AWARD NUMBER:

W81XWH-13-1-0354

TITLE:

“Targeting the Adipocyte-Tumor Cell Interaction in Prostate Cancer Treatment”

PRINCIPAL INVESTIGATOR:

Jorge Moscat, PhD

CONTRACTING ORGANIZATION:

Sanford-Burnham Medical Research Institute
La Jolla, CA 92037

REPORT DATE: December 2016

TYPE OF REPORT:

Final

PREPARED FOR: U.S. Army Medical Research and Materiel Command
Fort Detrick, Maryland 21702-5012

REPORT DOCUMENTATION PAGE

Form Approved
OMB No. 0704-0188

1. REPORT DATE	2. REPORT TYPE	3. DATES COVERED
December 2016	Final	30 Sep 2013- 29 Sep 2016

4. TITLE AND SUBTITLE

"Targeting the Adipocyte-Tumor Cell Interaction in Prostate Cancer Cancer Treatment"

5a. CONTRACT NUMBER

5b. GRANT NUMBER W81XWH-13-1-0354

5c. PROGRAM ELEMENT NUMBER

6. AUTHOR(S)

Jorge Moscat, PhD

E-Mail: jmoscat@sbpdiscovery.org

5d. PROJECT NUMBER

5e. TASK NUMBER

5f. WORK UNIT NUMBER

7. PERFORMING ORGANIZATION NAME(S) AND ADDRESS(ES)

Sanford Burnham Medical Research
Institute
10901 North Torrey Pines
La Jolla, CA 92037

8. PERFORMING ORGANIZATION REPORT NUMBER

9. SPONSORING / MONITORING AGENCY NAME(S) AND ADDRESS(ES)

U.S. Army Medical Research and Materiel Command
Fort Detrick, Maryland 21702-5012

10. SPONSOR/MONITOR'S ACRONYM(S)

11. SPONSOR/MONITOR'S REPORT NUMBER(S)

12. DISTRIBUTION / AVAILABILITY STATEMENT

Approved for Public Release; Distribution Unlimited

13. SUPPLEMENTARY NOTES

14. ABSTRACT

Prostate cancer (PCa) is one of the leading causes of death among men in the United States. Obesity is another growing epidemic health problem in Western societies and in developing nations, and represents one of the greatest threats to global human health. Several epidemiological studies during the last decade have pointed to an association between obesity and increased risk factor for PCa progression and aggressiveness. However, despite the relatively high amount of epidemiological data available, little is known about the molecular basis underlying the association between PCa progression, obesity and inflammation, and the role of the adipocyte-cancer cell interaction in this process. The goal of this project is to test the hypothesis that p62 is a molecular link in the cross-talk between obesity, inflammation and prostate cancer progression. Here, we have generated a new mouse model to address this question. Unveiling the molecular mechanisms governing obesity-induced prostate cancer progression will have a great impact in our understanding of this process, and its relevance for potential more targeted and efficacious therapies in PCa.

15. SUBJECT TERMS

Prostate cancer, obesity, inflammation, p62, metastasis, adipocyte, mouse models

16. SECURITY CLASSIFICATION OF:			17. LIMITATION OF ABSTRACT	18. NUMBER OF PAGES	19a. NAME OF RESPONSIBLE PERSON
					USAMRMC
a. REPORT	b. ABSTRACT	c. THIS PAGE			19b. TELEPHONE NUMBER *(include area code)*
U Unclassified	U Unclassified	U Unclassified	UU Unclassified	90	

Table of Contents

Page

1. INTRODUCTION

Prostate cancer (PCa) is the leading cancer diagnosis and the second-leading cause of death among men in the United States[1]. Obesity is another growing epidemic in Western societies and in developing nations, and represents one of the greatest threats to global human health[2,3]. Importantly, there is emerging support for a positive association between obesity and increased risk of PCa, with stronger links to more aggressive fatal disease[4,5]. However, despite the relatively high amount of epidemiological data available, little is known about the molecular basis underlying the association among PCa progression, obesity, and inflammation, or the role of the adipocyte-cancer cell interaction in this process. Therefore, biochemical and genetic studies using physiologically relevant models that mimic the complexity of these processes are sorely needed. Given the current obesity epidemic, it is urgent to explore possible interventions to disrupt the obesity-PCa link. Identifying the molecular mechanisms governing obesity-induced PCa progression will have a great impact on our understanding of this process, and will help in the design of more targeted and efficacious therapies in PCa. Collaborative efforts between our two laboratories (Diaz-Meco and Moscat) have identified p62 as a novel player in PCa and in obesity-induced inflammation, providing us with a unique in vivo model to study, at a cellular and molecular level, the mechanisms regulating the obesity-PCa interface. Understanding the role of p62 in the cellular and molecular pathways controlling PCa progression in obesity is critical for the design of new therapeutic strategies aimed at targeting the tumor microenvironment. Interfering with adipocyte-tumor cell interactions to disrupt PCa progression could be a much-needed new therapeutic avenue.

2. KEYWORDS

Prostate cancer; obesity; inflammation; p62; tumor microenvironment; adipocyte; IL-6; mouse models; stroma; mTORC1; c-Myc; nutrient sensing.

3. OVERALL PROJECT SUMMARY

This report corresponds to the final report of the Synergistic Idea Development Awards W81XWH-13-1-0353 (PI: Dr. Diaz-Meco) and W81XWH-13-1-0354 (Partnering PI: Dr. Moscat).

The goal of this synergistic project was to test the hypothesis that p62 is a molecular link that connects obesity, inflammation, and PCa progression. This was addressed in three Specific Aims:

Aim 1. Investigate the in vivo role of p62 in the relationship between adipose tissue and PCa progression.

Aim 2. Determine the role of p62-mediated inflammation in the PCa tumor microenvironment.

Aim 3: Explore the role of p62 in the adipocyte-PCa cell interaction through cellular and mechanistic in vitro studies.

The overall progress of the project has been excellent. We have fully developed the project and successfully completed the tasks planned according to the approved SOW and also expanded some unanticipated experiments based on the obtained results.

Task 1: Breeding of the required mice for experiments (Months 1-16; Diaz-Meco & Moscat). This task was completed as planned and as reported in 1st and 2nd Annual reports.

Task 1.1. Diaz-Meco lab bred TRAMP+ mice with $p62^{Adipo}$ mice provided by Moscat lab and generated the required experimental mice for analysis in the different tasks.

Task 1.2. Moscat lab bred WT, p62 KO, IL-6 KO and p62/IL-6 DKO mice required for the planned experiments.

Task 2: Analysis of the PCa phenotype of $TRAMP^{+}/p62^{Adipo}$ and $TRAMP^{+}$ mice (Months 4-16; Diaz-Meco) was completed as reported in 2nd Annual report.

Task 2.1. Disease-free survival curves (Kaplan-Meier plots) have been completed. No changes in survival were observed comparing the groups of both genotypes (Fig. 1A). This was most probably due to the huge volume of the primary tumor in both groups.

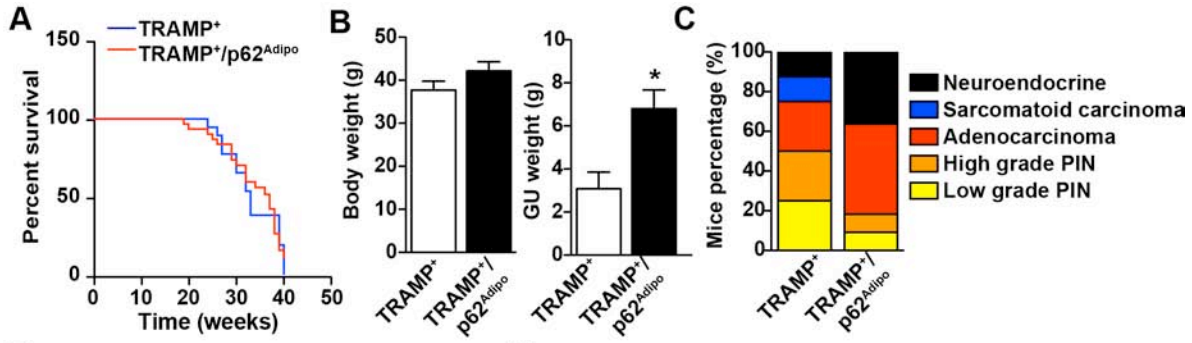

D

Genotype	Metastasis incidence
TRAMP+	28.6% (4/14)
TRAMP+/p62Adipo	36.7% (11/30)

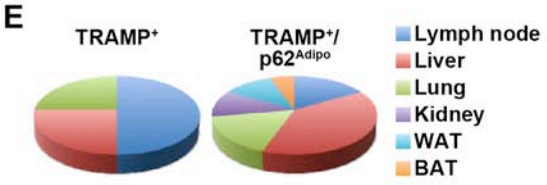

F

Genotype	Site of metastasis					
	Lymph nodes	Liver	Lung	Kidney	WAT	BAT
TRAMP+	14.3% (2/14)	7.1% (1/14)	7.1% (1/14)	0.0% (0/14)	0.0% (0/14)	0.0% (0/14)
TRAMP+/p62Adipo	10.0% (3/30)	23.3% (7/30)	10.0% (3/30)	6.7% (2/30)	6.7% (2/30)	3.3% (1/30)

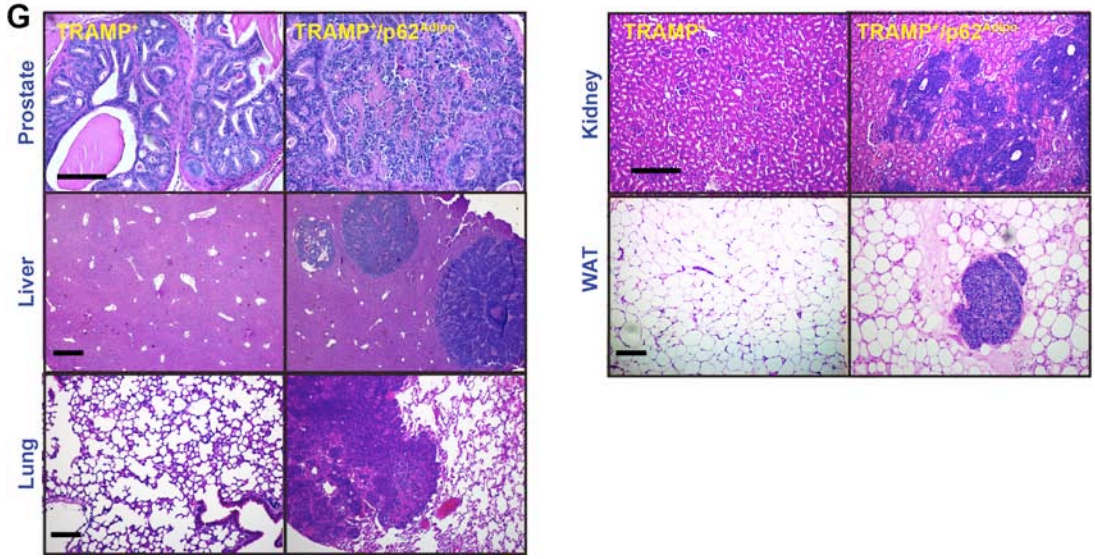

Figure 1. Analysis of the PCa phenotype of TRAMP^{+} and TRAMP^{+}/p62^{Adipo} mice. (**A**) Kaplan-Meier survival curve of TRAMP^{+} (n=20), compared with TRAMP^{+}/p62^{Adipo} (n=31). (**B**) Graph showing body weight and genitourinary (GU) tract weight of TRAMP^{+} (n=10) and TRAMP^{+}/p62^{Adipo} (n=20) mice at 30-40 weeks of age. (**C**) Histological analysis of prostrates of the indicated genotypes. **(D)** Table showing incidence of metastases from TRAMP^{+} (n=14) compared with TRAMP^{+}/p62^{Adipo} mice (n=30). **(E and F)** Pie chart and table showing the distribution of metastasis sites. (**G**) H&E staining of prostates and metastasis in different tissues of the indicated genotypes at 37 weeks of age. Scale bar=100 mm. Results are shown as means ± SEM, *p<0.05.

Task 2.2. Analysis of PCa progression in TRAMP^{+}/p62^{Adipo} and TRAMP^{+} mice: Diaz-Meco lab completed the characterization of the phenotype of TRAMP^{+}/p62^{Adipo}. The results of these tasks are presented in Fig. 1. Body weight and GU weight was determined at the endpoint of the experiment. Although there was a tendency of higher body weight in the TRAMP^{+}/p62^{Adipo} mice, there were not significant differences in this parameter between both groups (Fig. 1B). This result was unexpected,

but suggested that the presence of the tumor could have a profound effect in the whole metabolism of the host. Thus, whereas our previously published results[6] demonstrated that $p62^{Adipo}$ mice are significantly more obese that WT control mice in regular as well as in high-fat diet, however $TRAMP^{+}/p62^{Adipo}$ mice loose weight and their body weight is not significantly different from that of $TRAMP^{+}$ mice. This intriguing result suggested us the possibility that these mice could be suffering cachexia as a result of the PCa tumor. In contrast to body weight, the GU weight was significantly increased in $TRAMP^{+}/p62^{Adipo}$ mice as compared to control group (Fig. 1B). Most importantly, we found that $TRAMP^{+}/p62^{Adipo}$ mice developed a more aggressive PCa phenotype with higher incidence of adenocarcinoma and neuroendocrine tumors than $TRAMP^{+}$ control mice (Figs. 1C). Interestingly, $TRAMP^{+}/p62^{Adipo}$ mice also had a higher metastasis incidence as compared to the control group (Fig. 1D). Of note, there was also a tissue preference for the metastasis in the $TRAMP^{+}/p62^{Adipo}$ mice with increased incidence in liver and lung (Figs. 1E-1G). Furthermore, we also found metastasis in kidney, WAT and BAT in $TRAMP^{+}/p62^{Adipo}$ mice that were not detected in $TRAMP^{+}$ (Figs. 1E-1G). Collectively, these results suggest that the loss of p62 selectively in the adipose tissue drives tumorigenesis and invasiveness in PCa. This is consistent the increased risk associated with more aggressive PCa to obesity found in multiple epidemiological data[7,8]. In addition, these results demonstrate a cause and effect molecular link to start dissecting the mechanism connecting obesity and PCa progression in a suitable, physiologically relevant genetic in vivo model independent of food intake and diet.

Task 3: Analysis of the general metabolic characterization of TRAMP+/p62Adipo and TRAMP+ mice (Months 4-16; Moscat). A cohort of 6 mice of each genotype was analyzed for metabolic studies (CLAMS and DXA). The results of these tasks are presented in Fig. 2. As planned in Task 3.1, we monitored the body weight of a large cohort of mice during 10 months. In agreement with our results of Fig. 1B, there was a tendency of higher body weight in the $TRAMP^{+}/p62^{Adipo}$ mice group, however that was not overall significant (Fig. 2A). Furthermore, there were not significant changes in percentage of lean mass or fat mass as determined by body composition (Fig. 2B). Oil red staining to assess lipid accumulation in liver also revealed not significant differences between both genotypes (Fig. 2C). Next, we performed full metabolic characterization by using an automated indirect calorimetry system (CLAMS). The analysis of all the metabolic parameters measured including food intake, drinking, horizontal and vertical activity, volume of O_2 (VO_2), volume of CO_2 (VCO_2), respiratory exchange ratio (RER) and energy expenditure (EE) did not show significance changes between the $TRAMP^{+}/p62^{Adipo}$ mice group as compared to the control $TRAMP^{+}$ mice (Figs. 2D-2L). These surprising results are extremely interesting because they unveiled the impact that the PCa tumor has in the metabolism. As mentioned above in regard to the lack of differences in body weight, these metabolic results suggest that $TRAMP^{+}/p62^{Adipo}$ mice are suffering a cancer-associated cachexia phenotype. In fact, a similar metabolic analysis performed in $p62^{Adipo}$ mice showed decreased energy expenditure accompanied by a significant reduction in locomotor activity as compared to WT control mice[6]. This indicates that the presence of tumor in $TRAMP^{+}/p62^{Adipo}$ mice provoked a metabolic dysfunction in the $p62^{Adipo}$ mice increasing their metabolic rate to reach the same energy expenditure than $TRAMP^{+}$ mice. This is consistent with the increased energy expenditure and activation of thermogenesis that have been proposed as causative for cancer-associated cachexia [9,10,11]. Of note, $TRAMP^{+}/p62^{Adipo}$ mice that have no longer increased body weight or energy expenditure alterations, they however still displayed an insulin resistance phenotype. Thus, $TRAMP^{+}/p62^{Adipo}$ mice have defects in glucose and insulin responses as measured in glucose tolerance (GTT) and insulin tolerance (ITT) tests (Figs. 2M-2N) and the levels of triglycerides and cholesterol were also normalized with no differences between both genotype groups (Fig. 2O). These results open a new aspect of investigation in our project, since not only the adipose tissue talks to the tumor to make it more aggressive, but also the tumor impacts the metabolism of the host.

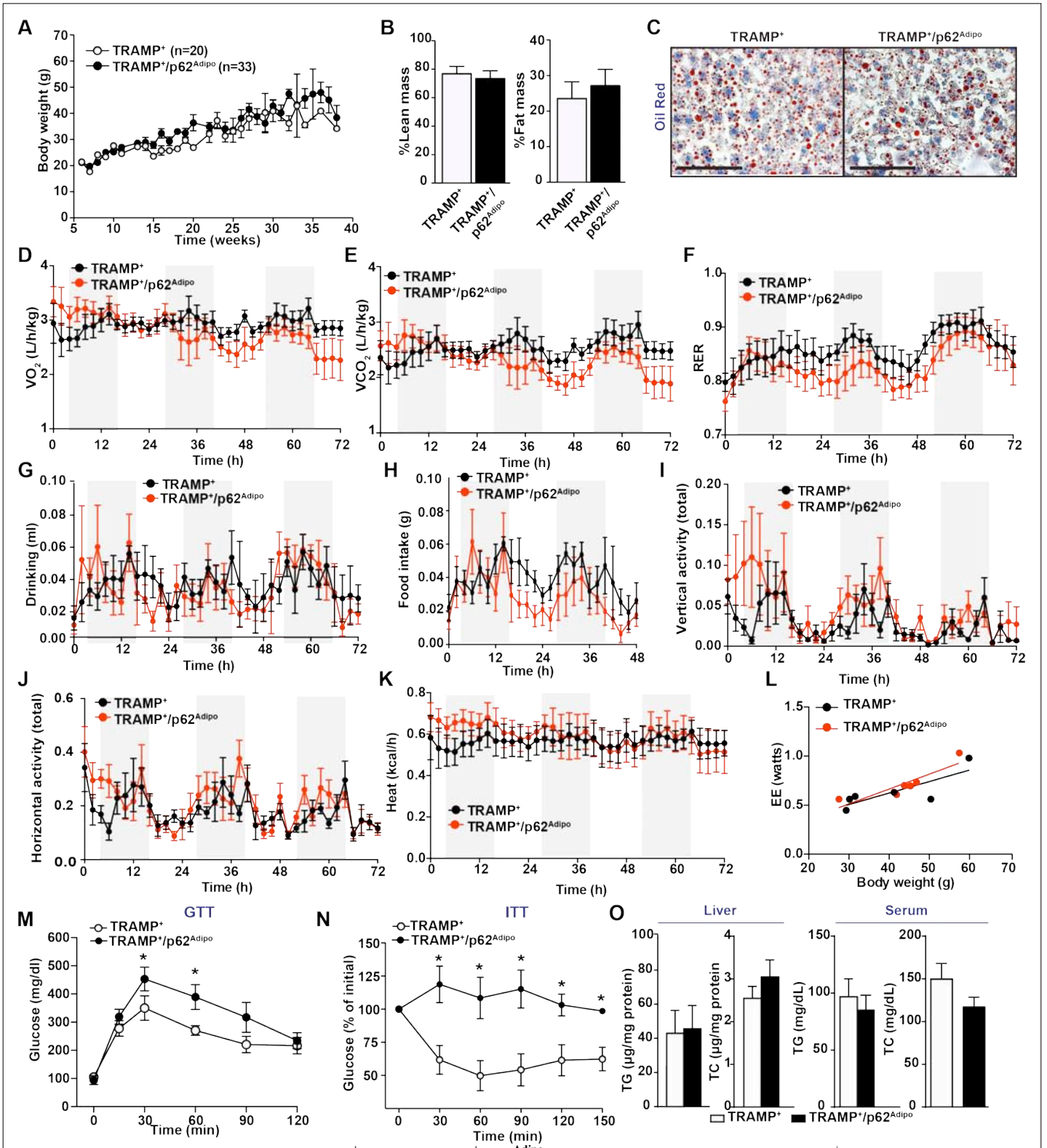

Figure 2. Metabolic analysis of TRAMP^{+} and TRAMP^{+}/p62^{Adipo} mice. (A) Body weight of TRAMP^{+} (n=20), compared with TRAMP^{+}/p62^{Adipo} (n=33) from 6 to 40 weeks of age. **(B)** DEXA analysis of mice of 7 month of age. Fat and lean mass as the percentage of total body weight. **(C)** Representative pictures of Oil Red staining from TRAMP^{+} and TRAMP^{+}/p62^{Adipo} livers. **(D-L)** Mice were housed in a metabolic chamber and monitored using Comprehensive Lab Animal Monitoring System CLAMS. **(D)** Oxygen consumption. **(E)** Carbon Dioxide production. **(F)** Respiratory Exchange Rate. **(E)** Drinking volume. **(H)** Food intake. **(I-J)** Locomotor activity. **(K)** Heat production. **(L)** Energy expenditure in relation to body weight. **(M)** Glucose tolerance and **(N)** insulin sensitivity tests. (O) Triglycerides (TG) and total cholesterol (TC) in liver and serum of TRAMP^{+} and TRAMP^{+}/p62^{Adipo} mice. n=6 mice per genotype. Scale bar=100 µm.

Tasks 4 and 5. Gene expression studies and metabolic profile of prostate and metabolic tissues in TRAMP^{+}/p62^{Adipo} and TRAMP mice (Months 12-22; Diaz-Meco & Moscat). We decided to modify the SOW regarding these tasks and to take a more global and unbiased approach to analyze gene expression. Instead of performing gene chip microarray analysis of PCa tumors and qPCR of a very limited number of metabolic genes and doing a limited metabolic analysis in these tissues, we decided to do RNAseq of both white adipose tissue (WAT, Moscat) and of the PCa tumors (Diaz-Meco). We think that this more comprehensive analysis could be more useful to understand the mechanism of

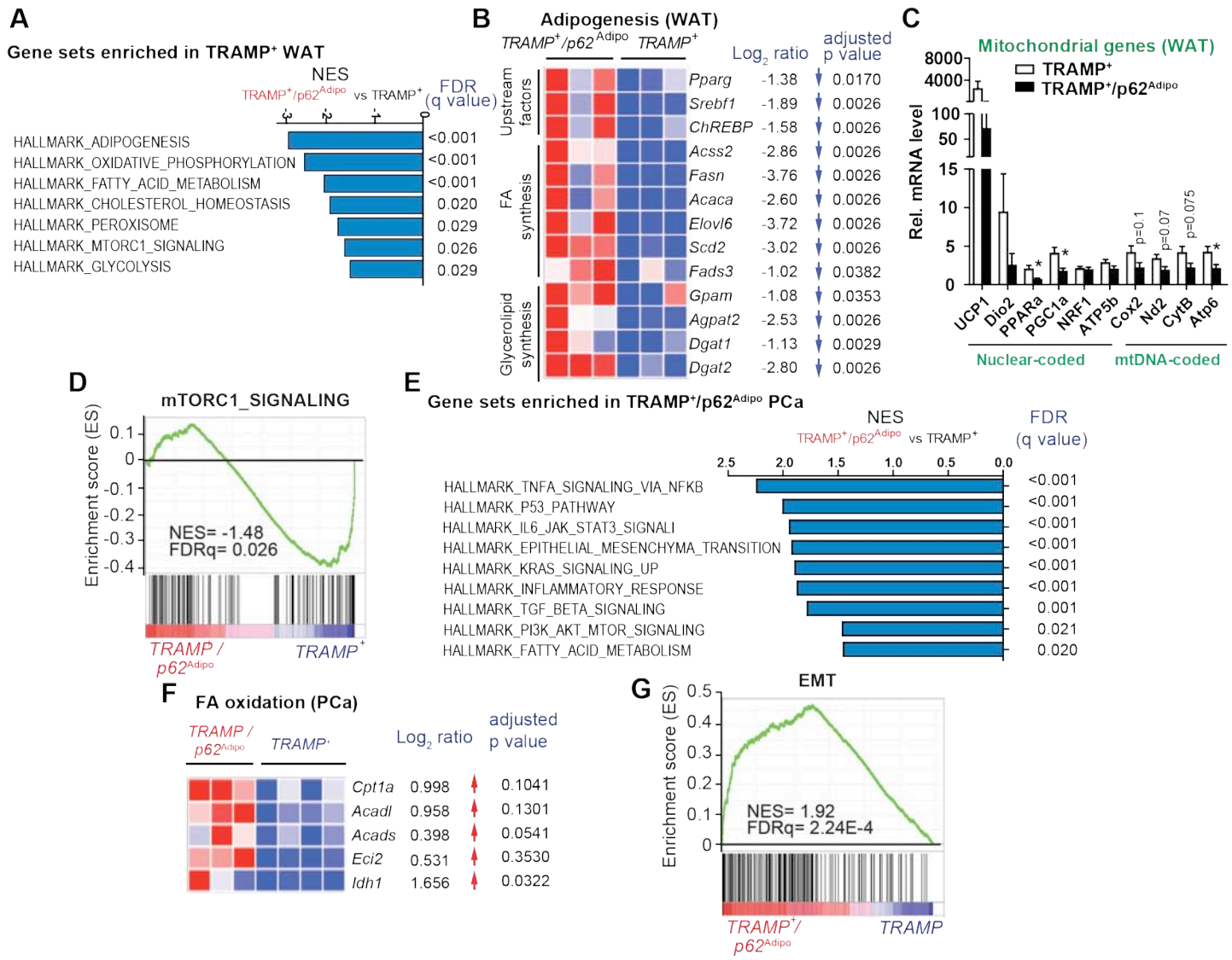

Figure 3. Whole-genome transcriptome analysis of WAT and PCa tumors in TRAMP^{+} and TRAMP^{+}/p62^{Adipo} mice. (**A**) Gene set enrichment analysis (GSEA) showing that p62 ablation in adipocyte in TRAMP tumor bearing mice rewires metabolic pathways in WAT. Top metabolic hallmark gene sets sorted by normalized enrichment score (NES) comparing TRAMP^{+}/p62^{Adipo} versus TRAMP^{+} mice (n=3). (**B**) Heatmap representation of downregulated genes associated with "adipogenesis" in TRAMP^{+}/p62^{Adipo} relative to TRAMP^{+} WAT (n=3) including Log$_2$FC and adjusted p value. (**C**) qRT-PCR analysis showing the downregulated expression of mitochondrial genes in TRAMP^{+}/p62^{Adipo} relative to TRAMP^{+} WAT (n=7). (**D**) Enrichment graph of mTORC1_SIGNALING dataset in WAT (n=3). (**E**) GSEA showing that p62 ablation in adipocytes has distal influences on PCa. Top different hallmark gene sets in PCa sorted by NES. (**F**) Heatmap of representative genes associated with FA oxidation upregulated in PCa tumor of TRAMP^{+}/p62^{Adipo} (n=3) versus TRAMP^{+} mice (n=4). (**G**) GSEA showing an Epithelial-Mesenchymal-Transition (EMT) signature in PCa of TRAMP^{+}/p62^{Adipo} mice (n=3).

action of p62 in these two compartments and to decipher how the tumor impacts the adipose tissue and, at the contrary, how the adipose tissue promotes tumor growth. Interestingly, bioinformatics analysis of the whole-transcriptome of WAT of both mouse genotypes (Moscat) revealed a profound impact on the metabolic functions upon deletion of p62. Thus, gene set enrichment analysis (GSEA) using the

curated gene set compilation Hallmark (MSigDb H) showed enrichment in metabolic gene sets in genes downregulated in TRAMP^{+}/p62^{Adipo} WAT. These included "adipogenesis", "oxidative phosphorylation", and "fatty acid metabolism" among the three top enriched gene sets (Fig. 3A). These results indicate that the PCa tumors abrogate critical adipocyte functios such as adipogenesis and mitochondrial oxidative phosphorylation in p62^{Adipo} WAT to shut down of the metabolism in the adipose tissue to provide nutrients for the benefit of the tumor to support tumor growth and progression. In agreement with this model, a broad spectrum of genes involved in fatty acid and glycerolipid synthesis for lipogenesis and mitochondrial oxidation their respective upstream regulators were profoundly repressed in TRAMP^{+}/p62^{Adipo} WAT (Figs. 3B and 3C). In addition, we also found that a signature of mTORC1 signaling was impaired in WAT upon p62 deletion (Fig. 3D). This is an important observation based on the fact that mTOCR1 is a well recognized regulator of lipogenesis via SREBP1[12] as well as a key player in "browning", a process characterized by β-AR-dependent UCP1 expression and expansion of beige/brite adipocytes[13]. Furthermore, the Diaz-Meco lab has recently established the importance of p62 in mTORC1 activation[14,15]. Therefore, it is conceivable that the loss of p62 in adipocytes may cause inhibition of mTORC1signalling that account for the suppression of both adipogenesis and browning and is responsible for the metabolic reprograming in the adipose tissue to save nutrients for the benefit of the tumor.

Next, we analyzed RNAseq data of PCa tumors from TRAMP^{+} and TRAMP^{+}/p62^{Adipo} mice (Diaz-Meco) to study the impact of metabolic alterations in the adipose tissue on the tumor. Of note, and in contrast with the general repression of metabolism in the adipose tissue of the p62^{Adipo} mice, GSEA of PCa tumors of these mice revealed a marked enrichment of gene sets associated with fatty acid metabolism in genes upregulated in TRAMP^{+}/p62^{Adipo} tumors as compared to those of TRAMP^{+} (Fig. 3E). Importantly, there was a robust increase in fatty acid oxidation as indicated by upregulation of CPT1a and Acyl-CoA Dehydrogenase (Acad) expression (Fig. 3F). These opposite results in adipose tissue and PCa tumors in fatty acid oxidation might indicate a metabolic switch of excessive energy flow from "host-to-WAT" in normal mice to "host-to-tumor" in TRAMP^{+}/p62^{Adipo} mice. Importantly, such metabolic rewiring is accompanied by an induction of Epithelial-Mesenchymal-Transition (EMT) signature as shown by GSEA analysis (Fig. 3G), which is consistent with the increased metastasis incidence observed in TRAMP^{+}/p62^{Adipo} WAT (Fig.1D).

Task 6. <u>In vivo characterization of inflammation in PCa tumors, and adipose tissue (Months 23-30; Diaz-Meco & Moscat)</u>. We have fully characterized the inflammation in both adipose tissue (Moscat) as well as in PCa tumors (Diaz-Meco) from TRAMP^{+} and TRAMP^{+}/p62^{Adipo} mice. To analyze the infiltration of specific immune cell populations, we applied CIBERSORT, a computational approach using the RNAseq data of both tissues. Interestingly, there was a significant decreased in the infiltration of M1 macrophages in TRAMP^{+}/p62^{Adipo} adipose tissue as compared to TRAMP^{+} controls (Fig. 4A). In addition, there was a reduction in the recruitment of resting natural killer T cells (NK) and a concomitant decreased in activated NK cells in the WAT of TRAMP^{+}/p62^{Adipo} mice (Fig. 4A). Other immune populations did not show significant changes by this computational method. Further analysis of RNAseq data to characterize the immunological profile of the adipose tissue revealed a general increased in inflammation upon p62 deletion in this tissue including increased expression of macrophage markers (F4/80 and CD68), the monocyte chemoatractant (MCP1) and osteopontin (SPP1) (Fig. 4B). Interestingly, it has been shown that M2 macrophages express high levels of SPP1, which is important for remodeling the adipogenic cell niche[16]. Interestingly, we also found a switch from the expected M1 phenotype in adipose tissue from obese subjects to an M2 profile, as indicated by increased expression of classical M2 markers such as arginase (Arg1) or interleukin-4 (IL-4). Of note, a similar immunological landscape was also observed in the PCa tumors of TRAMP^{+}/p62^{Adipo} mice with an increased recruitment of macrophages, M2 switch and reduction of activated NK cells (Figs. 4C and 4D). These results are consistent with a change in the host upon p62 deletion in the adipose tissue that will favor tumor progression and metastasis. In line with the potential role of inflammation in tumor progression, we have tested the hypothesis that p62-deficiency-induced obesity promotes

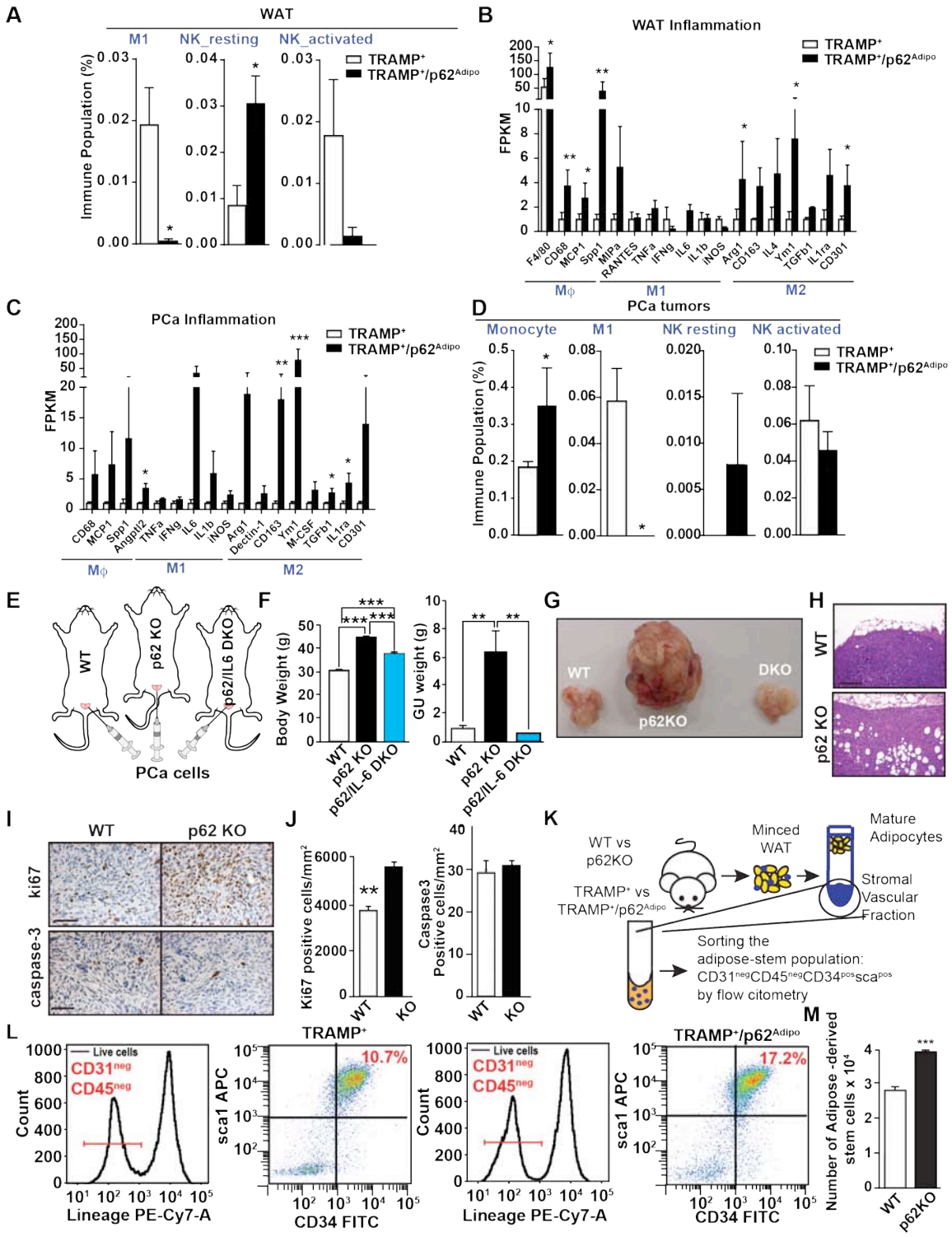

Figure 4. Role of inflammation in p62-mediated tumorigenesis. (A) Alterations in immune cell infiltration in WAT from TRAMP^{+} and TRAMP^{+}/p62^{Adipo} mice determined by CIBERSORT analysis. **(B)** mRNA expression of immunological profile of WAT from both genotypes. **(C)** Alterations in immune cell infiltration in PCa tumors from TRAMP^{+} and TRAMP^{+}/p62^{Adipo} mice determined by CIBERSORT analysis. **(D)** mRNA expression of immunological profile of PCa tumors from both genotypes. **(E)** IL-6 is required for p62's role in the tumor microenvironment. Orthotopic injection of TRAMP-C2Re3 cells into the prostates of syngeneic WT and p62 KO mice. Orthotopic tumors were allowed to grow for two months. **(F)** Body weight and GU tract weight. **(G)** Pictures of representative orthotopic tumors . n = 5 or 6 mice per genotype. (**H**) Infiltration of adipocytes in orthotopic tumors of p62 KO. H&E staining of orthotopic tumors from WT and p62 KO mice. Scale bar = 200 μm. **(I)** Increased proliferation in p62 KO orthotopic tumors. Immunostaining of Ki67 and cleaved caspase 3 in orthotopic tumors of WT and p62 KO mice. **(J)** Quantification of Ki67-positive cells and caspase3 positive cells. Results are the means ± SEM of counts from 10 different fields per mouse. n=5 mice, $^{**}p<0.01$. Scale bar = 50 μm. (**K**) Schematic representation of FACS-purification of adipose-derived stem cells from white adipose tissue of the indicated genotypes. **(L)** Histograms and dot-plots showing FACS staining profiles and gating of adipose stem cells from TRAMP^{+} and TRAMP^{+}/p62^{Adipo} mice. The live cells were sorted for CD31^{neg}CD45^{neg} (histograms in the left). These cells were then sorted on the basis of expression of CD34 and sca1 (dot plots in the right). The percentage yield of CD31^{neg}CD45^{neg}CD34^{pos}sca1^{pos} cells (adipose-derived stem cells) for each genotype is indicated. **(M)** Quantification of adipose-derived stem cells from WT and p62KO mice isolated as described above. $^{*}p<0.05$, $^{***}p<0.001$.

carcinogenesis through increased adipose tissue and systemic inflammation, resulting in enhanced IL-6 production. These results were reported in the 1st Annual report. We used orthotopic injections of PCa cells into the prostates of WT, p62 and p62/IL-6 DKO mice (Fig. 4E), and determined body and genitourinary weight (Fig. 4F). Interestingly, orthotopic tumors grew faster in the prostates of p62 KO mice as compared with WT controls, and importantly, tumor growth was completely abolished when the injections were performed in the p62/IL6 DKO prostates, indicating that IL-6 is required in vivo for the role of p62 in the tumor microenvironment (Fig. 4G). H&E staining of the orthotopic tumors grown in p62 KO mice showed infiltration of periprostatic adipocytes into the tumor whereas in the WT tumors the adipocytes were restricted to the periphery (Fig. 4H). p62 KO tumors have a higher proliferation rate with no changes in apoptosis as determined by Ki67 and cleaved Caspase-3 staining, respectively (Figs. 4I and 4J).

To complete this task, we also determine the potential role of adipose stem cells (ASC) in the tumor progression promoted by p62 deletion in adipose tissue. We first determined ASC in adipose tissue of $TRAMP^{+}/p62^{Adipo}$ and $TRAMP^{+}$ mice and of WT and p62 KO as described (Fig. 4K). Cells were initially selected by size, on the basis of forward scatter (FSC) and side scatter (SSC), followed by exclusion of dead cells on the basis of uptake of DAPI. Then, live cells were gated on both SSC and FSC singlets, ensuring that the staining of individual cells was analyzed. Next, the cells were separated on the basis of the cell-surface markers indicated. Of note, we found that adipose tissue from both TRAMP+/p62Adipo or p62 KO had more ASCs than their corresponding controls (Figs. 4L and 4M). These results demonstrate that there is an expansion of the ASC population as a consequence of p62-deficiency that could impact tumor progression.

Task 7. 3D Organotypic cultures to study the adipocyte-PCa cell interaction in vitro (Months 30-36; Diaz-Meco & Moscat).

We next explored the role of p62 in the adipocyte-PCa cell interaction in in vitro studies using organotypic cultures. This 3D culture recapitulates, in an amenable in vitro system, the tumor microenvironment and its interactions with the tumor cell, closely mimicking the physiological situation and the cellular architecture. We have developed this in vitro system to study the interactions of tumor cells with adipose tissue. Culturing mature adipocytes is technically challenging because of their large lipid droplets, which precludes their attachment. To overcome this difficulty, we have successfully set up 3D cultures with adipocytes embedded in a matrix of collagen I and Matrigel that maintains the unilocular structure and active functions of adipocytes in vitro (Fig. 5A). Our first analysis using this approach demonstrates that both the vascular stromal fractions (SVF) containing preadipocytes, endothelial, immune, and ASC cells as well as mature adipocytes were able to promote PCa cell invasion (Figs. 5B and 5C) consistent with the notion that there is in fact an interaction between adipocytes and PCa cells that can be recapitulated in vitro. To address how p62 regulates the crosstalk of the adipose tissue with tumor cells to promote carcinogenesis, we first used minced adipose tissue from mice of each genotype embedded in the collagen I/Matrigel matrix combined with PCa cells seeded on top of the gel, and evaluate the impact on prostate cell invasion. Of note, WAT from p62 KO mice promoted an enhanced effect on PCa cells invasion as compared to WAT from WT mice (Figs. 5D and 5E). To further dissect the cellular components responsible for p62-mediated role in PCa invasion, we separated mature adipocytes and SVF containing preadipocytes, endothelial, macrophages, and ASC cells, and test in organotypic cultures their contribution to the phenotype. Interestingly, we found that all these cellular fractions including mature adipocytes and ASCs from p62 KO mice produced a marked increase in PCa invasion (Figs. 5F-5K). Next, we tested the role of IL-6 as a critical mediator of p62 actions using this in vitro system. Notably, genetic deletion of IL-6 abrogated the p62-mediated PCa-invasion by mature adipocytes or SVF (Figs. 5F-5I). Furthermore, addition of IL-6 to organotypic cultures of PCa cells alone or in the presence of stromal cells was sufficient to promote PCa invasion. These results indicate the critical role of IL-6 mediating p62 actions and are fully consistent with our in vivo data (Figs. 4E-4G).

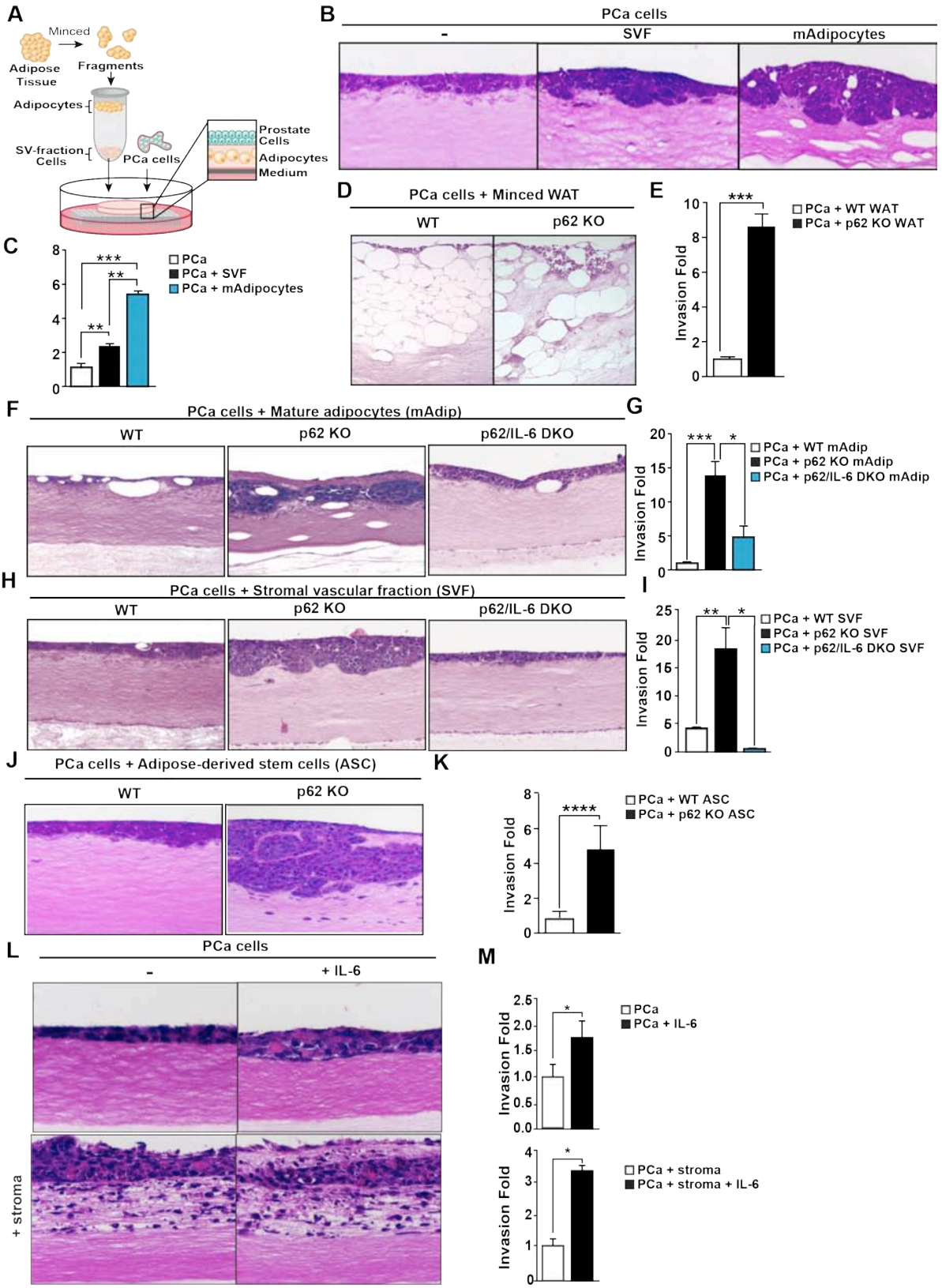

Figure 5. Role of p62 in the adipocyte-PCa cell interaction in vitro. (A) Schematic representation of 3D organotypic cultures used to study the interaction between adipose tissue and PCa cells. **(B)** H&E-stained sections of Myc-Cap cells cultured in an organotypic system in the presence of stromal vascular fraction (SVF) or mature adipocyte embedded in the collagen/matrigel matrix. **(C)** Quantification of PCa cell invasion of experiment shown in **(B)**. **(D-E)**. H&E staining of organotypic gels of Myc-Cap cells cultured in the presence of minced WAT from WT or p62 KO mice **(D)** and quantification of PCa cell invasion **(E)**. **(F-K)** H&E staining of organotypic gels of Myc-Cap cells cultured in the presence of mature adipocytes **(F)**, SVF **(H)** or ASCs **(J)** from the indicated genotypes and quantification of PCa cell invasion of these cultures **(G, I-K)**. **(L-M)** H&E staining of organotypic gels of Myc-Cap cells alone or mixed with stromal cells and cultured in the presence or not of IL-6 (L) and quantification of PCa cell invasion (M). Results are presented as mean ± SEM. n=4. *p < 0.05, **p < 0.01. ***p < 0.001. ****p < 0.0001.

Currently, experiments are underway testing the potential role of the changes in fatty acid oxidation observed in PCa tumors from TRAMP^{+}/p62^{Adipo} mice in tumor invasion using organotypic cultures. We are now finishing these experiments and preparing a publication that will report all the unpublished data presented in this final report.

In addition, we have also complemented these studies with research aimed to understand how p62 senses nutrients. These results have been recently published in the top-notch journal Cell Reports[17] (see Appendix). The ability to sense and response to fluctuation in nutrient levels is a requisite for life. During food abundance, nutrient sensing pathways engage anabolism and storage, whereas scarcity triggers homeostatic mechanisms, such as the mobilization of internal stores through autophagy. Importantly, nutrient-sensing pathways are commonly deregulated in human metabolic disease such as obesity. Central to this process is the nutrient-sensitive kinase complex mTORC1 that integrate the response to growth factors, energy levels and nutrients, specifically amino acids. Interestingly, we have found a nutrient sensing pathway that is selectively activated in response to amino acids and that is critical for PCa cells. We have identified a kinase cascade that is highly upregulated in PCa and that is essential for tumor development. Because kinases are eminently druggable targets, our findings have the potential to open new avenues for designing novel treatments for cancer.

Furthermore, we have recently published a Minireview in Cell[18] on the role of p62 in cancer and highlighting its novel role as a tumor suppressor in the stroma. The results of this project further emphasize the role of p62 in the tumor microenvironment and specifically in the adipose tissue as a critical player in tumor progression and metastasis. These results also unveiled the cellular interactions that take place between obesity and cancer and advance our understanding of this complex process to facilitate the design of novel therapeutic strategies in this area.

4. KEY RESEARCH ACCOMPLISHMENTS

- Identification of p62 as a novel tumor suppressor in the stroma in PCa.
- Demonstration that p62-mediated inflammation in the stroma is key for prostate tumorigenesis.
- Identification of the inflammatory cytokine IL-6 as a major player in mediating p62 actions in the tumor stroma.
- Characterization of a molecular network linking p62 to mTORC1 and c-Myc operating in the stroma to influence tumorigenesis in the prostate epithelium.
- Identification of c-Myc as a novel tumor suppressor in the stroma in PCa, opposite to its role as an oncogene in the epithelium.
- The use of mTORC1 inhibitors in PCa could have deleterious effect through its role in the stroma.
- The identification of the mechanisms that reduce p62 levels in the stroma could constitute a novel strategy to intervene in PCa.
- p62 deficiency in the adipose tissue expands the adipose-stem cell population.
- p62 selective deficiency in the adipose tissue promotes a more aggressive PCa phenotype, providing a link between obesity and adiposity and PCa progression.
- p62 selective deficiency in the adipose tissue changes the metastasis incidence and the tissue preference for metastasis.
- Generation of a new mouse model to study cancer-associated cachexia.
- Full metabolic characterization of mice with selective deficient of p62 in the adipose tissue and PCa tumors revealed a phenotype of cancer-associated cachexia.
- Identification of a novel kinase cascade that regulates nutrient sensing to control mTORC1 activation.
- Novel nutrient sensing mechanism critical for PCa cell growth and autophagy.
- The p62-kinase cascade identified is overexpressed in human PCa tumors and is required for PCa tumor growth.
- p62 selective deficiency in the adipose tissue promotes a metabolic shutdown in the adipose tissue blocking nutrient utilization and storage in adipose tissue to make nutrients available for tumor growth.
- p62 selective deficiency in the adipose tissue promotes an inflammation switch towards an M2 macrophage phenotype in both adipose tissue and PCa tumors to favor tumor progression.
- p62 selective deficiency in the adipose tissue impairs adipose tissue fatty acid oxidation but increase fatty acid oxidation in PCa tumors. The metabolic rewiring benefits tumor growth.

5. CONCLUSION

The main conclusions from this project are:

1) The full characterization of the prostate phenotype caused in vivo by p62 selective deficiency in the adipose tissue that has lead to the important conclusion that obesity drives a more aggressive PCa phenotype with higher incidence of metastasis.
2) The metabolic studies at whole body level as well as a cellular level that have identified a cancer-associated cachexia phenotype in the obese p62 adipose-deficient mice harboring PCa

tumors. This opens the need to investigate not only how the adipose tissue influences the PCa tumor, but also how the tumor instructs and transforms the adipose tissue for its own benefit. p62 selective deficiency in the adipose tissue promotes a metabolic rewiring to benefit tumor progression.

3) The study of the adipocyte-PCa cell link in vitro in a 3D organotypic culture that recapitulates in vitro the interactions mediated by the tumor microenvironment.
4) The complementary studies at understanding the molecular mechanisms how p62 senses nutrients that have allowed the identification of a druggable kinase cascade as potential novel therapeutic strategies for PCa.

6. PUBLICATIONS, ABSTRACTS, AND PRESENTATIONS

Publications:

✓ Peer-Reviewed Scientific Journals:

Valencia, T., Kim, J.Y., Abu-Baker, S., Moscat-Pardos, J., Ahn, C.S., Reina-Campos, M., Duran, A., Castilla, E.A., Metallo, C.M., Diaz-Meco, M.T.*, and Moscat, J*. (2014) Metabolic reprogramming of stromal fibroblasts through p62-mTORC1 signaling promotes inflammation and tumorigenesis. **Cancer Cell** 26, 121-135 (*equal contribution and corresponding author)

This publication has been highlighted in the following scientific articles:

- Ubaldo E. Martinez-Outschoorn, Federica Sotgia, Michael P. Lisanti. (2014). Metabolic Asymmetry in Cancer: A "Balancing Act" that Promotes Tumor Growth. **Cancer Cell**, Volume 26, Issue 1, 14 July 2014, 5-7
- Research Watch: Tumor Microenvironment: p62 loss reprograms stromal metabolism to promote tumor growth. (2014) **Cancer Discovery** Published Online First July 17, 2014; doi:10.1158/2159-8290.CD-RW2014-152
- Alderton, G.K. (2014). Stromal metabolism has paracrine effects. Nature Reviews **Cancer**, Research Highlight. 14, 515.

Linares J.F., Duran A., Reina-Campos M., Aza-Blanc P., Campos A., Moscat J., Diaz-Meco M.T. (2015). Amino Acid Activation of mTORC1 by a PB1-Domain-Driven Kinase Complex Cascade. **Cell Rep.** 12, 1339-52. PMCID: PMC4551582

Moscat J., Richardson A., Diaz-Meco M.T. (2015). Nutrient stress revamps cancer cell metabolism. **Cell Research** 25:537-38.

Moscat J., Karin, M., Diaz-Meco, M.T. (2016). p62 in cancer: signaling adaptor beyond autophagy . **Cell** (Leading Edge Minireview) 167: 606-609.

✓ Lay press:

Our publication in Cancer Cell has been reviewed in several lay articles:

- Newswise – La Jolla, CA, July 3, 2014. "New study reveals how tumors remodel their surroundings to grow"
- EurekAlert. AAAS, July 3, 2014. "New study reveals how tumors remodel their surroundings to grow"

- Science Daily. July 3, 2014. "How tumors remodel their surroundings to grow".

Our publication in Cell Reports has been reviewed in several lay articles:

- Health Innovations. August 14, 2015. "Study identifies mTOR pathway that controls cancer proliferation via nutrients".
- Science Daily. August 13, 2015. "Scientists discover a pathway that controls cancer cell proliferation by nutrients".

Our work on the obesity-PCa link has been reviewed also in the following lay articles:

- Our research was highlighted on the CDMRP website:

  http://cdmrp.army.mil/pcrp/research_highlights/16diaz-meco_highlight.shtml
- Onclive – May 007, 2016. "Novel protein research may help unravel obesity-cancer link".
- KUSI TV: Sep 30, 2016. Moscat talks about prostate cancer research.

Abstracts and presentations:

"Nutrient sensing and Cancer Metabolism by the p62 autophagy pathway" University of Pennsylvania, Philadelphia, 2014. Speaker (Moscat).

"New role of metabolic reprograming in stroma-induced tumorigenesis" Centre for Genome Regulation, Barcelona, Spain, 2014. Speaker (Moscat).

"Metabolic Reprogramming by the p62 Pathway in Cancer" in the "2014 ASIP Annual Meeting at Experimental Biology 2014" (San Diego, 2014). Speaker (Moscat).

"mTORC1 activation by p62" in the SBMRI Workshop on "Cancer Metabolism, autophagy and nutrient sensing" (La Jolla, USA, 2014). Speaker and co-organizer (Moscat)

"Metabolic reprograming by the mTORC1/p62 complex in the tumor stroma" in the SBMRI Workshop on "Cancer Metabolism, autophagy and nutrient sensing" (La Jolla, USA, 2014). Speaker and co-organizer (Diaz-Meco)

"Metabolic reprogramming in the stroma promotes inflammation and tumorigenesis". CDSN / MDP Metabolism Retreat. (Carlsbad, USA, 2014). Speaker (Diaz-Meco)

"Metabolic Reprogramming in the Tumor Stroma by the p62/mTORC1 Pathway" Case Western Reserve, Cleveland, 2014. Speaker (Moscat).

"Autophagy and Metabolic Reprograming in the Tumor Stroma" in the Major Symposium on "Autophagy and Cancer" at the Annual AACR meeting, Philadelphia, 2015. Speaker (Moscat).

"Dual role of p62/mTORC1 in the tumor microenvironment". The San Diego Center for Systems Biology. UCSD (San Diego, 2015). Speaker (Moscat).

"Metabolic reprograming in cancer" C3 Cancer Centers Consortium Retreat, UCSD, 2015. Speaker (Moscat).

"Targeting Metabolic Reprograming in Cancer" Centro Nacional de Biotecnologia, Madrid, Spain, 2015. Speaker (Moscat)

"Cell Death and Survival Networks". Helmholtz Zentrum München, Munich, 2015 Speaker (Moscat)

"Nutrient Sensing in Cancer". Helmholtz Zentrum München, Munich, 2015 Speaker (Diaz-Meco)

"Metabolic reprograming of the tumor microenvironment through p62". 2nd Annual Meeting of International Ovarian Cancer Consortium in conjunction with the International Symposium on Tumor Microenvironment and Therapy Resistance –Oklahoma City, 2015, Speaker (Diaz-Meco)

"Nutrient Sensing and Metabolic Reprograming in the Tumor Stroma" at the 46th International Symposium of the Princess Takamatsu Cancer Research Fund on "Onco-metabolomics", Tokyo, Japan, 2015 Speaker (Moscat)

"p62: Metabolism and the tumor microenvironment" in the Education Session "Metabolic Interplay Between Tumor and Microenvironment" at the Annual AACR meeting, New Orleans, 2016 Speaker (Moscat)

"p62 at the crossroad of stroma-epithelium interactions in Cancer" at the SBP Symposium on "Cancer Metabolism, autophagy and nutrient sensing" La Jolla, 2016 Speaker (Moscat)

"Control of p62 homeostasis by autophagy in cancer" at the Banbury Center, Cold Spring Harbor Laboratory Meeting on "Autophagy and Cancer" Cold Spring Harbor, USA, 2016 Speaker (Moscat)

"Cross-talks at the tumor microenvironment by autophagy adapters" at the 28th Pezcoller Symposium on "initial steps on the route to tumorigenesis" Trento, Italy, 2016 Speaker (Moscat)

7. INVENTIONS, PATENTS AND LICENSES

Nothing to report.

8. REPORTABLE OUTCOMES

- New mouse model to study the link of obesity and prostate cancer.
- New 3D organotypic model to provide a physiological and amenable system to study the biology and the relationships of the different cell types in the tumor microenvironment.
- Four manuscripts (in Cancer Cell, Cell Reports, Cell Research and Cell) co-authored by both laboratories (Moscat and Diaz-Meco) (see above in Publications).

9. OTHER ACHIEVEMENTS

Nothing to report.

10. REFERENCES

1. American Society of Clinical, O. The State of Cancer Care in America, 2016: A Report by the American Society of Clinical Oncology. *J Oncol Pract* **12**, 339-383 (2016).
2. Finkelstein, E.A., Ruhm, C.J. & Kosa, K.M. Economic causes and consequences of obesity. *Annual review of public health* **26**, 239-257 (2005).
3. Finkelstein, E.A. How big of a problem is obesity? *Surg Obes Relat Dis* **10**, 569-570 (2014).

4. Wright, M.E., *et al.* Prospective study of adiposity and weight change in relation to prostate cancer incidence and mortality. *Cancer* **109**, 675-684 (2007).
5. Mondul, A.M., Giovannucci, E. & Platz, E.A. A prospective study of obesity, and the incidence and progression of lower urinary tract symptoms. *J Urol* **191**, 715-721 (2014).
6. Muller, T.D., *et al.* p62 links beta-adrenergic input to mitochondrial function and thermogenesis. *The Journal of clinical investigation* **123**, 469-478 (2013).
7. Joshu, C.E., *et al.* Weight gain is associated with an increased risk of prostate cancer recurrence after prostatectomy in the PSA era. *Cancer Prev Res (Phila)* **4**, 544-551 (2011).
8. Haque, R., *et al.* Association of body mass index and prostate cancer mortality. *Obes Res Clin Pract* **8**, e374-381 (2014).
9. Blum, D., *et al.* Cancer cachexia: a systematic literature review of items and domains associated with involuntary weight loss in cancer. *Crit Rev Oncol Hematol* **80**, 114-144 (2011).
10. Tsoli, M., *et al.* Activation of thermogenesis in brown adipose tissue and dysregulated lipid metabolism associated with cancer cachexia in mice. *Cancer Res* **72**, 4372-4382 (2012).
11. Petruzzelli, M., *et al.* A switch from white to brown fat increases energy expenditure in cancer-associated cachexia. *Cell Metab* **20**, 433-447 (2014).
12. Li, S., Brown, M.S. & Goldstein, J.L. Bifurcation of insulin signaling pathway in rat liver: mTORC1 required for stimulation of lipogenesis, but not inhibition of gluconeogenesis. *Proc Natl Acad Sci U S A* **107**, 3441-3446 (2010).
13. Liu, D., *et al.* Activation of mTORC1 is essential for beta-adrenergic stimulation of adipose browning. *J Clin Invest* **126**, 1704-1716 (2016).
14. Duran, A., *et al.* p62 is a key regulator of nutrient sensing in the mTORC1 pathway. *Mol Cell* **44**, 134-146 (2011).
15. Linares, J.F., *et al.* Amino Acid Activation of mTORC1 by a PB1-Domain-Driven Kinase Complex Cascade. *Cell reports* (2015).
16. Lee, Y.H., Petkova, A.P. & Granneman, J.G. Identification of an adipogenic niche for adipose tissue remodeling and restoration. *Cell Metab* **18**, 355-367 (2013).
17. Linares, J.F., *et al.* Amino Acid Activation of mTORC1 by a PB1-Domain-Driven Kinase Complex Cascade. *Cell reports* **12**, 1339-1352 (2015).
18. Moscat, J., Karin, M. & Diaz-Meco, M.T. p62 in Cancer: Signaling Adaptor Beyond Autophagy. *Cell* **167**, 606-609 (2016).

11. APPENDICES

Publications:

Valencia, T., Kim, J.Y., Abu-Baker, S., Moscat-Pardos, J., Ahn, C.S., Reina-Campos, M., Duran, A., Castilla, E.A., Metallo, C.M., Diaz-Meco, M.T.*, and Moscat, J*. (2014) Metabolic reprogramming of stromal fibroblasts through p62-mTORC1 signaling promotes inflammation and tumorigenesis. **Cancer Cell** 26, 121-135 (*equal contribution and corresponding author)

Linares J.F., Duran A., Reina-Campos M., Aza-Blanc P., Campos A., Moscat J., Diaz-Meco M.T. (2015). Amino Acid Activation of mTORC1 by a PB1-Domain-Driven Kinase Complex Cascade. **Cell Rep.** 12, 1339-52. PMCID: PMC4551582.

Moscat J., Richardson A., Diaz-Meco M.T. (2015). Nutrient stress revamps cancer cell metabolism. **Cell Research** 25:537-38.

Moscat J., Karin, M., Diaz-Meco, M.T. (2016). p62 in cancer: signaling adaptor beyond autophagy . **Cell** (Leading Edge Minireview) 167:606-609.

Cancer Cell
Article

Metabolic Reprogramming of Stromal Fibroblasts through p62-mTORC1 Signaling Promotes Inflammation and Tumorigenesis

Tania Valencia,[1] Ji Young Kim,[1] Shadi Abu-Baker,[2] Jorge Moscat-Pardos,[1] Christopher S. Ahn,[3] Miguel Reina-Campos,[1] Angeles Duran,[1] Elias A. Castilla,[2] Christian M. Metallo,[3,4] Maria T. Diaz-Meco,[1,5,*] and Jorge Moscat[1,5,*]
[1]Sanford-Burnham Medical Research Institute, 10901 N. Torrey Pines Road, La Jolla, CA 92037, USA
[2]University of Cincinnati Medical College, Cincinnati, OH 45267, USA
[3]Department of Bioengineering, University of California, San Diego, 9500 Gilman Drive, La Jolla, CA 92093, USA
[4]Moores Cancer Center, University of California, San Diego, 9500 Gilman, Drive, La Jolla, CA 92093
[5]Co-senior author
*Correspondence: mdmeco@sanfordburnham.org (M.T.D.-M.), jmoscat@sanfordburnham.org (J.M.)
http://dx.doi.org/10.1016/j.ccr.2014.05.004

SUMMARY

The tumor microenvironment plays a critical role in cancer progression, but the precise mechanisms by which stromal cells influence the epithelium are poorly understood. Here we show that p62 levels were reduced in the stroma of several tumors and that its loss in the tumor microenvironment or stromal fibroblasts resulted in increased tumorigenesis of epithelial prostate cancer cells. The mechanism involves the regulation of cellular redox through an mTORC1/c-Myc pathway of stromal glucose and amino acid metabolism, resulting in increased stromal IL-6 production, which is required for tumor promotion in the epithelial compartment. Thus, p62 is an anti-inflammatory tumor suppressor that acts through the modulation of metabolism in the tumor stroma.

INTRODUCTION

Primary tumors are initiated as a result of the stepwise acquisition of genetic alterations within the epithelial compartment (Shen and Abate-Shen, 2010). However, increasing evidence supports the notion that the tumor microenvironment also plays a critical role in cancer progression in many types of neoplasias, including prostate cancer (PCa), although relatively little is known about the signaling pathways that mediate communication between the stromal and epithelial compartments (Ammirante et al., 2010; Erez et al., 2010; Santos et al., 2009; Trimboli et al., 2009). Inflammation and metabolism are two critical factors contributing to the protumorigenic properties of the stroma (DeBerardinis and Thompson, 2012; Grivennikov et al., 2010; Hanahan and Coussens, 2012; Metallo and Vander Heiden, 2013; Vander Heiden, 2013). Although not totally understood, some evidence suggests that the metabolic state of the tumor stroma can decisively influence the tumorigenic potential of the tumor epithelial compartment (Lisanti et al., 2013). Here we have addressed this fundamental biological question in the context of p62 deficiency in the nonepithelial tumor compartment. Our laboratory initially identified p62, also known as sequestosome-1, as a scaffold protein for the atypical protein kinase C isozymes and later implicated p62 in other cell stress responses (Diaz-Meco and Moscat, 2012; Moscat and Diaz-Meco, 2012; Moscat et al., 2007; Sanchez et al., 1998). p62 binds Raptor, a key component of the mTOR-orchestrated nutrient-sensing complex and an important activator of anabolic pathways that are instrumental in metabolic reprogramming during cell transformation (Duran et al., 2011; Moscat and Diaz-Meco, 2011). Nonetheless, nothing is known about the signaling cascades that p62 regulates in stromal cells or to

Significance

Inappropriate activation of the stroma as a consequence of the tumorigenic process can potentiate the growth and transformation of epithelial tumor cells, thus facilitating the progression of cancers toward more malignant stages. Using prostate cancer as a model system, we show that the loss of the signaling adaptor p62 in stromal cells triggers an inflammatory response that leads to activation of cancer-associated fibroblasts that enhances tumorigenesis in vitro and in vivo. Deficiency in p62 results in reduced mTORC1 activity and deregulation of metabolic pathways controlling inflammation. Because the stroma is increasingly recognized as a potential source of therapeutic targets, this study suggests that targeting stromal metabolic reprogramming can decisively influence the tumorigenic potential of the tumor epithelial compartment.

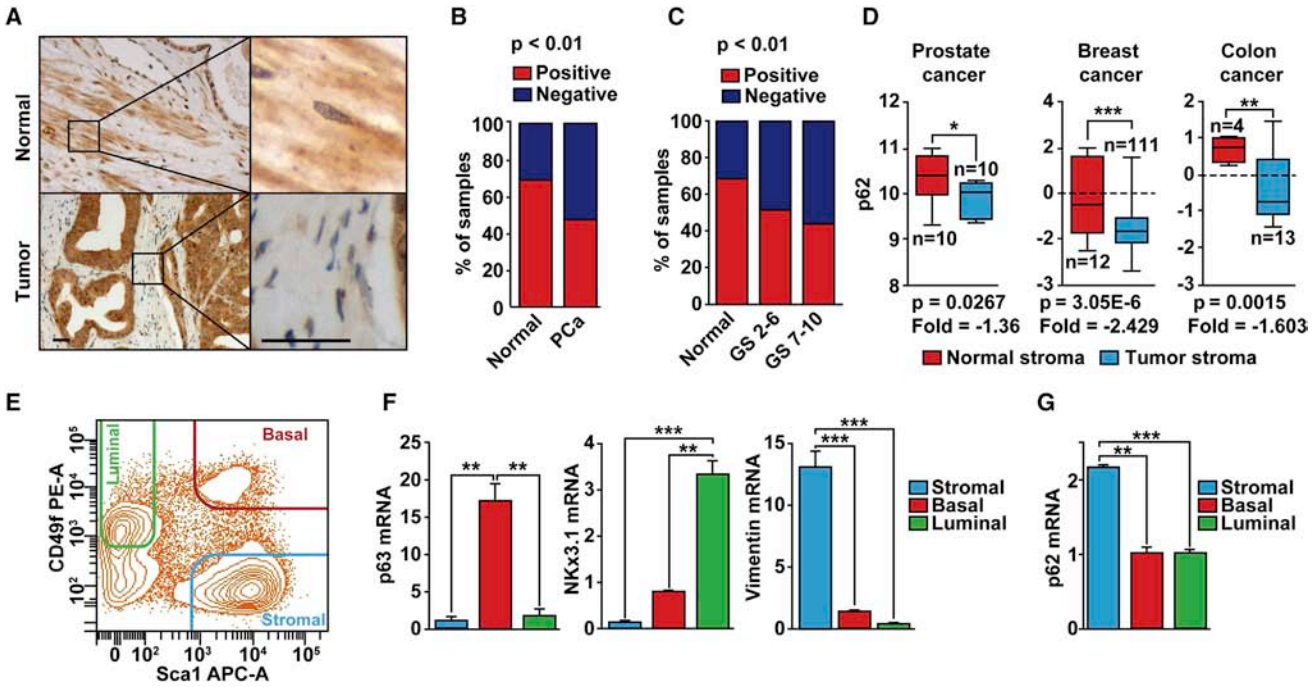

Figure 1. p62 Levels Are Reduced in the Stroma of Human Prostate Tumors

(A) Representative examples of p62 staining of normal and primary prostate cancer (tumor) samples. The scale bars represent 25 μm.

(B) Quantification of p62 staining in the stroma of primary PCa tumors compared with normal; n = 22 (normal), n = 202 (PCa). Fisher's exact test, $p < 0.01$.

(C) p62 levels are reduced upon PCa progression; n = 22 (normal), n = 70 (GS 2–6), n = 132 (GS 7–10). Chi-square test, $p < 0.01$.

(D) p62 mRNA levels in stroma of human cancer samples. Data were collected from public data sets of gene expression in the tumor stroma of several human cancers: GSE34312 (prostate cancer), GSE9014 (breast cancer), and GSE35602 (colon cancer).

(E) FACS-sorted adult murine prostate cell lineages. Prostate basal, luminal, and stromal cells are $Lin^{-}Sca\text{-}1^{+}CD49f^{Hi}$, $Lin^{-}Sca\text{-}1^{-}CD49f^{Low}$, and $Lin^{-}Sca\text{-}1^{+}CD49f^{-}$, respectively.

(F) RT-PCR of specific markers for each prostate cell population (n = 3): p63 (basal), Nkx3.1 (luminal), and vimentin (stromal).

(G) RT-PCR for p62 in prostate cell populations (n = 3).

*$p < 0.05$, **$p < 0.01$, ***$p < 0.001$. Results are presented as mean ± SEM. See also Figure S1.

what extent these pathways influence the epithelial-stromal interaction in the tumor microenvironment. Cancer-associated fibroblasts (CAFs) have been proposed to be key mediators of the crosstalk between malignant tumor cells and their microenvironment (Barron and Rowley, 2012; Franco and Hayward, 2012). CAFs and the complex set of signaling molecules they secrete generate an environment conducive to inflammation, and this in turn maintains the protumorigenic status of the stromal cells. Among these proteins, interleukin-1β (IL-1β), interleukin-8, and interleukin-6 (IL-6) have been implicated as part of the proinflammatory signature of the PCa stroma (Erez et al., 2010; Franco and Hayward, 2012; Schauer et al., 2008). Furthermore, IL-6 has received increasing attention as a key proinflammatory and protumorigenic molecule in many types of cancer, including PCa (Azevedo et al., 2011; De Marzo et al., 2007; Guo et al., 2012; Schafer and Brugge, 2007). Here we address the role of p62 in the stroma in the control of the inflammatory environment in PCa.

RESULTS

p62 Expression Levels in the Tumor Microenvironment

The initial evidence suggesting that p62 plays a role in the regulation of the tumor microenvironment in PCa came from the histological analysis of a tissue panel comprising 202 primary human PCa tumors, 8 metastases, and 22 adjacent normal prostate tissue samples. This study revealed that p62 was expressed in the prostate epithelium and also in the stroma (Figure 1A). p62 protein levels were downregulated in the stroma of human primary PCa tumors compared with the stroma of normal samples (Figures 1A and 1B). Furthermore, when the tumor samples were grouped on the basis of low Gleason score (GS) (2–6) or high GS (7–10), p62 levels in the stroma were significantly reduced upon progression to the most aggressive stage (Figure 1C). p62 was also overexpressed in the epithelial compartment of the PCa human samples (Figure 1A; Figures S1A and S1B available online). This is consistent with previous observations suggesting that p62 is upregulated in many cancers, including lung cancer (Duran et al., 2008; Inoue et al., 2012), liver cancer (Inami et al., 2011), glioblastoma (Galavotti et al., 2013), breast cancer (Rolland et al., 2007; Thompson et al., 2003), and kidney cancer (Li et al., 2013). However, because those studies did not report on expression in the stromal component, it is not clear whether p62 was downregulated in the stroma in those samples, as we have shown in the samples analyzed here. Moreover, bioinformatics analysis of public data sets of stromal gene expression also demonstrated that p62 was significantly downregulated in the tumor stroma, compared

with normal stroma, in several types of cancers, including prostate, breast, and colon cancers (Figure 1D). In addition, fluorescence-activated cell sorting (FACS) analysis of adult mouse prostates showed that p62 is more highly expressed in cells of the stroma than in those of basal or luminal lineages (Figures 1E–1G). Quantitative RT-PCR analyses of the sorted prostate cell populations showed that transcripts for the basal marker p63, the luminal cell marker Nkx3.1, and the stroma marker vimentin were enriched in their corresponding cell populations, demonstrating successful cell fractionation (Figures 1E and 1F). Of note, p62 expression was highly enriched in the stromal compartment compared with the other two cell populations (Figure 1G). These results suggest that p62 could exert its effect as a tumor suppressor in the tumor microenvironment, likely in the stroma.

p62 Is a Suppressor of Inflammation and the CAF Phenotype in the Tumor Microenvironment

To test whether p62 deficiency in the tumor microenvironment is relevant to the transforming properties of epithelial cells, we performed orthotopic injections of syngeneic murine PCa cells (TRAMP-C2Re3) (Olson et al., 2006) into the prostates of wild-type (WT) and p62 knockout (KO) mice and then assessed tumor growth. The resulting tumors were bigger in the prostates of p62 KO mice than in those of WT mice (Figures 2A–2C), supporting the notion that a loss of p62 in the tumor microenvironment promotes PCa growth. We next carried out transcriptomic profiling of the orthotopic tumors in the WT and p62 KO mice. NextBio analysis revealed important correlations between genes upregulated in the p62 KO orthotopic tumors with a gene signature in the category of "response to wounding" (Figure S2A). In addition, gene set enrichment analysis (GSEA) also identified "response to wounding" as significantly enriched of the gene ontology (GO) biological-process categories (Figure 2D; Figures S2B and S2C) and "stromal stimulation" in the C2 curated gene set library (Figures S2D and S2E). Because CAFs acquire an "activated phenotype" during tumor progression that resembles that of fibroblasts during the wound-healing repair process, these results suggested that the p62 KO stroma is likewise activated (Barron and Rowley, 2012; Bissell and Radisky, 2001; Franco and Hayward, 2012; Schäfer and Werner, 2008) and has a more CAF-like phenotype than the WT stroma. In support of this notion, we observed an increase in the expression of α smooth muscle actin (α-SMA) in sections from orthotopic tumors in p62 KO mice compared to WT controls (Figure 2E), as well as an increase in transforming growth factor β (TGF-β) transcripts as determined by RT-PCR in the same samples (Figure 2F). TGF-β and α-SMA are two bona fide markers of the CAF phenotype (Barron and Rowley, 2012; Franco and Hayward, 2012). Consistent with this, Ingenuity Pathway Analysis identified TGF-β1 as a predicted upstream regulator in the p62 KO orthotopic tumors ($p = 1.47 \times 10^{-7}$, activation Z score = 3.890). To determine the potential cell-autonomous effect of p62 in this important function, we used FACS to isolate prostate stromal cells from mice of both genotypes, as described in Figures 1E and 1F. Interestingly, we found that p62-deficient stromal cells also showed characteristics of CAFs, as determined by increased expression levels of α-SMA, TGF-β, and vimentin (Figure 2G). To facilitate subsequent studies, we generated prostate fibroblasts from WT and p62 KO mice and determined their "CAF activation" state. In these cells, the loss of p62 resulted in increased CAF transcript markers (Figure 2H), as well as in the secretion of TGF-β, as determined by ELISA (Figure 2I). This is important because TGF-β is essential for the acquisition and maintenance of the CAF/myofibroblast phenotype (Kojima et al., 2010; Ostman and Augsten, 2009). Therefore, p62 loss modifies the stroma by inducing a CAF phenotype, which in turn drives tumor progression.

Further bioinformatics GSEA revealed a hyperinflammatory phenotype in the p62 KO orthotopic tumors. That is, we found "humoral immune response" and "inflammatory response" as second GO categories enriched in the p62 KO transcriptome profile (Figure 2J; Figures S2F and S2G). RT-PCR analysis of the tumors from p62 KO mice showed increases in the transcripts of inflammatory cytokines such as IL-6, IL-1β, and keratinocyte chemoattractant (Figure 2K), as well as in the secretion of IL-6 as determined by ELISA (Figure 2L). We hypothesized that IL-6 could be an important mediator of the stromal p62-dependent signals that influence PCa progression in the epithelium. To test this possibility, we carried out an orthotopic injection experiment using p62/IL-6 double-KO (DKO) mice as hosts. Notably, the increased tumor growth observed in p62 KO mice was completely reversed in the DKO mice (Figures 2M and 2N), demonstrating that p62 plays a tumor-suppressive role in the tumor microenvironment during PCa progression by inhibiting CAF activation and blocking inflammation.

p62 in Stromal Fibroblasts Regulates an IL-6/TGF-β Cascade Essential for Tumor Invasion

We next set up a 3D organotypic culture model that recapitulates, in a genetically accessible system, the tumor microenvironment and its interactions with the tumor epithelial cell, closely mimicking the physiological situation and the cellular architecture (Gaggioli et al., 2007; Kim et al., 2013; Nyström et al., 2005; Ridky et al., 2010). Because our genome-wide transcriptomic analysis suggested that the loss of p62 in the tumor microenvironment is associated with a CAF-like signature, and because fibroblasts are a critical component of the stroma, we next tested whether p62 KO prostate fibroblasts were able to recapitulate the in vivo phenotype in 3D organotypic cultures. To do this, we cocultured in this organotypic system prostate fibroblasts from p62 KO and WT mice with TRAMP-C2Re3 PCa cells (Figure 3A). Importantly, p62 KO prostate fibroblasts (versus WT counterparts) enhanced the invasiveness and proliferation index of PCa epithelial tumor cells (Figures 3B–3D). Similar results were obtained with other PCa cell lines, such as mouse Myc-CaP (Figure S3A), or human PC3 cells (Figure S3B). Mouse fibroblasts from p62 KO mice also enhanced the invasiveness and proliferation index of human normal prostate epithelial cells compared with similar organotypic cultures with WT fibroblasts (Figure S3C). Altogether, this indicates that p62 deficiency in the stromal fibroblasts has a pivotal role in mediating cancer cell proliferation and invasion.

To follow up on our findings that IL-6 levels were increased in orthotopically injected tissues and that increased IL-6 expression was associated with enhanced tumorigenicity in vivo (Figures 2K–2N), we further investigated the role of this cytokine in the protumorigenic microenvironment created by p62 deficiency

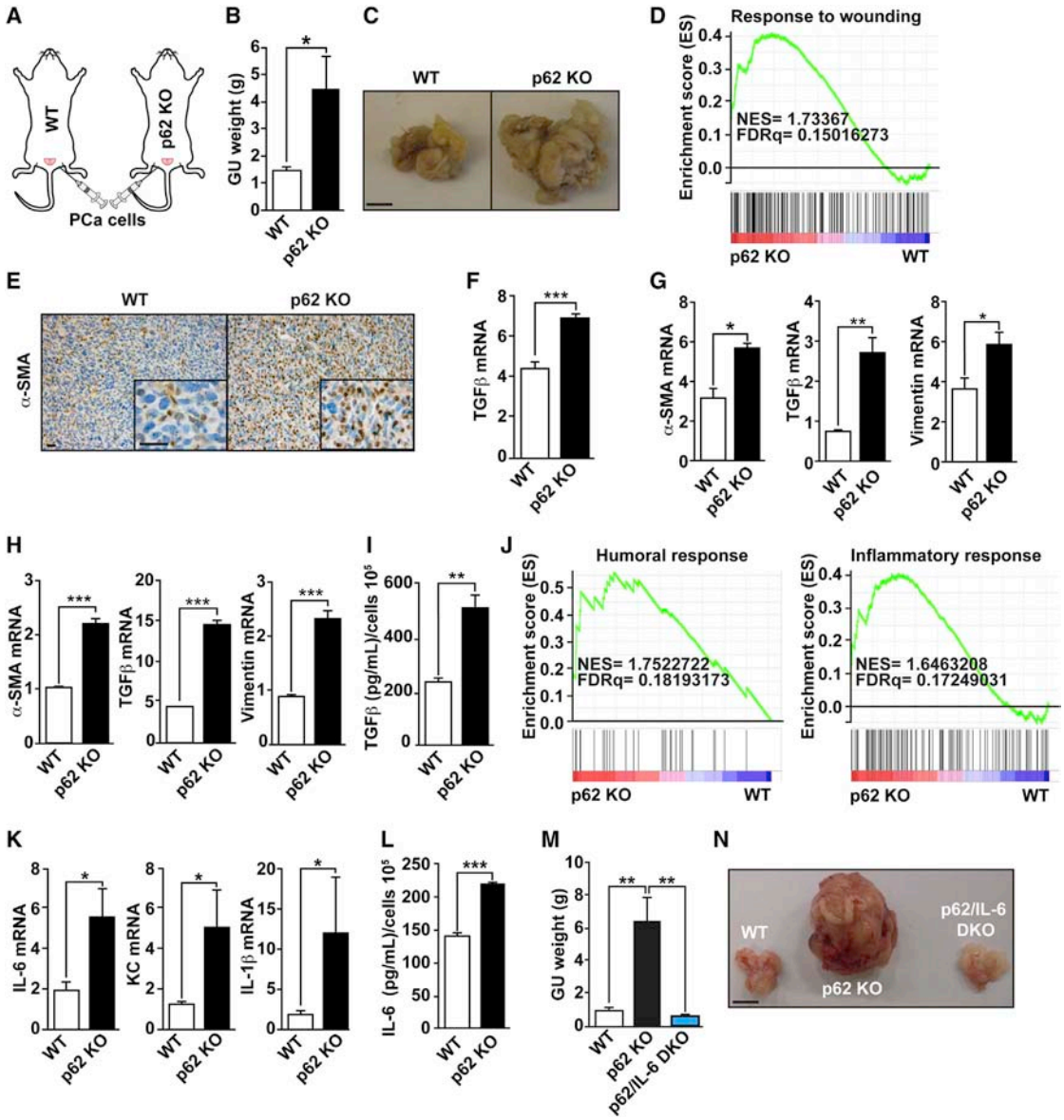

Figure 2. IL-6 Is Required for p62's Role in the Tumor Microenvironment

(A) Orthotopic injection of TRAMP-C2Re3 cells into the prostates of syngeneic WT and p62 KO mice. Orthotopic tumors were allowed to grow for two months.

(B and C) GU tract weight (B) and pictures (C) from (A); n = 5 or 6 mice per genotype. The scale bar represents 1 cm.

(D) "Response to wounding" GSEA plot of enrichment of gene expression in p62 KO orthotopic tumors.

(E) α-SMA staining of orthotopic tumors from WT and p62 KO mice. The scale bars represent 25 μm.

(F) RT-PCR of TGF-β in orthotopic tumors from WT and p62 KO mice (n = 3).

(G and H) RT-PCR of CAF markers (α-SMA, TGF-β, and vimentin) in FACS-sorted prostate stromal fraction from WT and p62 KO mice (G) and in WT and p62 KO prostate fibroblasts (H); n = 3.

(I) TGF-β production in prostate fibroblasts was determined by ELISA.

(J) GSEA plots of enrichment of gene expression in p62 KO orthotopic tumors.

(K) RT-PCR of inflammatory cytokines in orthotopic tumors of WT and p62 KO mice; n = 5 or 6 animals per group versus WT.

(L) IL-6 ELISA in fibroblasts.

(M and N) Orthotopic injection of TRAMP-C2Re3 cells into the prostates of mice of different genotypes (n = 5 or 6 mice). GU weights (M) and pictures (N). The scale bar represents 1 cm.

*p < 0.05, **p < 0.01, ***p < 0.001. Results are presented as mean ± SEM. See also Figure S2.

in the stroma. The two major sources of IL-6 in the tumor microenvironment are macrophages and stromal fibroblasts (Hanahan and Coussens, 2012). Notably, 3D organotypic culture experiments established that fibroblasts (Figures 3B and 3C), but not macrophages (Figure S3D), from p62 KO mice recapitulated the p62 KO phenotype in the orthotopic tissue grafting

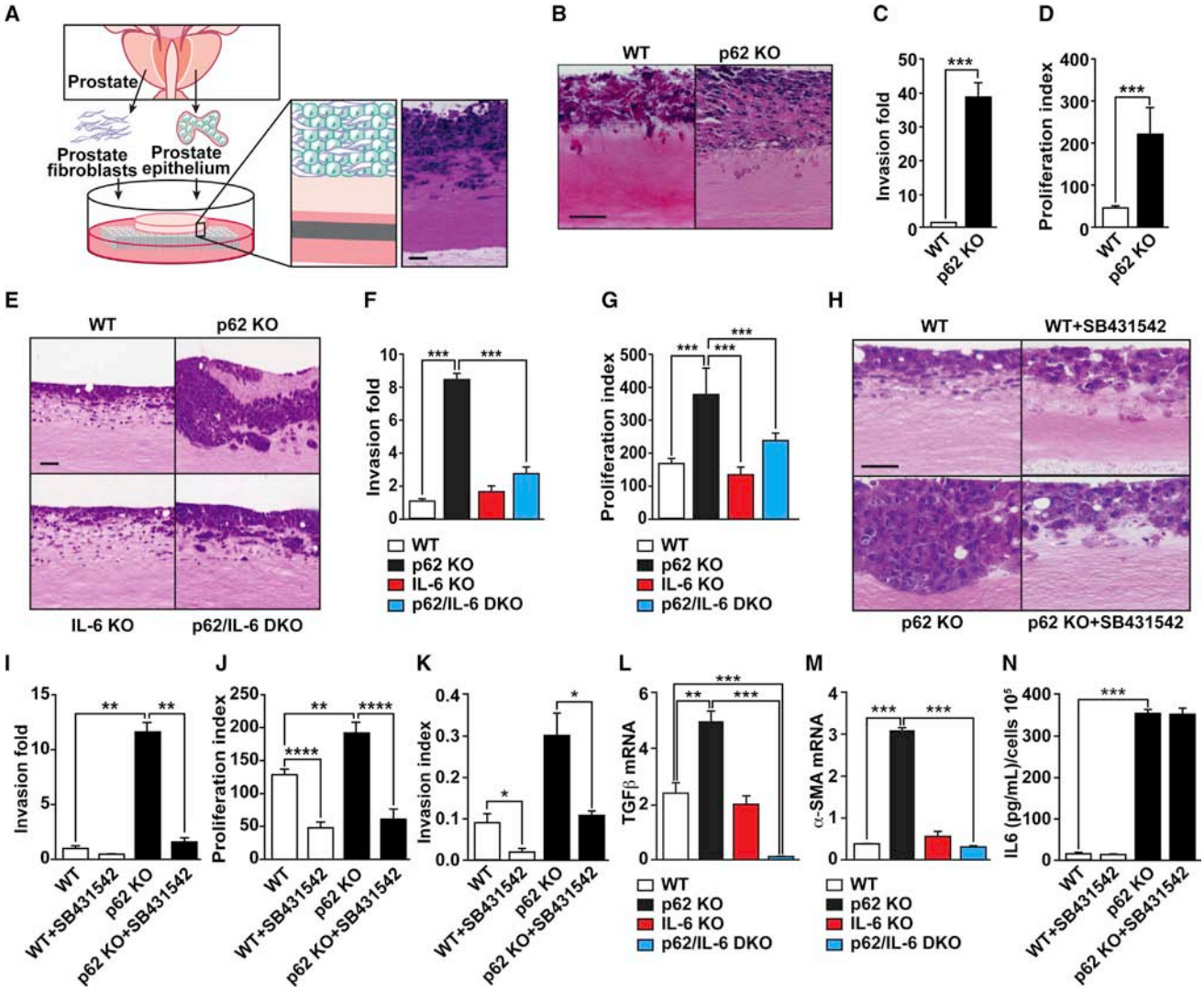

Figure 3. p62-Deficient Stroma-Mediated Invasion Is IL-6 and TGF-β Dependent

(A) Schematic representation of 3D organotypic cultures.

(B) H&E-stained sections of TRAMP-C2Re3 cells cultured in an organotypic system in the presence of primary prostate fibroblasts from WT and p62 KO mice.

(C and D) Quantification of PCa cell invasion (C) and proliferation index (D) of experiment shown in (B); n = 4.

(E) H&E staining of organotypic gels combining Myc-CaP cells with prostate fibroblasts from mice of different genotypes (n = 4).

(F and G) Quantification of PCa cell invasion (F) and proliferation index (G) of experiment shown in (E); n = 4.

(H) H&E staining of organotypic gels combining Myc-CaP cells with prostate fibroblasts from mice WT and p62 KO mice in the presence or absence of the TGF-β inhibitor SB431542 (10 μM).

(I and J) PCa cell invasion quantification (I) and proliferation index (J) of (H); n = 4.

(K) Invasion index determined by modified Boyden chamber assay with conditioned media from WT and p62 KO fibroblasts in the presence or absence of SB431542 (10 μM); n = 3.

(L and M) RT-PCR of TGF-β (L) and α-SMA (M) mRNA levels in fibroblasts of mice of different genotypes (n = 4).

(N) IL-6 production by WT and p62 KO fibroblasts in the presence or absence of the TGF-β inhibitor SB431542 (n = 4).

*p < 0.05, **p < 0.01, ***p < 0.001, ****p < 0.0001. Results are presented as mean ± SEM. The scale bars represent 100 μm. See also Figure S3.

experiment, and this effect was abolished when p62/IL-6 DKO fibroblasts were used in the 3D system (Figures 3E–3G). Furthermore, when TGF-β signaling was inhibited by incubating the organotypic cultures with the TGF-β inhibitor SB431542 (Inman et al., 2002), the protumorigenic phenotype of p62-deficient fibroblasts was reverted, consistent with the notion that TGF-β is important for the CAF phenotype and PCa proliferation (Figures 3H–3J). Likewise, the TGF-β inhibitor reverted the increased invasion index of PCa cells incubated with p62-deficient fibroblast conditioned medium in a Boyden chamber invasion assay (Figure 3K). Results shown in Figure S3E demonstrate the effectiveness of this inhibitor to block the TGF-β pathway. Moreover, the enhanced TGF-β production observed in the p62 KO fibroblasts, as well as that of α-SMA, was completely abrogated in

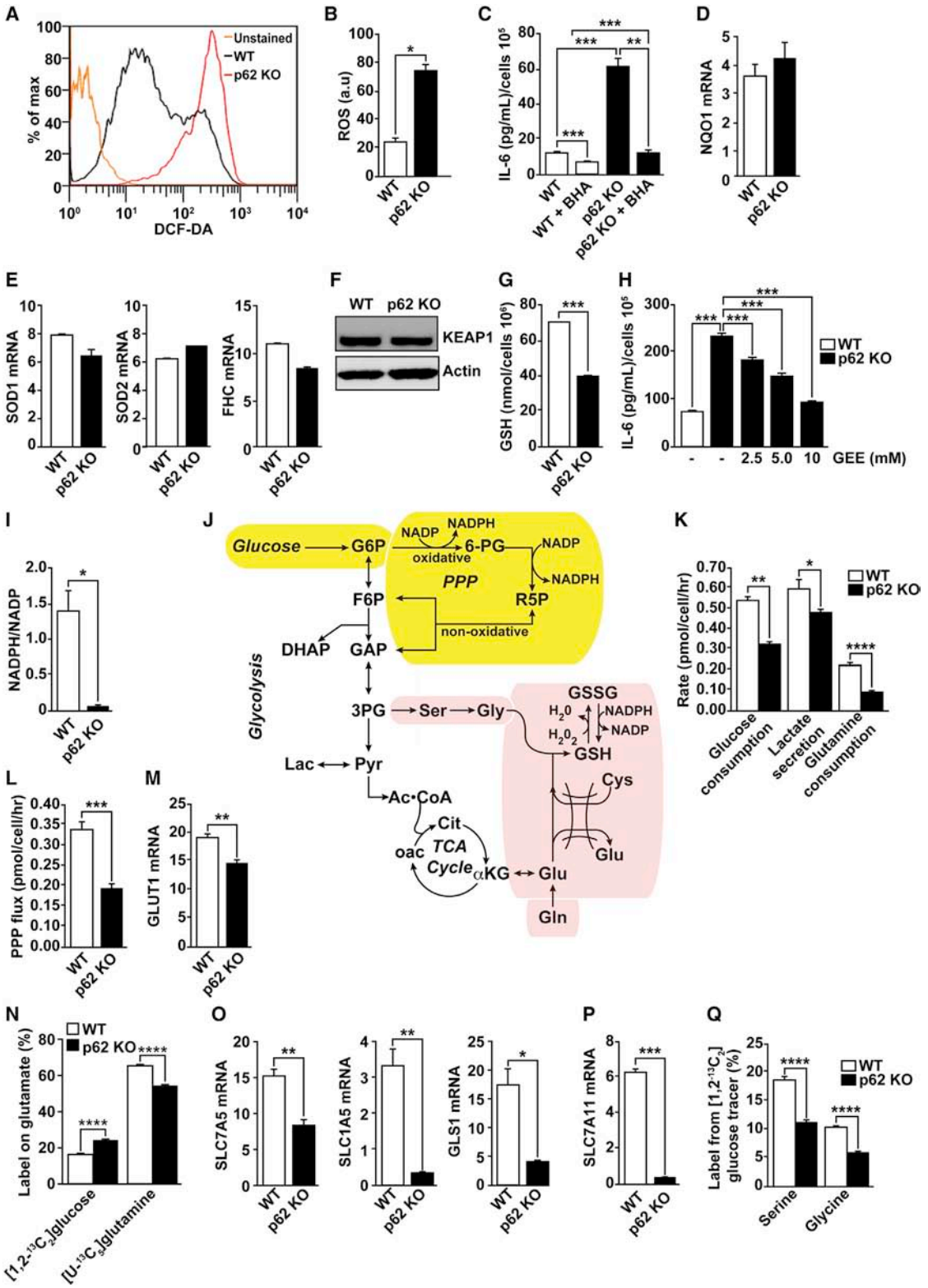

Figure 4. Metabolic Reprogramming in p62-Deficient Stroma

(A and B) Total intracellular levels of ROS in WT and p62 KO fibroblasts (A) and quantification (B); n = 4.

(C) IL-6 ELISA of WT and p62 KO fibroblasts treated with vehicle or the ROS scavenger BHA (100 μM) for 12 hr (n = 4).

(D and E) RT-PCR of NQO1 (D) and SOD1, SOD2, and FHC (E) mRNA levels in fibroblasts (n = 4).

(legend continued on next page)

the DKO fibroblasts (Figures 3L and 3M). Consistently, the knockdown of IL-6 in p62 KO fibroblasts impaired IL-6 secretion and, more important, also reverted TGF-β production and PCa invasion (Figures S3F–S3H). Furthermore, incubation of p62/IL-6 DKO fibroblasts with exogenously added IL-6 restored TGF-β levels to those of p62 KO cells as well as PCa invasion (Figure S3I and S3J). All this is consistent with a cell-autonomous role of the p62-IL-6 axis in the control of the CAF phenotype. However, incubation of p62 KO fibroblasts with the TGF-β signaling inhibitor SB431542 did not affect the overproduction of IL-6 in p62 KO fibroblasts (Figure 3N). These are important observations that establish a sequential p62/IL-6/TGF-β axis in the tumor fibroblastic compartment contributing to the control of epithelial tumorigenesis during PCa progression.

p62 Controls IL-6 Levels by Repressing Reactive Oxygen Species Production through Metabolic Reprogramming

We next sought to determine how p62 controls IL-6 production in fibroblastic stromal cells and whether the mechanisms mediating IL-6 production are relevant to stroma-driven tumorigenesis. It should be noted that p62 KO fibroblasts have increased levels of reactive oxygen species (ROS) (Figures 4A and 4B) and that the inhibition of ROS production (by the ROS scavenger butylated hydroxyanisole [BHA]) completely reverts the IL-6 hyperproduction phenotype (Figure 4C). This indicates that the mechanism whereby p62 represses IL-6 production in fibroblasts involves the control of ROS levels. It has previously been reported that p62 can activate NF-κB and NRF2 (Duran et al., 2008; Komatsu et al., 2010; Moscat and Diaz-Meco, 2009), which suggests that these molecules could play a role in the ability of p62 to repress ROS production and the subsequent activation of IL-6. The expression of critical detoxifying NF-κB- or NRF2-dependent genes (Figures 4D and 4E), as well as the levels of the NRF2 inhibitor Keap1 (Figure 4F), was not affected by the loss of p62 in fibroblasts. However, we found that p62 KO fibroblasts displayed lower levels of reduced glutathione (GSH) than the WT controls (Figure 4G). These are important observations because GSH is central to the control of ROS levels. In fact, treatment of p62 KO fibroblasts with the GSH analog GSH-reduced ethyl ester (GEE) reduced IL-6 to levels comparable with those of WT fibroblasts (Figure 4H). These results demonstrate that the loss of p62 results in lower GSH levels, thus promoting ROS accumulation, which is required for IL-6 overproduction in p62-deficient fibroblasts.

We observed a striking decrease in the reduced nicotinamide adenine dinucleotide phosphate (NADPH)/nicotinamide adenine dinucleotide phosphate (NADP) ratio in p62-deficient fibroblasts (Figure 4I). This ratio provides additional information on the cellular redox status, as the relative concentration of GSH versus oxidized GSH depends on the cellular content of NADPH. Glycolytic metabolism plays a critical role in maintaining NADPH production through the oxidative pentose phosphate pathway (PPP) (Figure 4J, yellow shading). Indeed, p62 KO cells exhibited decreased glucose uptake and lactate secretion (Figure 4K). This reduction in glycolytic rate resulted in decreased flux through the oxidative PPP, as determined by stable isotope tracing with [1,2-$^{13}C_2$]glucose (Figure 4L). These metabolic changes correlated with a reduction in GLUT1 levels in p62-deficient fibroblasts (Figure 4M), providing evidence that transcriptional changes associated with p62 loss influence metabolic flux.

Amino acids are critical for the production of GSH, a peptide composed of glutamate, cysteine, and glycine (Figure 4J, pink shading). Glutamine serves as an important precursor for glutamate, and loss of p62 in fibroblasts leads to lower glutamine consumption compared with WT cells (Figure 4K). We also observed a decrease in the direct conversion of [U-$^{13}C_5$] glutamine to glutamate in p62 KO fibroblasts, with a relative increase in the fraction of glutamate derived from [1,2-$^{13}C_2$]glucose (Figure 4N). In good agreement with these changes in glutamine metabolism, we observed reduced levels of the glutamine transporters SLC7A5 and SLC1A5, as well as glutaminase-1 (GLS1) (Figure 4O), a critical enzyme in the pathway that catalyzes the conversion of glutamine into glutamate (Figure 4J). Consistent with reduced levels of GSH, p62 KO fibroblasts also exhibit a dramatic reduction in the levels of SLC7A11, the xCT cystine/glutamate antiporter, which is the major driver of cystine uptake, a critical and rate-limiting step in the synthesis of GSH in several cell types, including fibroblasts (Figure 4P) (Bannai and Tateishi, 1986; Gout et al., 1997). Finally, we observed significant decreases in labeling of both serine and glycine from [1,2-$^{13}C_2$] glucose (Figure 4Q). Serine serves as a precursor to glycine and cysteine (when synthesized from methionine), so this decrease in label transfer provides evidence that there is less demand for GSH synthesis in p62-deficient cells. These results collectively demonstrate that loss of p62 in fibroblasts influences metabolic pathways controlling cellular redox, including NADPH production in the PPP and GSH synthesis.

p62 Is a Critical Regulator of c-Myc Levels

Previous data from other laboratories have established the critical role of c-Myc in the regulation of glutamine and glucose metabolism (Dang, 2012). We found significantly reduced levels of c-Myc in p62 KO fibroblasts as well as in WT fibroblasts in which p62 has been knocked down by small hairpin RNA (shRNA)

(F) Immunoblot analysis of KEAP1 in cell lysates from WT and p62 KO fibroblasts. Results are representative of three experiments.
(G) Cellular GSH levels in WT and p62 KO fibroblasts (n = 4).
(H) IL-6 ELISA of fibroblasts treated with increasing concentrations of the GSH analog GEE (n = 4).
(I) Cellular NADPH/NADP levels in WT and p62 KO fibroblasts (n = 4).
(J) Metabolic scheme depicting biosynthetic routes to NAPDH (yellow shading) and GSH (pink shading) from glucose and glutamine.
(K) Glucose consumption, lactate secretion, and glutamine consumption rates determined by spent medium analysis from WT and p62 KO fibroblasts (n = 3).
(L) PPP flux estimates from metabolic flux analysis in WT and p62 KO fibroblast cultures labeled with [1,2-$^{13}C_2$]glucose (n = 3).
(M) RT-PCR of GLUT1 mRNA (n = 4).
(N) Glutamate labeling in WT and p62 KO fibroblasts grown in either [1,2-$^{13}C_2$]glucose and unlabeled glutamine or [U-$^{13}C_5$]glutamine and unlabeled glucose (n = 3).
(O and P) RT-PCR of SLC7A5, SLC1A5, and GLS1 (O) and SLC7A11 (P) mRNA levels in WT and p62 KO fibroblasts (n = 3).
(Q) Labeling of serine and glycine from [1,2$^{13}C_2$]glucose (n = 3).
*p < 0.05, **p < 0.01, ***p < 0.001, ****p < 0.0001. Results are presented as mean ± SEM.

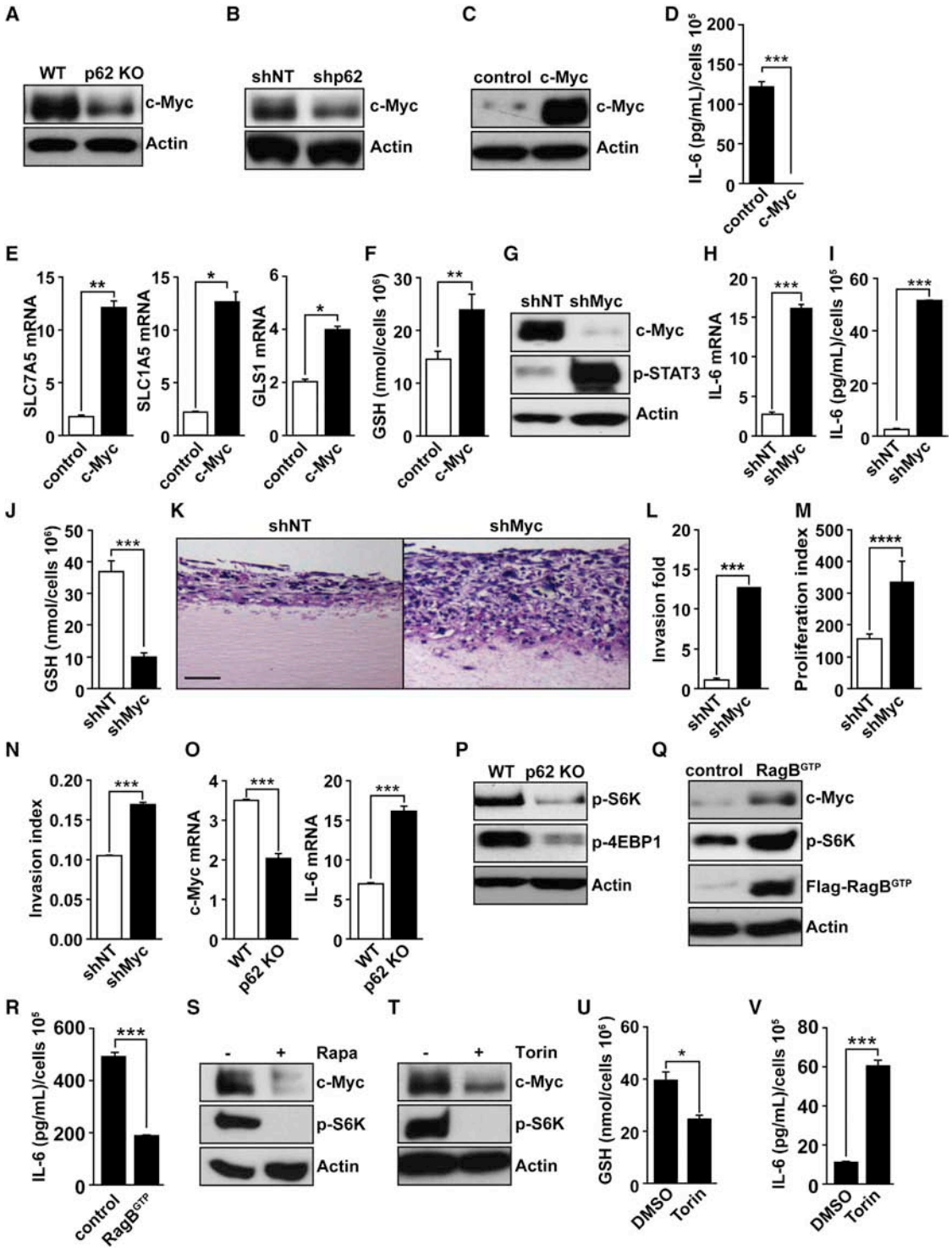

Figure 5. c-Myc-Mediated Metabolism in p62-Deficient Stroma

(A–C) Immunoblot analysis of c-Myc levels in WT and p62 KO fibroblasts (A), in WT fibroblasts lentivirally infected with shRNA nontargeted control (shNT) or shRNA specific for p62 (shp62) (B), and in p62 KO fibroblasts retrovirally infected with control vector (control) or with c-Myc expression vector (c-Myc) (C). Results are representative of three experiments.

(D) IL-6 ELISA in control and c-Myc cells (n = 4) as in (C).

(E) RT-PCR of SLC7A5, SLC1A5, and GLS1 mRNA in control and c-Myc cells (n = 3).

(F) Intracellular GSH levels in control and c-Myc cells (n = 3).

(G) Immunoblot analysis of c-Myc and p-STAT3 in WT fibroblasts infected with shNT or shRNA for c-Myc (shMyc).

(legend continued on next page)

(Figures 5A and 5B) and reductions in the levels of the key glutamine transporters SLC7A5 and SLC1A5, and GLS1 (Figure 4O), which are targets of c-Myc (Dang, 2012). Interestingly, ectopic expression of c-Myc in p62 KO fibroblasts (Figure 5C) reverted the p62-deficient phenotype in terms of IL-6 production (Figure 5D) and the levels of glutamine transporters and GLS1 (Figure 5E) and GSH (Figure 5F). On the contrary, c-Myc knockdown in WT fibroblasts (Figure 5G) resulted in increased IL-6 production at the mRNA and protein levels (Figures 5H and 5I). c-Myc knockdown in fibroblasts led to decreased levels of GSH (Figure 5J), as well as enhanced PCa cell invasion and proliferation in organotypic cell cultures (Figures 5K–5M). Also, the knockdown of c-Myc in fibroblasts resulted in increased PCa cell invasion index in a Boyden chamber assay (Figure 5N). Of note, this cause-and-effect correlation between p62 deficiency, c-Myc expression, and IL-6 production was also found in FACS-isolated prostate stromal cells from WT and p62 KO mice (Figure 5O). Collectively these results demonstrate that p62 repression of c-Myc expression in the stroma fibroblasts accounts for its tumor suppressive role in PCa.

IL-6 Is Regulated by a p62/mTORC1/c-Myc Cascade

Consistent with previously published observation (Duran et al., 2011), we found that p62 KO cells displayed reduced mTORC1 activity (Figure 5P). We hypothesized that the reduction in c-Myc levels found in p62 KO fibroblasts could be the consequence of mTORC1 inhibition. Importantly, we rescued c-Myc inhibition in p62 KO fibroblasts by expressing a permanently active mutant of the small-guanosine triphosphatase RagB, which is a critical activator of mTORC1 (Figure 5Q). IL-6 levels were likewise reduced under these conditions (Figure 5R). These results demonstrate that reduced mTORC1 activity in p62 KO fibroblasts accounts for the low levels of c-Myc and the subsequent increase in IL-6 production in these mutant cells. Treatment of WT fibroblasts with rapamycin or Torin, two different inhibitors of mTORC1, effectively reduced c-Myc levels (Figures 5S and 5T), promoting a significant reduction in GSH levels (Figure 5U) and a concomitant increase in IL-6 production (Figure 5V). Therefore, p62's ability to regulate mTORC1 in the stroma is essential for its control of the c-Myc/GSH/IL-6 axis.

p62 KO Mice Develop Prostate Hyperplasia and Prostatic Intraepithelial Neoplasia upon Aging

On the basis of these results, we hypothesized that the loss of p62 at an organismal level, which would include both the prostate stroma and epithelium, might be sufficient to drive prostate epithelium toward neoplasia. We characterized the prostates of p62 KO mice by histological analysis, which revealed no abnormalities in development or morphology at early stages. However, at 9 months of age, prostates from p62 KO mice developed hyperplasia, with a concomitant increase in Ki67 staining (Figures 6A and 6B). These lesions progressed to prostatic intraepithelial neoplasia (PIN) at 1 year of age (Figure 6C). This indicated that, whereas in xenograft experiments PCa epithelial cells with reduced p62 displayed inhibited tumorigenesis (Duran et al., 2011), the total loss of p62 in vivo promoted prostate epithelial cell growth. These observations are in good agreement with our model whereby p62 in the stromal fibroblasts normally acts as a tumor suppressor, and the total KO of p62 results in p62-deficient stromal fibroblasts that drive the prostate epithelium to a malignancy-prone state. To further test this hypothesis, we crossed total p62 KO mice with two well-established mouse models of PCa ($PTEN^{+/-}$ and $TRAMP^{+}$) (Di Cristofano et al., 1998; Greenberg et al., 1995) and asked whether total ablation of p62 inhibited or promoted prostate tumor development. Figures 6D and 6E show hematoxylin and eosin (H&E) analyses of $PTEN^{+/-}$/p62 KO prostrates demonstrating an increase in the percentage of glands with high-grade PIN at the age of 6 months. Furthermore, $TRAMP^{+}$/p62 KO mice had reduced survival (Figure 6F), increased percentages of poorly differentiated adenocarcinoma (Figure 6G) and neuroendocrine tumors (Figure 6H), as well as a larger number of metastases (Figure 6I), of which a higher percentage were in the liver (Figure 6J). Consistent with our model, prostate fibroblasts from $PTEN^{+/-}$/p62 KO mice showed increased IL-6 and reduced c-Myc expression compared with those from p62-proficent $PTEN^{+/-}$ mice (Figures S4A–S4C). Interestingly, immunohistochemical analysis of prostates from $PTEN^{+/-}$ mice confirmed reduced expression of p62 in the stromal compartment compared with those from WT mice (Figure S4D). To further support the role of p62 deficiency in the stroma in driving tumorigenesis in vivo, we coinjected syngeneic PCa cells (TRAMP-C2Re3) with WT or p62 KO fibroblasts and assessed the effect that fibroblasts exert on tumor growth. Tumors coinjected with p62 KO fibroblasts grew significantly faster and were larger than tumors in mice injected with WT fibroblasts, consistent with the cell-autonomous tumor-promoting activity of p62-deficient fibroblasts on epithelial PCa cells (Figures 6K and 6L). In agreement with this, bromodeoxyuridine (BrdU) incorporation was increased in the p62 KO fibroblast-driven tumors (Figures 6M and 6N).

(H and I) RT-PCR of IL-6 mRNA (H) and IL-6 ELISA (I) in the same cells (n = 3) as in (G).
(J) Quantification of intracellular GSH levels in WT shNT and shMyc cells (n = 3).
(K) H&E-stained organotypic gels of TRAMP-C2Re3 cells with shNT or shMyc fibroblasts. The scale bar represents 100 μm.
(L and M) Quantification of PCa cell invasion (L) and proliferation index (M) of experiment shown in (K).
(N) Invasion index determined by modified Boyden chamber assay of Myc-CaP cells cocultured with shNT and shMyc fibroblasts.
(O) RT-PCR of c-Myc and IL-6 mRNA levels in FACS-isolated prostate stromal cells from WT and p62 KO mice (n = 3).
(P) Immunoblot analysis with the indicated antibodies of cell lysates of WT and p62 KO fibroblasts.
(Q) Immunoblot analysis for the specified proteins of cell lysates from p62 KO fibroblasts retrovirally infected with control vector (control) or FLAG-$RagB^{GTP}$ expression vector ($RagB^{GTP}$). Results are representative of three experiments.
(R) IL-6 ELISA (n = 3) in cells shown in (Q).
(S and T) Immunoblot analysis of c-Myc and p-S6K in fibroblasts treated with rapamycin (S) or Torin1 (T) for 12 hr.
(U) Intracellular GSH levels in fibroblasts treated with Torin1.
(V) IL-6 ELISA in fibroblasts treated with Torin1 (n = 3).
*p < 0.05, **p < 0.01, ***p < 0.001, ****p < 0.0001. Results are presented as mean ± SEM.

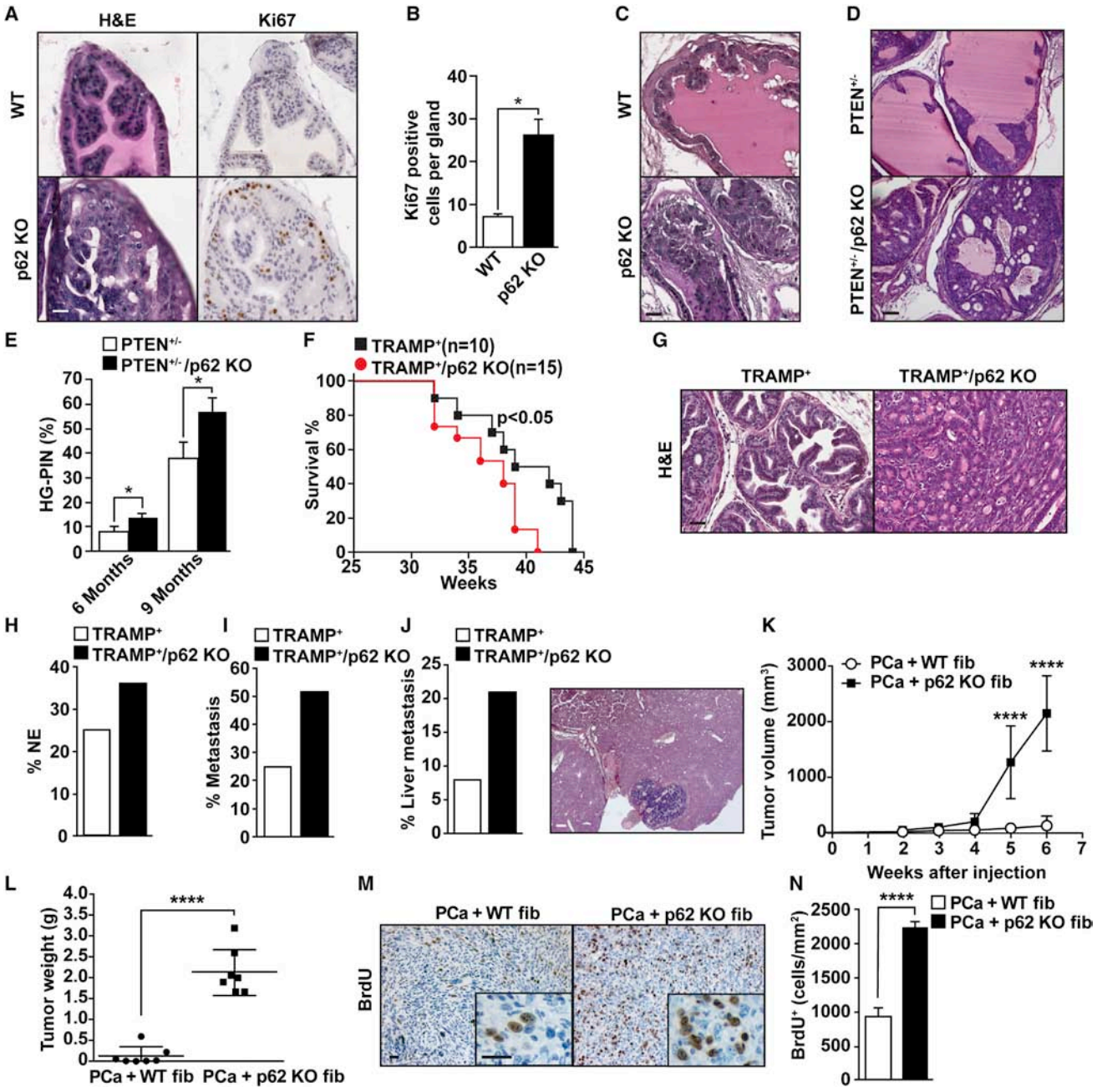

Figure 6. p62 Deficiency Accelerates Prostate Tumor Progression in Different Mouse Models of Prostate Cancer

(A) Hyperplasia in the prostatic anterior lobe of p62 KO mice. H&E and Ki67 staining of prostates from 9-month-old WT and p62 KO mice (n = 5).

(B) Quantification of Ki67-positive cells in the prostate sections shown in (A). Results are the means ± SD of counts from 10 different fields per mouse (n = 5).

(C) PIN in the dorsolateral lobes of prostates from 12-month-old p62 KO mice.

(D) Representative examples of H&E staining of dorsolateral lobes of prostates from $PTEN^{+/-}$ and $PTEN^{+/-}$/p62 KO mice at 6 months of age (n = 5).

(E) Percentage of glands with HG-PIN (n = 5 mice).

(F) Kaplan-Meier survival curve of $TRAMP^{+}$ mice (n = 10), compared with $TRAMP^{+}$/p62 KO mice (n = 15).

(G) Representative H&E staining of mouse prostate sections from $TRAMP^{+}$ and $TRAMP^{+}$/p62 KO mice (n = 10).

(H) Incidence of neuroendocrine tumors in $TRAMP^{+}$ (n = 12) and $TRAMP^{+}$/p62 KO mice (n = 19).

(I and J) Incidence of metastasis (I) and liver metastasis (J) in $TRAMP^{+}$ compared with $TRAMP^{+}$/p62 KO mice.

(K–M) Coinjection of syngeneic TRAMPC2-Re3 PCa cells with either WT or p62 KO fibroblasts in C57BL/6 mice. (K) Tumor volume assessed at different time points after injection (n = 7 mice). (L) Tumor weight at 6 weeks after injection (n = 7 mice). (M) BrdU staining in tumor sections.

(N) Quantification of BrdU positive cells of (M).

Results are presented as mean ± SEM (n = 10). *p < 0.05, ****p < 0.001. The scale bars represent 25 μm. See also Figure S4.

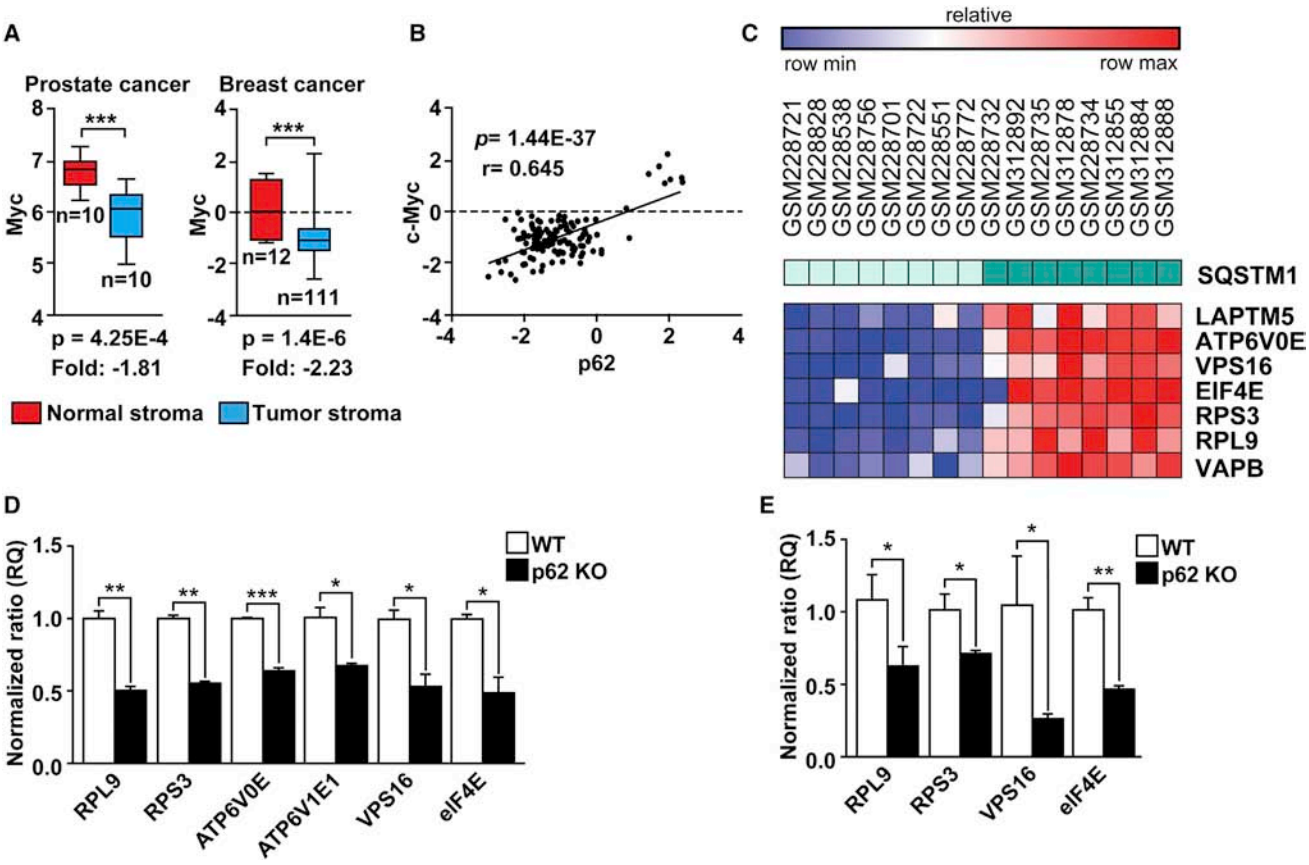

Figure 7. The p62-Myc-mTORC1 Cassette Is Downregulated in Prostate Tumor-Associated Stroma in Human Samples

(A) Myc levels are downregulated in the tumor stroma of human tissue samples. Data were collated from public data sets of gene expression in tumor stroma in several human cancers: GSE34312 (prostate cancer) and GSE9014 (breast cancer). The p value, fold change of expression, and size of the sample (n) for each study are indicated in the corresponding panels.

(B) Positive correlation between p62 and Myc levels in the stroma.

(C) Heatmap of mTORC1 signature selected from p62 neighboring genes in human stroma. p62 levels are indicated as SQSTM1.

(D and E) RT-PCR analysis of mTORC1 genes in WT and p62 KO fibroblasts (D) and in FACS sorted mouse prostate stromal fraction (E).

*p < 0.05, **p < 0.01, ***p < 0.001. Results are presented as mean ± SEM (n = 3). See also Figure S5.

p62/mTORC1/c-Myc Connection in Human Cancer Stroma

To determine whether the identified link between p62 and c-Myc through mTORC1 has relevance to the role of the stroma in human cancer, we used bioinformatics to analyze c-Myc transcript levels in two sets of human gene-expression arrays from prostate and breast cancer stroma. Stroma of human tumors displayed reduced levels of c-Myc (Figure 7A), and there was a statistically significant correlation between c-Myc and p62 expression in tumor stroma (Figure 7B), emphasizing the clinical relevance of the p62-Myc connection in the stroma. To further explore the link between p62 and mTORC1 in the tumor stroma of human cancers, we identified expression neighbors of p62. We developed this gene signature by using the human cancer stroma data set shown in Figure 7A, in which we classified tumors on the basis of p62 expression levels and selected for analysis only those samples in the top and bottom 25%. Interestingly, this analysis revealed a statistically significant correlation between p62 expression and that of genes previously reported to be controlled by mTORC1 activity (Figure 7C; Figure S5) (Peña-Llopis et al., 2011). We determined the expression levels of a selection of these genes by RT-PCR and found that their expression was reduced in p62 KO fibroblasts compared with WT (Figure 7D). The same results were obtained when these were analyzed in prostate stromal cell preparations from p62 KO and WT mice (Figure 7E). Furthermore, we found a clear statistically significant correlation between p62 expression and that of these genes in human cancer stroma (Figures S5B–S5H). Altogether, these results demonstrate that the p62/mTORC1/c-Myc connection is not only relevant in the mouse prostate stroma but it is also important in human cancer stroma.

DISCUSSION

Tumorigenesis is a slow process that is initiated by the successive accumulation of genetic and epigenetic changes that result in the activation of cell growth and survival genes and the inactivation of tumor suppressors (Hanahan and Weinberg, 2011). However, for tumor development to take place, initiation is not sufficient. Other signals are required to drive tumor promotion

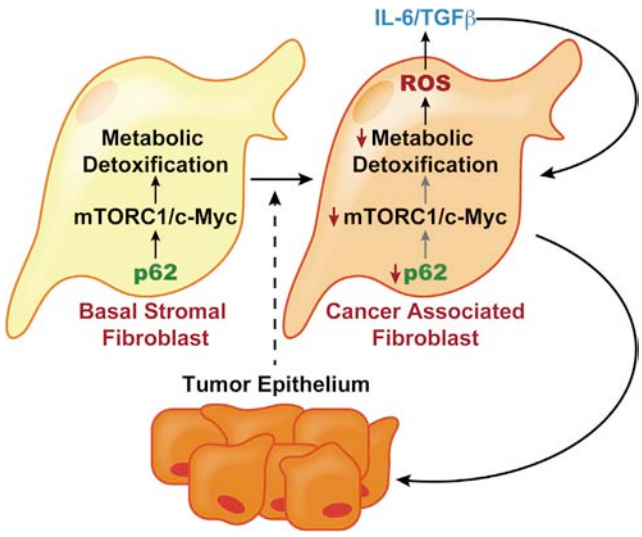

Figure 8. Stromal Activation by p62 Deficiency in Cancer
Tumor epithelium promotes the downregulation of p62 in stromal fibroblasts, leading to reduced mTORC1 activity and c-Myc expression, which results in impaired metabolic detoxification and the subsequent release of ROS and IL-6. An autocrine pathway promotes TGF-β and the induction of CAF phenotype, which further increases epithelial invasion and tumorigenesis.

and progression and the development of the fully malignant stage. The progression phase is most likely orchestrated via the tumor microenvironment by nonepithelial cells in which metabolic stress and inflammation create an environment in which epithelial tumor-derived cells propagate and acquire more aggressive phenotypes (Hanahan and Coussens, 2012; Hanahan and Weinberg, 2011). Immune cells, such as tumor-associated macrophages, are among the cell types in the tumor microenvironment that contribute to inflammation (Coussens and Werb, 2002; Johansson et al., 2008). On the other hand, a crosstalk between metabolic pathways in the stromal and epithelial compartments of the tumor may drive the survival and growth of epithelial cancer cells (Lisanti et al., 2013). However, it has not been thoroughly investigated whether metabolic reprogramming in the stromal cells of the tumor microenvironment exerts any control over inflammation and the malignant characteristics of the transformed epithelium.

Here we demonstrate that the inactivation of mTORC1 in p62-deficient stromal fibroblasts results in metabolic reprogramming through c-Myc inactivation (Figure 8). This reprogramming leads to increased levels of IL-6, which promotes epithelial cell invasion and proliferation. Therefore, because of its regulation of mTORC1, p62 emerges as a tumor suppressor that acts by regulating c-Myc and thus inducing an inflammatory response. These results are in marked contrast to the role played by p62 and mTORC1 in epithelial cancer cells. That is, we have recently demonstrated that p62 inactivation in PCa and lung adenocarcinoma epithelial cells inhibits the proliferation and tumorigenic properties of these cells and correlates with decreased mTORC1 activation. Moreover, the increased IL-6 phenotype can be reverted by expression of a permanently active mutant of the mTORC1 activator RagB. This has important implications from a therapeutic point of view because inhibition of p62 and/or mTORC1 may result in opposite effects in the stroma and the epithelium of the tumor, thus reducing the efficacy of broadly applied mTORC1-based chemotherapeutic approaches. In this regard, these results are reminiscent of the dual role that mTORC1 might play as a regulator of autophagy, which can have a tumor-suppressing or a tumor-promoting effect, depending of the stage of the tumor (Guo et al., 2013; Levine and Kroemer, 2008), and also on whether the manipulation takes place in the epithelium or in the stroma (Lisanti et al., 2013). Our data using KO mice clearly reveal that p62 deficiency creates a protumorigenic environment for p62-proficient PCa cells in orthotopic experiments and also show that, even under normal conditions, it drives PIN formation in the endogenous epithelium in the absence of any other induced mutations. Furthermore, in two PCa models, the lack of p62 at an organismal level results in increased tumorigenesis, despite the fact that p62 is absent not only in the stroma but also in the transformed epithelium. These results are very important because they demonstrate that even though p62 is required for epithelial cancer cells to proliferate in vitro and in xenografts (Duran et al., 2011), the p62-deficient tumor microenvironment overrides the requirement for p62 in the epithelium. Our in vitro and in vivo findings establish that increased IL-6 levels generated by stromal fibroblasts are a critical event in that process. Therefore, it can be predicted that total ablation of p62 at an organismal level, either genetically or pharmacologically, may increase tumorigenesis, rather than inhibiting it, depending on the contribution of the stroma and the ability of p62 deficiency to reprogram stromal metabolism to generate ROS and inflammation. Our data shown here demonstrate that this is the case in prostate tumorigenesis and suggest that it could be a relevant mechanism in other tumor types as well. The proinflammatory microenvironment in the p62-deficient stroma results in a CAF-activated phenotype that is maintained by stromal TGF-β production. This is consistent with previous results in colon cancer demonstrating that a TGF-β-activated tumor microenvironment is critical for fully aggressive cancer cells to metastasize (Calon et al., 2012).

Metabolic reprogramming in cancer is emerging as a central process in tumor cell survival and growth (DeBerardinis and Thompson, 2012; Metallo and Vander Heiden, 2013; Vander Heiden, 2013). The so-called Warburg effect supports the importance of an atypical glucose metabolism tailored to the cancer cell's need for efficient anabolic utilization of nutrients (Vander Heiden et al., 2009). More recently, different types of reprogramming events have been unveiled that constitute specific responses of the tumor cell to a nutrient-deficient environment. These include the metabolism of serine or the utilization of the PPP to alleviate oxidative stress conditions during tumorigenesis (Locasale, 2013; Ma et al., 2013; Possemato et al., 2011; Vander Heiden et al., 2010). In the current study, we show that metabolic reprogramming triggered by p62 deficiency in the tumor stroma is critical for the creation of a protumorigenic inflammatory environment driven by IL-6. Moreover, we have shown that this involves an mTORC1/c-Myc/ROS cascade that is controlled by p62. In this regard, previous results from our and other laboratories have shown that p62 represses ROS by inducing the activation of NF-κB- or NRF2-dependent detoxifying molecules (Duran et al., 2008; Komatsu et al., 2010; Ling et al., 2012). Surprisingly, neither of these two transcription factors nor Keap1

levels were affected in p62-deficient stromal fibroblasts, indicating that p62 may use diverse cascades in different cellular compartments of the tumor. Interestingly, our previous data demonstrate that under conditions of Ras-induced transformation, p62 deficiency leads to increased cell death and reduced tumorigenesis due to enhanced ROS production (Duran et al., 2008). In contrast, we show here that the enhanced ROS observed in the untransformed stromal fibroblasts does not result in increased cell death but rather in the creation of a proinflammatory phenotype. The main conclusion of these results is that increased ROS production induced by p62 deficiency has different outcomes depending on the cell type and the mechanisms whereby ROS is produced. The outcome also depends on whether or not the levels of ROS are high enough to engage a c-Jun N-terminal kinase-driven cell-death pathway, as found in the Ras-tumor cell, as opposed to increased IL-6 production and a protumorigenic effect on epithelial cells, as we demonstrated in the stromal nontransformed fibroblasts.

Importantly, we were able to show that the implication of the p62/mTORC1/c-Myc cascade is relevant not only in mouse model systems but also in human samples, in which this pathway is inactivated in the tumor stroma. Therefore, our findings support a more comprehensive approach when devising therapeutic strategies in cancer, which should take into account not only the altered pathways in the transformed epithelial compartment but also how the inhibition of these cascades might affect the surrounding stroma. Our observations suggest that pharmacological inhibition of IL-6 and/or TGF-β to target stromal activation could be beneficial in combination with epithelial-targeted therapies.

EXPERIMENTAL PROCEDURES

Mice

WT, p62 KO, PTEN$^{+/-}$, and TRAMP^{+} mice were previously described (Durán et al., 2004; Di Cristofano et al., 1998; Greenberg et al., 1995). All mouse strains were generated in a C57BL/6 background. All mice were born and maintained under pathogen-free conditions. All genotyping was done by PCR. Mice were sacrificed and genitourinary (GU) sections were dissected. Mice were injected with 5-bromo-2′-deoxyuridine intraperitoneally and sacrificed 2 hr after injection. Animal handling and experimental procedures conformed to institutional guidelines (Sanford-Burnham Medical Research Institute Institutional Animal Care and Use Committee).

Cell Lysis and Western Immunoblotting

Cells were rinsed once with ice-cold PBS and lysed in radioimmunoprecipitation assay buffer (1 × PBS, 1% Nonidet P-40, 0.5% sodium deoxycholate, 0.1% SDS, 1 mM phenyl methyl sulfonyl fluoride, and protease inhibitors). Cell extracts were denatured, subjected to 8% to 14% SDS-PAGE, transferred to nitrocellulose-enhanced chemiluminescence membranes (GE Healthcare), and immunoblotted with the specific antibodies. Chemiluminescence was used to detect the proteins (Thermo Scientific).

Statistical Analysis

Significant differences between groups were determined using Student's t test. Scoring of immunostaining of human prostate tissue microarrays was analyzed using Fisher's exact test. The significance level for statistical testing was set at $p < 0.05$.

ACCESSION NUMBERS

The Gene Expression Omnibus accession number for the microarray data reported in this paper is GSE55587.

SUPPLEMENTAL INFORMATION

Supplemental Information includes Supplemental Experimental Procedures and five figures and can be found with this article online at http://dx.doi.org/10.1016/j.ccr.2014.05.004.

AUTHOR CONTRIBUTIONS

T.V., J.Y.K., S.A.-B. and A.D. performed experiments. J.M.-P. and M.R.-C. performed bioinformatics analysis. E.A.C. provided pathologist expertise for histological analysis. C.S.A. and T.V. performed the metabolic experiments. C.M.M., M.D.M., and J.M. designed and analyzed metabolic data. M.D.M. and J.M conceived and supervised the project with equal contribution. M.D.M. and J.M. wrote the manuscript with assistance from all the authors.

ACKNOWLEDGMENTS

This work was funded by grants R01CA132847 (J.M.), R01CA172025 (J.M.), R01CA134530 (M.T.D.-M.), and 5P30CA030199 (M.T.D-M. and J.M.) from the NIH. Additional support was provided by grants W81XWH-13-1-0353 (M.T.D-M.), W81XWH-13-1-0354 (J.M.), and W81XWH-13-1-0105 (C.M.M.) from the U.S. Department of Defense. We thank Maryellen Daston for editing this manuscript; Diantha LaVine for the artwork; and Tomoko Yajima, Tom Hudson, Jessica Leung, and the personnel of the Cancer Metabolism, Flow Cytometry, Cell Imaging, Animal Facility, Histology, Functional Genomics and Viral Vectors Shared Resources at the Sanford-Burnham Medical Research Institute for technical assistance. We thank Neil Bhowmick for assistance in the preparation of prostate fibroblasts.

Received: December 24, 2013
Revised: March 17, 2014
Accepted: May 7, 2014
Published: July 3, 2014

REFERENCES

Ammirante, M., Luo, J.L., Grivennikov, S., Nedospasov, S., and Karin, M. (2010). B-cell-derived lymphotoxin promotes castration-resistant prostate cancer. Nature *464*, 302–305.

Azevedo, A., Cunha, V., Teixeira, A.L., and Medeiros, R. (2011). IL-6/IL-6R as a potential key signaling pathway in prostate cancer development. World J. Clin. Oncol. *2*, 384–396.

Bannai, S., and Tateishi, N. (1986). Role of membrane transport in metabolism and function of glutathione in mammals. J. Membr. Biol. *89*, 1–8.

Barron, D.A., and Rowley, D.R. (2012). The reactive stroma microenvironment and prostate cancer progression. Endocr. Relat. Cancer *19*, R187–R204.

Bissell, M.J., and Radisky, D. (2001). Putting tumours in context. Nat. Rev. Cancer *1*, 46–54.

Calon, A., Espinet, E., Palomo-Ponce, S., Tauriello, D.V., Iglesias, M., Céspedes, M.V., Sevillano, M., Nadal, C., Jung, P., Zhang, X.H., et al. (2012). Dependency of colorectal cancer on a TGF-β-driven program in stromal cells for metastasis initiation. Cancer Cell *22*, 571–584.

Coussens, L.M., and Werb, Z. (2002). Inflammation and cancer. Nature *420*, 860–867.

Dang, C.V. (2012). MYC on the path to cancer. Cell *149*, 22–35.

De Marzo, A.M., Platz, E.A., Sutcliffe, S., Xu, J., Grönberg, H., Drake, C.G., Nakai, Y., Isaacs, W.B., and Nelson, W.G. (2007). Inflammation in prostate carcinogenesis. Nat. Rev. Cancer *7*, 256–269.

DeBerardinis, R.J., and Thompson, C.B. (2012). Cellular metabolism and disease: what do metabolic outliers teach us? Cell *148*, 1132–1144.

Di Cristofano, A., Pesce, B., Cordon-Cardo, C., and Pandolfi, P.P. (1998). Pten is essential for embryonic development and tumour suppression. Nat. Genet. *19*, 348–355.

Diaz-Meco, M.T., and Moscat, J. (2012). The atypical PKCs in inflammation: NF-κB and beyond. Immunol. Rev. *246*, 154–167.

Durán, A., Serrano, M., Leitges, M., Flores, J.M., Picard, S., Brown, J.P., Moscat, J., and Diaz-Meco, M.T. (2004). The atypical PKC-interacting protein p62 is an important mediator of RANK-activated osteoclastogenesis. Dev. Cell *6*, 303–309.

Duran, A., Linares, J.F., Galvez, A.S., Wikenheiser, K., Flores, J.M., Diaz-Meco, M.T., and Moscat, J. (2008). The signaling adaptor p62 is an important NF-kappaB mediator in tumorigenesis. Cancer Cell *13*, 343–354.

Duran, A., Amanchy, R., Linares, J.F., Joshi, J., Abu-Baker, S., Porollo, A., Hansen, M., Moscat, J., and Diaz-Meco, M.T. (2011). p62 is a key regulator of nutrient sensing in the mTORC1 pathway. Mol. Cell *44*, 134–146.

Erez, N., Truitt, M., Olson, P., Arron, S.T., and Hanahan, D. (2010). Cancer-associated fibroblasts are activated in incipient neoplasia to orchestrate tumor-promoting inflammation in an NF-kappaB-dependent manner. Cancer Cell *17*, 135–147.

Franco, O.E., and Hayward, S.W. (2012). Targeting the tumor stroma as a novel therapeutic approach for prostate cancer. Adv. Pharmacol. *65*, 267–313.

Gaggioli, C., Hooper, S., Hidalgo-Carcedo, C., Grosse, R., Marshall, J.F., Harrington, K., and Sahai, E. (2007). Fibroblast-led collective invasion of carcinoma cells with differing roles for RhoGTPases in leading and following cells. Nat. Cell Biol. *9*, 1392–1400.

Galavotti, S., Bartesaghi, S., Faccenda, D., Shaked-Rabi, M., Sanzone, S., McEvoy, A., Dinsdale, D., Condorelli, F., Brandner, S., Campanella, M., et al. (2013). The autophagy-associated factors DRAM1 and p62 regulate cell migration and invasion in glioblastoma stem cells. Oncogene *32*, 699–712.

Gout, P.W., Kang, Y.J., Buckley, D.J., Bruchovsky, N., and Buckley, A.R. (1997). Increased cystine uptake capability associated with malignant progression of Nb2 lymphoma cells. Leukemia *11*, 1329–1337.

Greenberg, N.M., DeMayo, F., Finegold, M.J., Medina, D., Tilley, W.D., Aspinall, J.O., Cunha, G.R., Donjacour, A.A., Matusik, R.J., and Rosen, J.M. (1995). Prostate cancer in a transgenic mouse. Proc. Natl. Acad. Sci. USA *92*, 3439–3443.

Grivennikov, S.I., Greten, F.R., and Karin, M. (2010). Immunity, inflammation, and cancer. Cell *140*, 883–899.

Guo, Y., Xu, F., Lu, T., Duan, Z., and Zhang, Z. (2012). Interleukin-6 signaling pathway in targeted therapy for cancer. Cancer Treat. Rev. *38*, 904–910.

Guo, J.Y., Xia, B., and White, E. (2013). Autophagy-mediated tumor promotion. Cell *155*, 1216–1219.

Hanahan, D., and Weinberg, R.A. (2011). Hallmarks of cancer: the next generation. Cell *144*, 646–674.

Hanahan, D., and Coussens, L.M. (2012). Accessories to the crime: functions of cells recruited to the tumor microenvironment. Cancer Cell *21*, 309–322.

Inami, Y., Waguri, S., Sakamoto, A., Kouno, T., Nakada, K., Hino, O., Watanabe, S., Ando, J., Iwadate, M., Yamamoto, M., et al. (2011). Persistent activation of Nrf2 through p62 in hepatocellular carcinoma cells. J. Cell Biol. *193*, 275–284.

Inman, G.J., Nicolás, F.J., Callahan, J.F., Harling, J.D., Gaster, L.M., Reith, A.D., Laping, N.J., and Hill, C.S. (2002). SB-431542 is a potent and specific inhibitor of transforming growth factor-beta superfamily type I activin receptor-like kinase (ALK) receptors ALK4, ALK5, and ALK7. Mol. Pharmacol. *62*, 65–74.

Inoue, D., Suzuki, T., Mitsuishi, Y., Miki, Y., Suzuki, S., Sugawara, S., Watanabe, M., Sakurada, A., Endo, C., Uruno, A., et al. (2012). Accumulation of p62/SQSTM1 is associated with poor prognosis in patients with lung adenocarcinoma. Cancer Sci. *103*, 760–766.

Johansson, M., Denardo, D.G., and Coussens, L.M. (2008). Polarized immune responses differentially regulate cancer development. Immunol. Rev. *222*, 145–154.

Kim, J.Y., Valencia, T., Abu-Baker, S., Linares, J., Lee, S.J., Yajima, T., Chen, J., Eroshkin, A., Castilla, E.A., Brill, L.M., et al. (2013). c-Myc phosphorylation by PKCζ represses prostate tumorigenesis. Proc. Natl. Acad. Sci. U S A *110*, 6418–6423.

Kojima, Y., Acar, A., Eaton, E.N., Mellody, K.T., Scheel, C., Ben-Porath, I., Onder, T.T., Wang, Z.C., Richardson, A.L., Weinberg, R.A., and Orimo, A. (2010). Autocrine TGF-beta and stromal cell-derived factor-1 (SDF-1) signaling drives the evolution of tumor-promoting mammary stromal myofibroblasts. Proc. Natl. Acad. Sci. U S A *107*, 20009–20014.

Komatsu, M., Kurokawa, H., Waguri, S., Taguchi, K., Kobayashi, A., Ichimura, Y., Sou, Y.S., Ueno, I., Sakamoto, A., Tong, K.I., et al. (2010). The selective autophagy substrate p62 activates the stress responsive transcription factor Nrf2 through inactivation of Keap1. Nat. Cell Biol. *12*, 213–223.

Levine, B., and Kroemer, G. (2008). Autophagy in the pathogenesis of disease. Cell *132*, 27–42.

Li, L., Shen, C., Nakamura, E., Ando, K., Signoretti, S., Beroukhim, R., Cowley, G.S., Lizotte, P., Liberzon, E., Bair, S., et al. (2013). SQSTM1 is a pathogenic target of 5q copy number gains in kidney cancer. Cancer Cell *24*, 738–750.

Ling, J., Kang, Y., Zhao, R., Xia, Q., Lee, D.F., Chang, Z., Li, J., Peng, B., Fleming, J.B., Wang, H., et al. (2012). KrasG12D-induced IKK2/β/NF-κB activation by IL-1α and p62 feedforward loops is required for development of pancreatic ductal adenocarcinoma. Cancer Cell *21*, 105–120.

Lisanti, M.P., Martinez-Outschoorn, U.E., and Sotgia, F. (2013). Oncogenes induce the cancer-associated fibroblast phenotype: metabolic symbiosis and "fibroblast addiction" are new therapeutic targets for drug discovery. Cell Cycle *12*, 2723–2732.

Locasale, J.W. (2013). Serine, glycine and one-carbon units: cancer metabolism in full circle. Nat. Rev. Cancer *13*, 572–583.

Ma, L., Tao, Y., Duran, A., Llado, V., Galvez, A., Barger, J.F., Castilla, E.A., Chen, J., Yajima, T., Porollo, A., et al. (2013). Control of nutrient stress-induced metabolic reprogramming by PKCζ in tumorigenesis. Cell *152*, 599–611.

Metallo, C.M., and Vander Heiden, M.G. (2013). Understanding metabolic regulation and its influence on cell physiology. Mol. Cell *49*, 388–398.

Moscat, J., and Diaz-Meco, M.T. (2009). p62 at the crossroads of autophagy, apoptosis, and cancer. Cell *137*, 1001–1004.

Moscat, J., and Diaz-Meco, M.T. (2011). Feedback on fat: p62-mTORC1-autophagy connections. Cell *147*, 724–727.

Moscat, J., and Diaz-Meco, M.T. (2012). p62: a versatile multitasker takes on cancer. Trends Biochem. Sci. *37*, 230–236.

Moscat, J., Diaz-Meco, M.T., and Wooten, M.W. (2007). Signal integration and diversification through the p62 scaffold protein. Trends Biochem. Sci. *32*, 95–100.

Nyström, M.L., Thomas, G.J., Stone, M., Mackenzie, I.C., Hart, I.R., and Marshall, J.F. (2005). Development of a quantitative method to analyse tumour cell invasion in organotypic culture. J. Pathol. *205*, 468–475.

Olson, M.V., Lee, J., Zhang, F., Wang, A., and Dong, Z. (2006). Inducible nitric oxide synthase activity is essential for inhibition of prostatic tumor growth by interferon-beta gene therapy. Cancer Gene Ther. *13*, 676–685.

Ostman, A., and Augsten, M. (2009). Cancer-associated fibroblasts and tumor growth—bystanders turning into key players. Curr. Opin. Genet. Dev. *19*, 67–73.

Peña-Llopis, S., Vega-Rubin-de-Celis, S., Schwartz, J.C., Wolff, N.C., Tran, T.A., Zou, L., Xie, X.J., Corey, D.R., and Brugarolas, J. (2011). Regulation of TFEB and V-ATPases by mTORC1. EMBO J. *30*, 3242–3258.

Possemato, R., Marks, K.M., Shaul, Y.D., Pacold, M.E., Kim, D., Birsoy, K., Sethumadhavan, S., Woo, H.K., Jang, H.G., Jha, A.K., et al. (2011). Functional genomics reveal that the serine synthesis pathway is essential in breast cancer. Nature *476*, 346–350.

Ridky, T.W., Chow, J.M., Wong, D.J., and Khavari, P.A. (2010). Invasive three-dimensional organotypic neoplasia from multiple normal human epithelia. Nat. Med. *16*, 1450–1455.

Rolland, P., Madjd, Z., Durrant, L., Ellis, I.O., Layfield, R., and Spendlove, I. (2007). The ubiquitin-binding protein p62 is expressed in breast cancers showing features of aggressive disease. Endocr. Relat. Cancer *14*, 73–80.

Sanchez, P., De Carcer, G., Sandoval, I.V., Moscat, J., and Diaz-Meco, M.T. (1998). Localization of atypical protein kinase C isoforms into lysosome-targeted endosomes through interaction with p62. Mol. Cell. Biol. *18*, 3069–3080.

Santos, A.M., Jung, J., Aziz, N., Kissil, J.L., and Puré, E. (2009). Targeting fibroblast activation protein inhibits tumor stromagenesis and growth in mice. J. Clin. Invest. *119*, 3613–3625.

Schafer, Z.T., and Brugge, J.S. (2007). IL-6 involvement in epithelial cancers. J. Clin. Invest. *117*, 3660–3663.

Schäfer, M., and Werner, S. (2008). Cancer as an overhealing wound: an old hypothesis revisited. Nat. Rev. Mol. Cell Biol. *9*, 628–638.

Schauer, I.G., Ressler, S.J., Tuxhorn, J.A., Dang, T.D., and Rowley, D.R. (2008). Elevated epithelial expression of interleukin-8 correlates with myofibroblast reactive stroma in benign prostatic hyperplasia. Urology *72*, 205–213.

Shen, M.M., and Abate-Shen, C. (2010). Molecular genetics of prostate cancer: new prospects for old challenges. Genes Dev. *24*, 1967–2000.

Thompson, H.G., Harris, J.W., Wold, B.J., Lin, F., and Brody, J.P. (2003). p62 overexpression in breast tumors and regulation by prostate-derived Ets factor in breast cancer cells. Oncogene *22*, 2322–2333.

Trimboli, A.J., Cantemir-Stone, C.Z., Li, F., Wallace, J.A., Merchant, A., Creasap, N., Thompson, J.C., Caserta, E., Wang, H., Chong, J.L., et al. (2009). Pten in stromal fibroblasts suppresses mammary epithelial tumours. Nature *461*, 1084–1091.

Vander Heiden, M.G. (2013). Exploiting tumor metabolism: challenges for clinical translation. J. Clin. Invest. *123*, 3648–3651.

Vander Heiden, M.G., Cantley, L.C., and Thompson, C.B. (2009). Understanding the Warburg effect: the metabolic requirements of cell proliferation. Science *324*, 1029–1033.

Vander Heiden, M.G., Locasale, J.W., Swanson, K.D., Sharfi, H., Heffron, G.J., Amador-Noguez, D., Christofk, H.R., Wagner, G., Rabinowitz, J.D., Asara, J.M., and Cantley, L.C. (2010). Evidence for an alternative glycolytic pathway in rapidly proliferating cells. Science *329*, 1492–1499.

Cancer Cell, Volume *26*

Supplemental Information

Metabolic Reprogramming of Stromal Fibroblasts through p62-mTORC1 Signaling Promotes Inflammation and Tumorigenesis

Tania Valencia, Ji Young Kim, Shadi Abu-Baker, Jorge Moscat-Pardos, Christopher S. Ahn, Miguel Reina-Campos, Angeles Duran, Elias A. Castilla, Christian M. Metallo, Maria T. Diaz-Meco, and Jorge Moscat

Supplemental Data

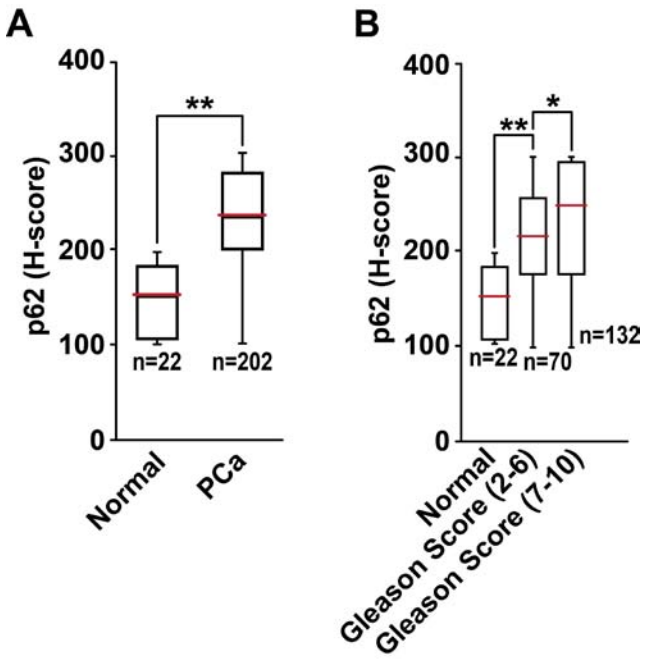

Figure S1, related to Figure 1. p62 is overexpressed in the epithelium of human prostate tumors.

(A) p62 levels are increased in the epithelium of primary PCa tumors as compared to normal samples, and (B) are upregulated upon PCa progression. Analysis of TMA of Figure 1A. The H-score, the staining intensity of p62 in epithelium x the proportion of cells with the observed intensity, was used to grade p62 expression levels in each sample. Students t test (*$p < 0.05$,**$p < 0.01$).

A

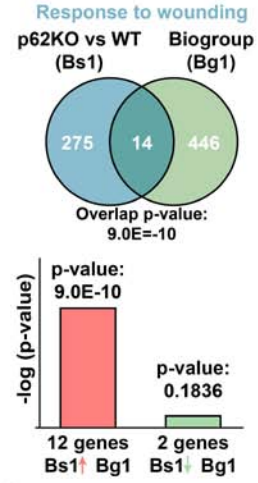

B

Gene sets enriched in phenotype p62 KO- Analysis with C5 database of MSigDB v. 3.1

RANK	MSigDB	Size	ES	NES	NOM p-val	FDR q-val	FWER p-val
1	GENERATION_OF_A_SIGNAL_INVOLVED_IN_CELL_CELL_SIGNALING	26	0.61	1.85	0.001	0.222	0.247
2	G_PROTEIN_SIGNALING_COUPLED_TO_CYCLIC_NUCLEOTIDE_SECOND_MESSENGER	95	0.46	1.82	0	0.166	0.344
3	CYCLIC_NUCLEOTIDE_MEDIATED_SIGNALING	97	0.46	1.78	0	0.181	0.499
4	HUMORAL_IMMUNE_RESPONSE	29	0.56	1.75	0.006	0.182	0.599
5	HORMONE_SECRETION	16	0.64	1.74	0.006	0.172	0.664
6	RESPONSE_TO_WOUNDING	171	0.41	1.73	0	0.15	0.685
7	DETECTION_OF_ABIOTIC_STIMULUS	19	0.61	1.73	0.007	0.137	0.708
8	CELL_CELL_SIGNALING	364	0.38	1.72	0	0.132	0.746
9	RESPONSE_TO_EXTERNAL_STIMULUS	274	0.38	1.71	0	0.125	0.771
10	NEGATIVE_REGULATION_OF_MULTICELLULAR_ORGANISMAL_PROCESS	27	0.55	1.69	0.008	0.14	0.838
11	SECOND_MESSENGER_MEDIATED_SIGNALING	141	0.41	1.69	0	0.137	0.861
12	NEUROLOGICAL_SYSTEM_PROCESS	343	0.37	1.68	0	0.135	0.876
13	INFLAMMATORY_RESPONSE	113	0.41	1.65	0.001	0.172	0.944
14	DETECTION_OF_STIMULUS	41	0.49	1.65	0.006	0.16	0.945
15	ECTODERM_DEVELOPMENT	69	0.44	1.65	0.004	0.15	0.945
16	POTASSIUM_ION_TRANSPORT	56	0.46	1.64	0.004	0.147	0.953
17	REGULATION_OF_MULTICELLULAR_ORGANISMAL_PROCESS	129	0.4	1.64	0.001	0.146	0.959
18	DEFENSE_RESPONSE	209	0.38	1.64	0.001	0.139	0.96
19	G_PROTEIN_SIGNALING_COUPLED_TO_CAMP_NUCLEOTIDE_SECOND_MESSENGER	60	0.45	1.63	0.009	0.136	0.964
20	SYNAPTIC_TRANSMISSION	162	0.38	1.62	0.001	0.141	0.975

C

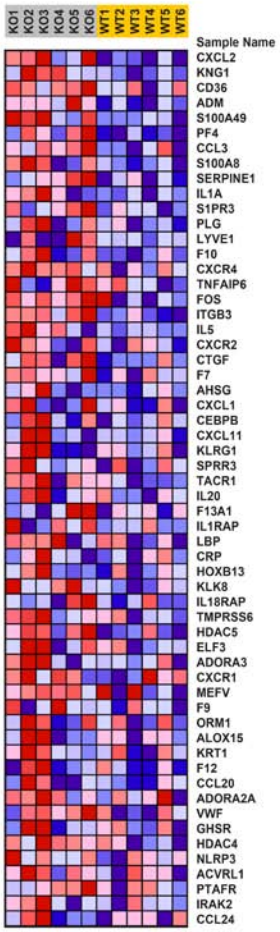

D

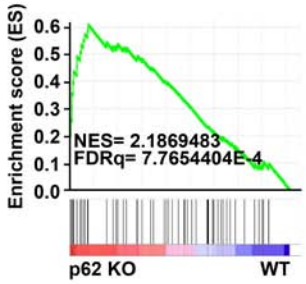

E

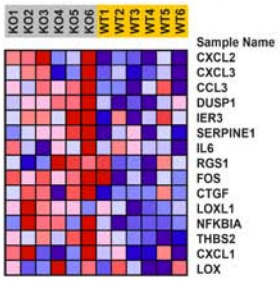

F

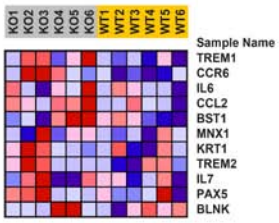

G

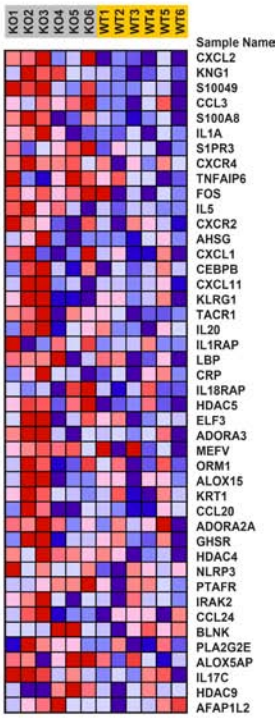

Figure S2, related to Figure 2. p62 deficiency in the stroma promotes a CAF and an inflammatory phenotype.

(A) Genes differentially expressed between orthotopic tumors from WT and p62 KO mice were subjected to NextBio analysis to identify biosets that contain similar genes. Venn diagrams show the number of common and unique genes in both sets. (B and C) Differentially expressed genes in orthotopic tumors from p62 KO mice analyzed by GSEA against C5 biological processes of the MSigDB database. (B) The top-ranked twenty gene sets enriched in p62 KO tumors are shown. (C) Leading edge genes of the “response to wounding” gene set. (D and E) Differentially expressed genes in orthotopic tumors from p62 KO mice analyzed by GSEA against C2 curated gene sets of the MSigDB database. (D) GSEA plot of the selected “stromal stimulation” gene set. (E) Leading edge genes of gene set of D. (F and G) Leading edge genes of selected gene sets enriched in p62 KO tumors from analysis shown in (B).

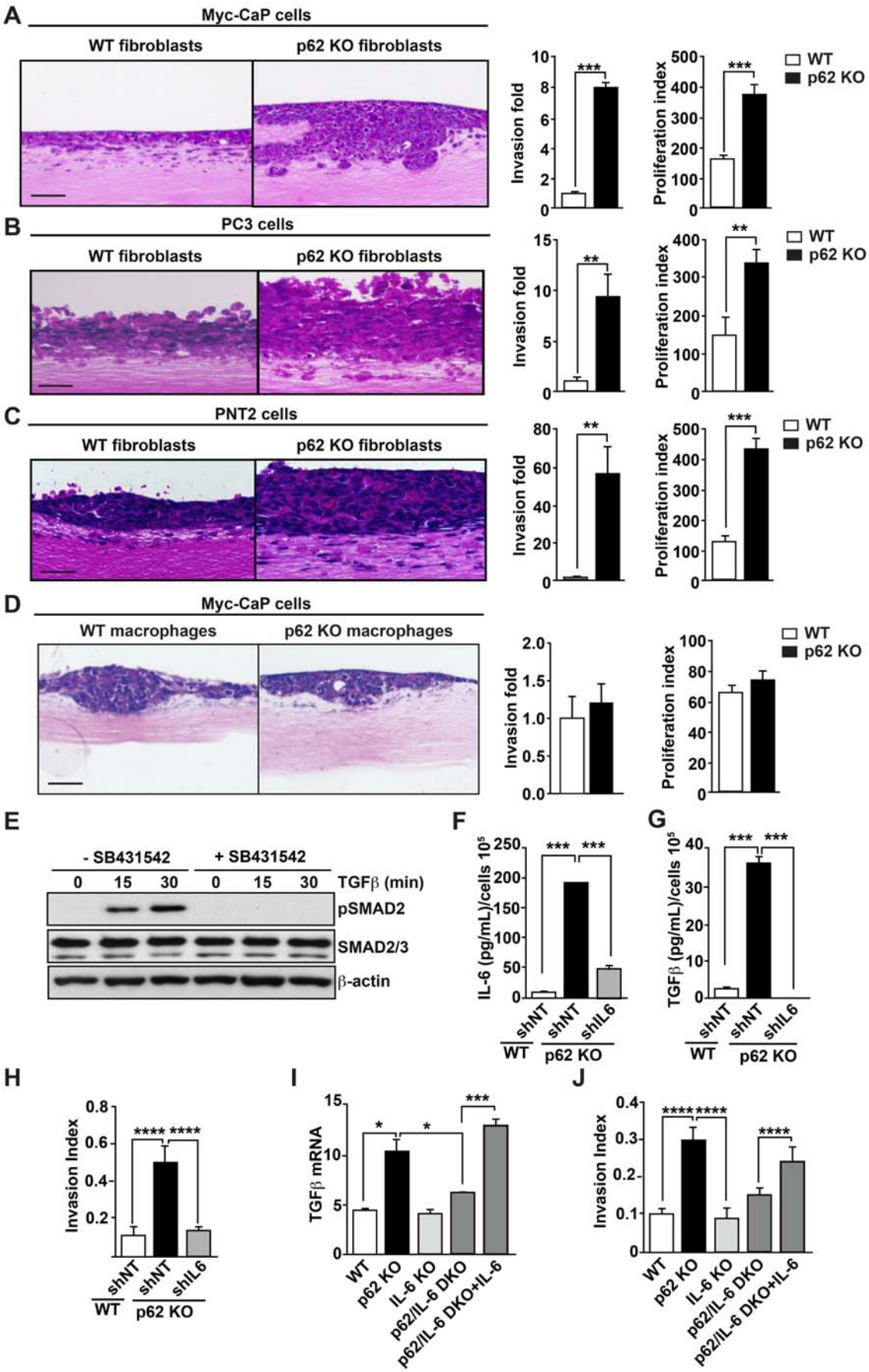
A
Myc-CaP cells
WT fibroblasts
p62 KO fibroblasts
Invasion fold
Proliferation index
WT
p62 KO
B
PC3 cells
C
PNT2 cells
D
Myc-CaP cells
WT macrophages
p62 KO macrophages
E
- SB431542
+ SB431542
0 15 30 0 15 30 TGFβ (min)
pSMAD2
SMAD2/3
β-actin
F
IL-6 (pg/mL)/cells 10^5
shNT
shIL6
WT
p62 KO
G
TGFβ (pg/mL)/cells 10^5
H
Invasion Index
I
TGFβ mRNA
WT
p62 KO
IL-6 KO
p62/IL-6 DKO
p62/IL-6 DKO+IL-6
J
Invasion Index

Figure S3, related to Figure 3. Loss of p62 in the prostate stroma promotes tumorigenesis in the prostate epithelium.

(A-C) H&E-stained organotypic cultures of different type of PCa cells: Myc-CaP (A), PC3 (B) and PNT2 (C) combined with fibroblasts from WT and p62 KO mice. Right panels show quantification of PCa cell invasion and proliferation of the organotypic experiments. (D) H&E-stained organotypic cultures of Myc-CaP cells with macrophages from WT and p62 KO mice. Right panels show quantification of PCa cell invasion and proliferation of the organotypic experiments. (E) The TGFβ inhibitor SB431542 effectively blocks TGFβ signaling as determined by immunoblot with pSMAD2. (F-H) Selective knockdown of IL-6 in p62 KO fibroblasts reverted increased IL-6 (F) and TGFβ (G) production as determined by ELISA, as well as PCa invasion as determined by modified Boyden chamber assay (H). (I) Addition of IL-6 to p62/IL-6 DKO fibroblasts restored TGFβ levels. IL-6 was added for 48 hr and TGFβ mRNA levels were determined by RT-PCR. (J) PCa invasion determined by modified Boyden chamber assay in fibroblasts from the different genotypes. IL-6 was exogenously added to p62/IL-6 DKO fibroblasts. Data are means ± SEM (n = 4). *$p < 0.05$, **$p < 0.01$. ***$p < 0.001$, ****$p < 0.0001$. Scale bars, 100 μm.

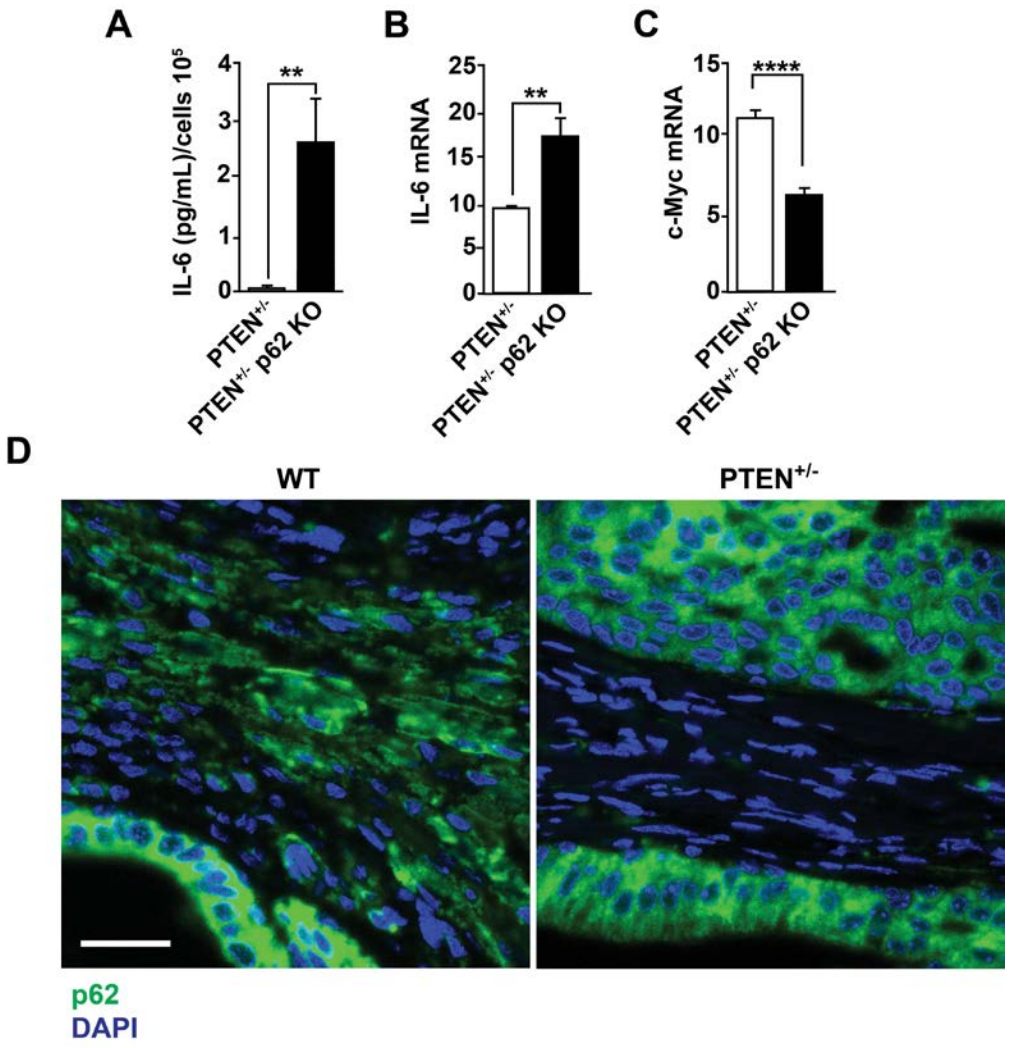

Figure S4, related to Figure 6. p62 role in prostate stroma of PTEN$^{+/-}$ mice.

(A-C) IL-6 ELISA (A) and RT-PCR of IL-6 (B) and c-Myc (C) in prostate stromal cells from PTEN$^{+/-}$ and PTEN$^{+/-}$/p62 KO mice (n = 6). (D) p62 levels are downregulated in the prostate stroma of PTEN$^{+/-}$ mice. Immunostaining of p62 (green) and DAPI (blue) were performed in prostate sections of WT and PTEN$^{+/-}$ mice of 9 months of age (n = 4). **p < 0.01, ****p < 0.0001. Scale bar, 25 μm. Results are presented as means ± SEM.

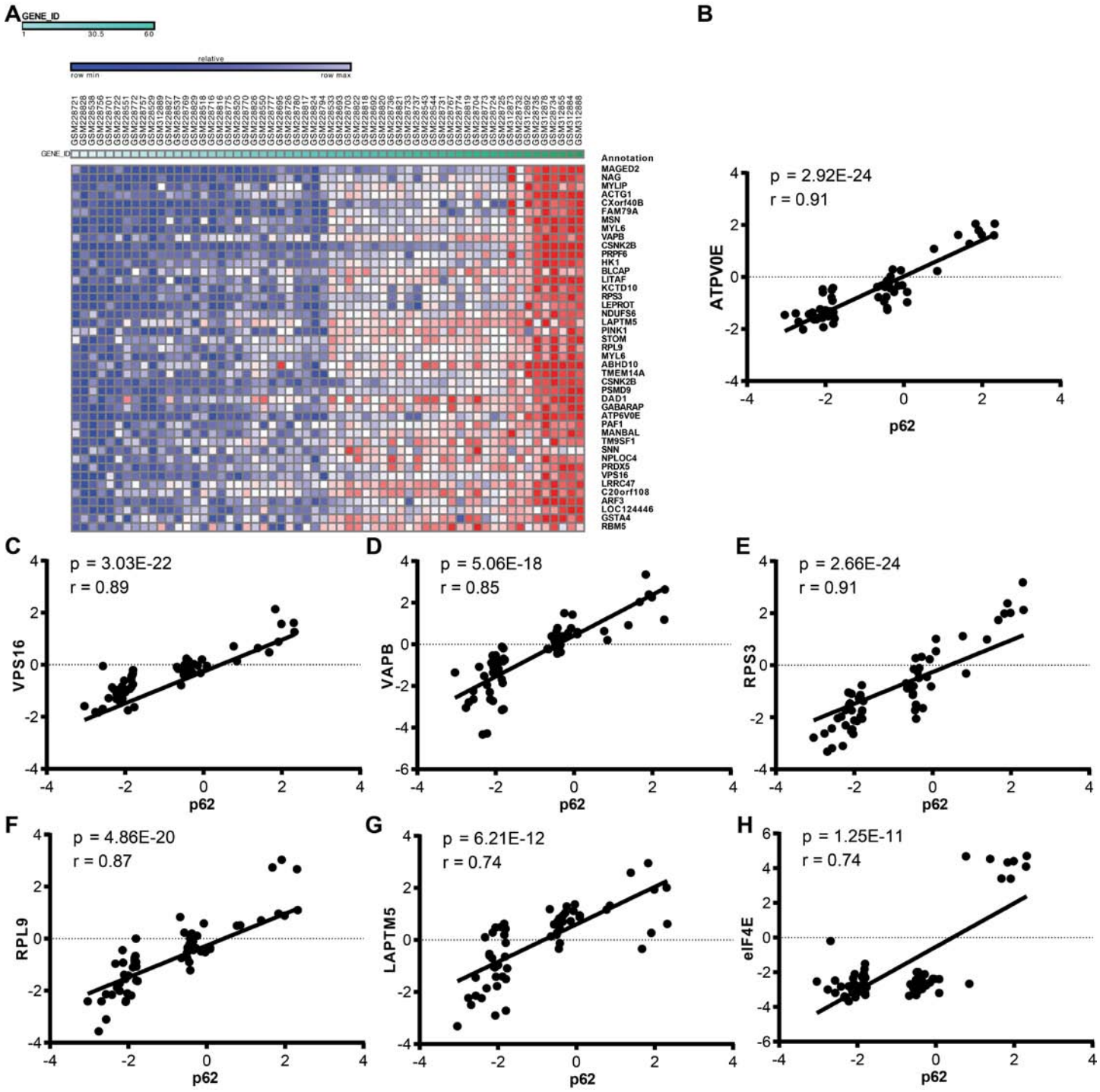
A
GENE_ID
1
30.5
60
relative
row min
row max
GENE_ID
Annotation
MAGED2
NAG
MYLIP
ACTG1
CXorf40B
FAM79A
MSN
MYL6
VAPB
CSNK2B
PRPF6
HK1
BLCAP
LITAF
KCTD10
RPS3
LEPROT
NDUFS6
LAPTM5
PINK1
STOM
RPL9
MYL6
ABHD10
TMEM14A
CSNK2B
PSMD9
DAD1
GABARAP
ATP6V0E
PAF1
MANBAL
TM9SF1
SNN
NPLOC4
PRDX5
VPS16
LRRC47
C20orf108
ARF3
LOC124446
GSTA4
RBM5
B
p = 2.92E-24
r = 0.91
ATPV0E
p62
C
p = 3.03E-22
r = 0.89
VPS16
p62
D
p = 5.06E-18
r = 0.85
VAPB
p62
E
p = 2.66E-24
r = 0.91
RPS3
p62
F
p = 4.86E-20
r = 0.87
RPL9
p62
G
p = 6.21E-12
r = 0.74
LAPTM5
p62
H
p = 1.25E-11
r = 0.74
eIF4E
p62

Figure S5, Related to Figure 7. p62 signature in human stroma.

(A) Heat map of the top 25 genes differentially expressed (FDR > 0.0002 and fold > 1.5) in the top 25% versus the bottom 25% of human stroma samples ranked by p62 expression levels. Expression data were extracted from the GSE9014 dataset. Blue and red in the heatmap indicate genes that are underexpressed or overexpressed, respectively. (B-H) A positive significant correlation of gene expression between p62 and ATPV0E (B), VPS16 (C), VAPB (D), RSP3 (E), RPL9 (F), LAPTM5 (G), and eIF4E (H) is shown for human stromal samples from the GSE9014 dataset.

Supplemental Experimental Procedures

Materials

Reagents were obtained from the following sources: Antibodies to KEAP1, actin, and HRP-labeled anti-mouse were from Santa Cruz Biotechnology. Antibodies to phospho-T389 S6K1, phospho-T37/46 4EBP1, phospho-Smad2-S465/467, HRP-labeled anti-rabbit secondary antibody and rapamycin were from Cell Signaling Technology. Antibody to Ki-67 was from ThermoScientific. Antibody to BrdU was from Millipore. Antibody to c-Myc [Y69] was from Abcam. Collagen, Matrigel, invasion chambers, NuSerum and antibody to human p62 were from BD biosciences; Antibody to murine p62 was from ThermoScientific. TGFβ and murine IL-6 was obtained from PeproTech. FLAG antibody, Butylated hydroxyanisole (BHA), Gluthatione Ethyl Ester (GEE), torin1, testosterone, methanol, chloroform, norvaline, 5-bromo-2'-deoxyuridine, and the glutathione assay kit were from Sigma Aldrich. TGFβ inhibitor, SB431542 was from StemRD. DMEM and fetal bovine serum were from Hyclone; X-tremeGENE and Dnase were from Roche. OneComp ebeads, antibodies CD31-FITC (clone 390), CD45-FITC (clone 30-F11), Ter119-FITC (clone TER-119), Sca-1-APC (clone D7), CD49f-PE (clone eBioGoH3), and TGF beta ELISA Ready-SET-GO were from eBioscience. αSMA was from DAKO. Trypsin, Insulin and collagenase were from Gibco. Crystal violet and 10% formalin were from Fisher Scientific. RNeasy RNA extraction kit was from Qiagen. High-Capacity cDNA reverse transcription kit was from Applied Biosystems. iTaq Universal SYBR green supermix was from Biorad. NADP/NADPH quantification colorimetric kit was from Biovision. CM-H_2DCFDA was from Molecular Probes. Alexa Fluor 488 tyramide signal amplification kit was from Life Technologies.

Cell Culture

HEK293T and PC-3 were from American Type Culture Collection (ATCC). PNT2 was obtained from Sigma. The Myc-CaP cell line was a generous gift from Dr. Charles Sawyers.

WT and p62 KO stromal prostate fibroblasts were isolated from mouse prostate, as described previously (Tuxhorn et al., 2002). Murine TRAMP-C2Re3 cells were previously described (Olson et al., 2006). Stromal prostate fibroblast cells were cultured in Dulbecco's modified Eagle's medium (DMEM) supplemented with 5% (vol/vol) fetal bovine serum (FBS), 5% (vol/vol) NuSerum IV, 1% glutamine, 1% penicillin-streptomycin, 0.01 μM testosterone, and 25 μg ml^{-1} of insulin, in an atmosphere of 95% air and 5% CO_2 at 37°C. Cells were stimulated with inhibitors (rapamycin, 100 nM; torin1, 100 nM; SB431542, 10 μM) or antioxidants (BHA [100 □M] and GEE [0, 2.5, 5.0, 10 mM]) for 12 h.

Mammalian Lentiviral shRNAs and Retroviral Transduction

pWZL-Hygro (Addgene plasmid 18750, donated by Scott, L), pWZL-Blast-Myc (Addgene, plasmid 10674) (Boehm et al., 2005), FLAG pLJM1 RagB 99L (Addgene, plasmid 19315) (Sancak et al., 2008), TRC lentiviral shRNA targeting murine c-Myc (TRCN0000234923) was obtained from Sigma Aldrich. TRC lentiviral shRNA targeting murine IL-6 (TRCN0000067548) was obtained from OpenBioSystems, Thermo Scientific. Actively growing HEK293T cells were co-transfected with shRNA-encoding plasmids, psPAX2 (Addgene, plasmid 12260) and pMD2.G (Addgene, plasmid 12259) packaging plasmids using X-tremeGENE transfection reagent. For retroviruses, pWZL-encoding plasmids were transfected into actively growing Phoenix cells with X-tremeGENE transfection reagent to produce viral particles, which were used to infect cells. Virus-containing supernatants were collected 48 and 72 hr post-transfection and filtered to remove cells. Target cells were infected in the presence of 8 μg ml^{-1} polybrene. Cells were selected with puromycin, hygromycin, or blasticidin after infection.

Gene-expression analyses

RNA was isolated using RNeasy mini kit from Qiagen (Valencia, USA). Total RNA (1 µg) was reverse-transcribed using the High-Capacity cDNA Reverse Transcription Kit (Applied Biosystems). Quantitative real-time PCR was performed using iTaq Universal SYBR green supermix (Biorad) on a Biorad CFX96 detection system. PCR primers were designed using the online primer tool Primer3 and purchased from Integrated DNA Technologies. 18S was used as the housekeeping gene for normalization, with a melting curve performed after each reaction.

Histological analysis

Excised prostates were fixed in 10% formalin, dehydrated, and embedded in paraffin. Samples were sectioned at 5 µm and subjected to staining with hematoxylin and eosin. For immunohistochemistry, samples were dewaxed and stained with anti-αSMA (clone 1A4, 1:400 dilution), with a ready to use anti-Ki-67 (1:10 dilution), or with anti-BrdU (clone PRB-1, 1:200 dilution). Secondary biotinylated antibody and ABC complex (Vectastain Elite, Vector Labs) were used for detection following manufacturer's instructions. Human prostate tissue microarrays (TMA) were obtained from US Biomax. This study had Institutional Review Board exempt status due to de-identification of the human samples. TMA were stained with anti-p62. TMA slides were scanned and imaged using the Scanscope XT system (Aperio) and Aperio ImageScope software, respectively. The scoring of staining intensity was done by a pathologist (E.C) in a blinded fashion. For immunofluorescence, sections were deparafinized as described above and incubated with anti-p62 antibody (1:100) overnight at 4°C. Alexa Fluor 488 tyramide signal amplification kit for p62 antibody was used. Stained sections were examined under an inverted laser scan microscope (LSM 710 NLO, Zeiss, Germany).

FACs-sorted murine stromal isolation

Prostates from 12-week-old mice were harvested and dissected. Prostate cell isolation has been described previously (Lukacs et al., 2010). Cells were stained with fluorescently labeled lineage markers (CD31-FITC, CD45-FITC, and Ter119-FITC), CD49f-PE, and Sca-1-APC. Unstained prostate cells were used as the control to set the background fluorescence. Single-color stained OneComp ebeads (eBioscience) were used for FACS Aria cell sorter equipment compensation. FMO compensations were also performed. Stromal cells were sorted at 4°C into FACS Collection media using the FACS Aria cell sorter and FACS Diva software (BD Biosciences). Stromal cell fractions were sorted based on the Lin^-, $Sca\text{-}1^+$, $CD49f^-$ profile.

Determination of ROS Levels

Cells were washed once with warm PBS and were incubated with 10 μM 5-(and-6)-chloromethyl-2',7'-dichlorodihydrofluorescein diacetate, acetyl ester (CM-H_2DCFDA, Molecular Probes) in warm PBS. After 30 min at 37°C, cells were washed, trypsinized, and re-suspended in PBS. Detection of ROS levels was carried out through flow cytometric analyses using a FACS Canto flow cytometer (Becton-Dickinson) with FlowJo software (BD Biosciences).

Measurement of NADPH/NADP ratio and GSH intracellular levels

Fibroblast cells were washed with cold PBS and extracted with NADP/NADPH extraction buffer. Quantification was carried out using the NADP/NADPH quantification colorimetric kit (Cat. No. K347-100, BioVision) according to the manufacturer's protocol. GSH was measured using the Glutathione Assay Kit (Cat No. CS0260, Sigma Aldrich). The plate reader was set to 412 nm with kinetic reads at 1 min intervals for 5 min. At least three independent measurements were carried out.

ELISAS

Culture supernatants were harvested, clarified by centrifugation, and frozen for the subsequent determination of IL-6 concentration by enzyme-linked immunosorbent assay (ELISA) according to the manufacturer's instructions (BD Bioscience). TGFβ□levels in culture supernatants were quantified using the Human/Mouse TGF beta 1 ELISA Ready-SET-Go! (eBioscience).

Invasion Assay

PCa cells (5 x 10^4) were plated onto 8 µm-pore Matrigel Invasion chambers (BD Biosciences) in 24-well plates. Conditioned media from WT, p62 KO, IL-6 KO, p62/IL-6 DKO, p62/IL-6 DKO + IL-6, WT shNT, p62 KO shNT, p62 KO shIL-6 fibroblasts were added to the lower chamber as a chemoattractant. Cells were allowed to invade for 22 hr at 37°C. Non-invading cells in the upper surface were removed and those on the lower surface fixed in methanol and stained with crystal violet. Cells in at least five randomly selected fields from each of three experiments were counted.

Co-culture invasion assays

Invasion assays were performed as described above with a few modifications. WT shNT or WT shMyc fibroblast (7.5 x 10^4) were seeded in TC-treated 24-well plates and allowed to attach for 6 hr before PCa cells were seeded on top of the invasion chamber. The chamber was then placed in the pre-seeded 24-well plate. Invasion was quantified after 22 hr.

Organotypic cultures

3D air liquid organotypic culture cultures have been used extensively in skin (Gaggioli et al., 2007), esophageal (Okawa et al., 2007), pancreas (Coleman et al., 2014), colon (Henriksson et al., 2011), breast (Chioni and Grose, 2012) and more recently in prostate cancer (Kim et al.,

2013), to determine the mechanisms of tumor invasion and the role of the stromal compartment (Chioni and Grose, 2008). To study the interaction between the prostate cancer cells and surrounding stroma to impact cancer cell proliferation and invasion, a 3D air liquid organotypic culture was set up as previously described (Kim et al., 2013) (Coleman et al., 2014). Briefly, gels were composed of one ml of a mixture of 1.75 volumes of Matrigel, 5.25 volumes of collagen type I, 1 volume of 1x DMEM, 1 volume of 10x DMEM, and 1 volume of filtered FBS. The mixture was plated onto 24-well plates coated with diluted collagen type I. Gels were allowed to equilibrate with 1 ml of 1x DMEM overnight at 37°C. 5 x 10^5 cells PCa cells and prostate stromal cells (50:50) were then seeded on top of the matrix as shown in the scheme below. For organotypic cultures with macrophages, whole bone marrow cells were obtained from WT and p62 KO mice and differentiated as previously described (Lee et al., 2010). Differentiated macrophages were embedded into the organotypic gels and PCa cells were seeded on top of the gel. Gel rafts were placed onto collagen-coated nylon sheets and lifted using a sterile supporting steel mesh to set up a raised air-liquid culture. Normal medium was changed in alternate days and organotypic cultures were allowed to grow for 14 days. Afterwards, organotypic gels were harvested, fixed in 10% neutroal buffered formalin, bisected and embedded in paraffin. H&E stained sections were analyzed with a Zeiss light microscope supplemented with Axiovision40 software. Quantification of the invasion assays was performed as described previously (Nystrom et al., 2005) using ImageProPlus software.

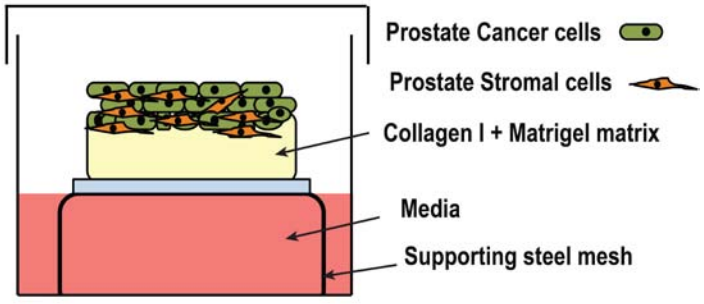

Schematic representation of air-liquid organotypic cultures

In vivo orthotopic tumor assay

Murine TRAMP-C2Re3 prostate carcinoma cells (5×10^4) were injected orthotopically into the prostates of WT, p62 KO, and p62/IL-6 DKO mice and harvested after 60 days, as previously described (Olson et al., 2006).

Xenograft experiments

Cell mixtures (1×10^6 cells) of equal ratios of PCa cells with fibroblasts in a 100 µl of BD Matrigel (BD Biosciences) were injected into the flanks of WT mice. Tumors were allowed to grow for 6 weeks. Tumor volume was measured every week.

Metabolic Extraction

For labeling experiments, 2×10^5 cells were seeded in 6-well plates. After 16 hr of incubation, cells were washed with PBS and incubated with DMEM, 10% dialyzed serum, and either 4 mM [U-$^{13}C_5$]glutamine and 25 mM unlabeled glucose or [1,2$^{13}C_2$]glucose and unlabeled glutamine. Spent medium from labeled cells was collected and analyzed for glucose, glutamine consumption, and lactate production using the YSI2950 analyzer. Cells were rinsed in ice-cold saline solution, and then ice-cold 100% HPLC-grade methanol was added to the cells. An equal volume of water containing norvaline as standard was added to the plate. Cells were scraped and mixed with ice-cold chloroform. Samples were vortexed for 10 min at room temperature and centrifuged at 3000 g for 10 min. Polar metabolites were separated and evaporated in a refrigerated vacuum centrifuge.

Derivatization, gas chromatography/mass spectrometry (GC/MS) analysis, and flux calculations

Polar metabolites were derivatized to form methoxime-tBDMS derivatives by first dissolving the evaporated samples in 20 µl of 2% (w/v) methoxylamine hydrochloride (MP Biomedicals, OH) in pyridine and incubating at 37°C for 60 min. Samples were then silylated by addition of 30 µl of N-tertbutyldimethylsily-N-methyltrifluoroacetamide (MTBSTFA) with 1% tert-butyldimethylchlorosilane (TBDMCS) (Regis Technologies, IL) and incubated at 37°C for 45 min. Samples were centrifuged at 14,000 rpm for 5 min and clarified supernatant was transferred to GC sample vials for analysis. Derivatized samples were analyzed by GC-MS using a DB-35MS (Agilent J&W Scientific) installed in an Agilent 7890A GC interfaced with an Agilent 5975C MS operating in electron impact mode scanning over the range 100-650 m/z. The GC method and metabolite peaks used for integration have been previously described (Grassian et al., 2011) (Metallo et al., 2012). Uptake and secretion fluxes of glucose, glutamine, and lactate were then calculated using an exponential growth model. PPP flux was determined by multiplying lactate secretion flux by the ratio of M1 to M2 lactate labeled from [1,2-$^{13}C_2$]glucose as described above.

Array and Gene Set Enrichment Analysis

Microarray studies were performed in the Genomics and Microarray Laboratory at the Department of Environmental Health, University of Cincinnati Medical Center. Briefly, total RNA was extracted from six independent orthotopic tumors from WT and p62 KO mice and hybridized on Affymetrix mouse ST 1.0 microarrays. Scanning of the images and the first pass processing of probe-level fluorescence intensities was performed using the Microarray Suite 5.0 software (MAS 5.0; Affymterix, Santa Clara, CA). The data was normalized, and the calculation of the gene-specific summary measures was performed by the robust multi-array average

(RMA) procedure (Irizarry et al., 2003) based on the Entrez gene-centric probe set definitions provided by the University of Michigan "brainarray" group (Dai et al., 2005). Statistical significance of genes differentially expressed between WT and p62 KO orthotopic tumors were assessed using Empirical Bayes linear model (Sartor et al., 2006). Gene set enrichment analysis was performed using GSEA v2.0.14 software (http://www.broadinstitute.org/gsea/index.jsp) with 5000 gene set permutations using the metric Signal-to-Noise ratio (S2N) and the collection C5.bp.v3.1.symbols or C2.all.v4.0.symbols (Subramanian et al., 2005Subramanian et al., 2005). Probe sets were collapsed using MoGene_1_0_st.chip. Meta-analyses to identify overlapping and associated genes with publically available data set were performed using the NextBio™ (NextBio, Cupertino, CA) on-line search engine (www.nextbio.com). Differentially expressed genes were further analyzed with the Ingenuity Pathways Analysis program (http://www.ingenuity.com/index.html).

Supplemental References

Boehm, J.S., Hession, M.T., Bulmer, S.E., and Hahn, W.C. (2005). Transformation of human and murine fibroblasts without viral oncoproteins. Mol Cell Biol 25, 6464-6474.

Chioni, A.M., and Grose, R. (2008). Organotypic modelling as a means of investigating epithelial-stromal interactions during tumourigenesis. Fibrogenesis & tissue repair 1, 8.

Chioni, A.M., and Grose, R. (2012). FGFR1 cleavage and nuclear translocation regulates breast cancer cell behavior. The Journal of cell biology 197, 801-817.

Coleman, S.J., Chioni, A.M., Ghallab, M., Anderson, R.K., Lemoine, N.R., Kocher, H.M., and Grose, R.P. (2014). Nuclear translocation of FGFR1 and FGF2 in pancreatic stellate cells facilitates pancreatic cancer cell invasion. EMBO Mol Med 6, 467-481.

Dai, M., Wang, P., Boyd, A.D., Kostov, G., Athey, B., Jones, E.G., Bunney, W.E., Myers, R.M., Speed, T.P., Akil, H., et al. (2005). Evolving gene/transcript definitions significantly alter the interpretation of GeneChip data. Nucleic acids research 33, e175.

Grassian, A.R., Metallo, C.M., Coloff, J.L., Stephanopoulos, G., and Brugge, J.S. (2011). Erk regulation of pyruvate dehydrogenase flux through PDK4 modulates cell proliferation. Genes & development 25, 1716-1733.

Henriksson, M.L., Edin, S., Dahlin, A.M., Oldenborg, P.A., Oberg, A., Van Guelpen, B., Rutegard, J., Stenling, R., and Palmqvist, R. (2011). Colorectal cancer cells activate adjacent fibroblasts resulting in FGF1/FGFR3 signaling and increased invasion. The American journal of pathology 178, 1387-1394.

Irizarry, R.A., Hobbs, B., Collin, F., Beazer-Barclay, Y.D., Antonellis, K.J., Scherf, U., and Speed, T.P. (2003). Exploration, normalization, and summaries of high density oligonucleotide array probe level data. Biostatistics 4, 249-264.

Lee, S.J., Kim, J.Y., Nogueiras, R., Linares, J.F., Perez-Tilve, D., Jung, D.Y., Ko, H.J., Hofmann, S.M., Drew, A., Leitges, M., et al. (2010). PKCzeta-regulated inflammation in the nonhematopoietic compartment is critical for obesity-induced glucose intolerance. Cell Metab 12, 65-77.

Lukacs, R.U., Goldstein, A.S., Lawson, D.A., Cheng, D., and Witte, O.N. (2010). Isolation, cultivation and characterization of adult murine prostate stem cells. Nat Protoc 5, 702-713.

Metallo, C.M., Gameiro, P.A., Bell, E.L., Mattaini, K.R., Yang, J., Hiller, K., Jewell, C.M., Johnson, Z.R., Irvine, D.J., Guarente, L., et al. (2012). Reductive glutamine metabolism by IDH1 mediates lipogenesis under hypoxia. Nature 481, 380-384.

Okawa, T., Michaylira, C.Z., Kalabis, J., Stairs, D.B., Nakagawa, H., Andl, C.D., Johnstone, C.N., Klein-Szanto, A.J., El-Deiry, W.S., Cukierman, E., et al. (2007). The functional interplay between EGFR overexpression, hTERT activation, and p53 mutation in esophageal epithelial

cells with activation of stromal fibroblasts induces tumor development, invasion, and differentiation. Genes & development 21, 2788-2803.

Sancak, Y., Peterson, T.R., Shaul, Y.D., Lindquist, R.A., Thoreen, C.C., Bar-Peled, L., and Sabatini, D.M. (2008). The Rag GTPases bind raptor and mediate amino acid signaling to mTORC1. Science 320, 1496-1501.

Sartor, M.A., Tomlinson, C.R., Wesselkamper, S.C., Sivaganesan, S., Leikauf, G.D., and Medvedovic, M. (2006). Intensity-based hierarchical Bayes method improves testing for differentially expressed genes in microarray experiments. BMC bioinformatics 7, 538.

Subramanian, A., Tamayo, P., Mootha, V.K., Mukherjee, S., Ebert, B.L., Gillette, M.A., Paulovich, A., Pomeroy, S.L., Golub, T.R., Lander, E.S., et al. (2005). Gene set enrichment analysis: a knowledge-based approach for interpreting genome-wide expression profiles. Proc Natl Acad Sci U S A 102, 15545-15550.

Tuxhorn, J.A., McAlhany, S.J., Dang, T.D., Ayala, G.E., and Rowley, D.R. (2002). Stromal cells promote angiogenesis and growth of human prostate tumors in a differential reactive stroma (DRS) xenograft model. Cancer Res 62, 3298-3307.

Article

Cell Reports

Amino Acid Activation of mTORC1 by a PB1-Domain-Driven Kinase Complex Cascade

Graphical Abstract

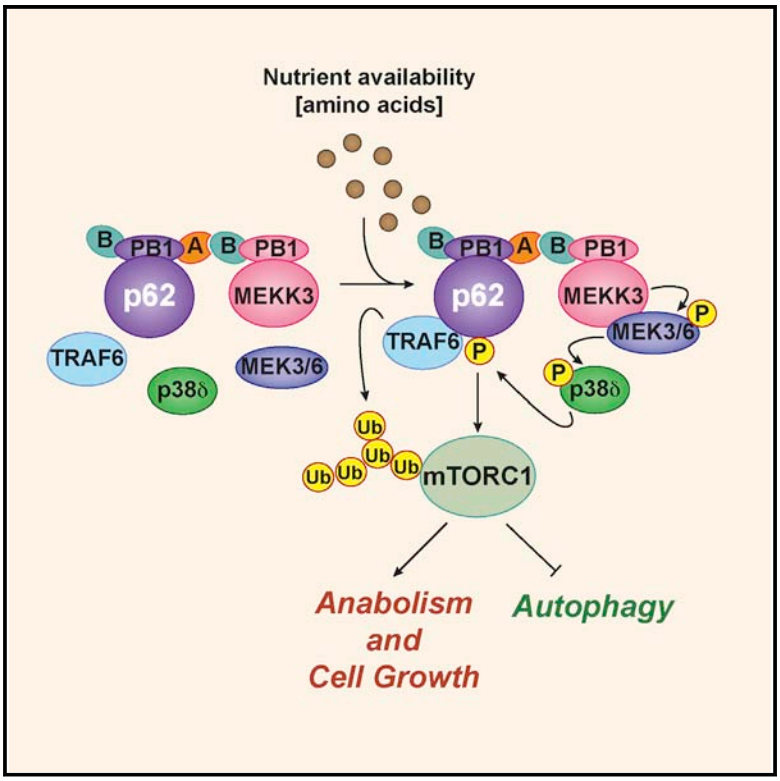

Authors

Juan F. Linares, Angeles Duran, Miguel Reina-Campos, ..., Alex Campos, Jorge Moscat, Maria T. Diaz-Meco

Correspondence

mdmeco@sbpdiscovery.org

In Brief

Linares et al. identify a kinase cascade that regulates the phosphorylation of the signal adaptor p62 in response to amino acids to control mTORC1 activation. This nutrient-sensing mechanism is relevant for autophagy regulation and tumor growth.

Highlights

- p62 is phosphorylated in response to amino acids by p38δ in a MEKK3-dependent manner
- p62 phosphorylation recruits TRAF6 and promotes mTORC1 translocation to lysosomes
- p38δ-mediated p62 phosphorylation is required for mTORC1 activation by amino acids
- The MEKK3/p38δ kinase cascade modulates autophagy and cancer growth via mTORC1

Linares et al., 2015, Cell Reports *12*, 1–14
August 25, 2015
http://dx.doi.org/10.1016/j.celrep.2015.07.045

CellPress

Please cite this article in press as: Linares et al., Amino Acid Activation of mTORC1 by a PB1-Domain-Driven Kinase Complex Cascade, Cell Reports (2015), http://dx.doi.org/10.1016/j.celrep.2015.07.045

Cell Reports
Article

Amino Acid Activation of mTORC1 by a PB1-Domain-Driven Kinase Complex Cascade

Juan F. Linares,[1] Angeles Duran,[1] Miguel Reina-Campos,[1] Pedro Aza-Blanc,[2] Alex Campos,[3] Jorge Moscat,[1] and Maria T. Diaz-Meco[1,*]
[1]Cell Death and Survival Networks Program
[2]Functional Genomics Core
[3]Proteomics Facility
Sanford Burnham Prebys Medical Discovery Institute, 10901 N. Torrey Pines Road, La Jolla, CA 92037, USA
*Correspondence: mdmeco@sbpdiscovery.org
http://dx.doi.org/10.1016/j.celrep.2015.07.045

SUMMARY

The mTORC1 complex is central to the cellular response to changes in nutrient availability. The signaling adaptor p62 contributes to mTORC1 activation in response to amino acids and interacts with TRAF6, which is required for the translocation of mTORC1 to the lysosome and the subsequent K63 polyubiquitination and activation of mTOR. However, the signal initiating these p62-driven processes was previously unknown. Here, we show that p62 is phosphorylated via a cascade that includes MEK3/6 and p38δ and is driven by the PB1-containing kinase MEKK3. This phosphorylation results in the recruitment of TRAF6 to p62, the ubiquitination and activation of mTOR, and the regulation of autophagy and cell proliferation. Genetic inactivation of MEKK3 or p38δ mimics that of p62 in that it leads to inhibited growth of PTEN-deficient prostate organoids. Analysis of human prostate cancer samples showed upregulation of these three components of the pathway, which correlated with enhanced mTORC1 activation.

INTRODUCTION

Cell metabolism is responsive to the availability of environmental and intracellular nutrients. The mTORC1 kinase complex is a key nutrient sensor and an essential mediator of this response via its actions as a regulator of anabolism and autophagy (Hay and Sonenberg, 2004; Laplante and Sabatini, 2012). The aberrant activation of mTORC1 has important repercussions in several diseases, including cancer (Guertin and Sabatini, 2007; Laplante and Sabatini, 2012; Sabatini, 2006). An essential step in amino-acid-induced activation of mTORC1 is its translocation to the lysosome, mediated by the Rag guanosine triphosphatases (GTPases), where it is activated by another GTPase termed Rheb (Durán and Hall, 2012; Sancak et al., 2008, 2010; Yuan et al., 2013). A lysosomal pentameric complex termed ragulator, along with the vacuolar-ATPase, have been proposed to promote the exchange of GDP for GTP on RagA or RagB in amino-acid-activated cells (Sancak et al., 2010). Additionally, the Rags have been shown to be regulated by other proteins including the GATOR1 complex (Bar-Peled et al., 2013), FLCN (Petit et al., 2013; Tsun et al., 2013), and sestrins (Budanov and Karin, 2008; Chantranupong et al., 2014). There is also evidence for Rag-independent mechanisms of mTORC1 activation. For example, it has recently been reported that Rab1A mediates mTORC1 activity in a Rag-independent manner through the formation of a Rheb-mTORC1 complex in the Golgi (Thomas et al., 2014). Moreover, RagA-null cells display a diffuse cytosolic localization of mTOR and RagC but can, nonetheless, maintain the activity of mTORC1 (Efeyan et al., 2014). Also, it has recently been shown that RheB-null cells retain significant levels of mTORC1 activity (Groenewoud et al., 2013). Moreover, very recent results suggest that the mechanism whereby glutamine activates mTORC1 differs from that of leucine as it is independent of the Rag-Ragulator cascade and is mediated by Arf-1 (Jewell et al., 2015). Therefore, it is clear that our comprehension of mTORC1 activation is still fragmentary and that more work is necessary to achieve a thorough understanding of the mechanisms that modulate its activity in response to nutrients.

The signaling adaptor p62 (also known as SQSTM1) is central to cell survival and proliferation through the activation of mTORC1 (Duran et al., 2008, 2011; Linares et al., 2013; Moscat and Diaz-Meco, 2009, 2011; Valencia et al., 2014). This is achieved through the interaction of p62 with raptor, a distinctive component of the mTORC1 complex, and by facilitating mTORC1 translocation to the lysosome, a process that likely involves the interaction of p62 with the Rag proteins (Duran et al., 2011). Our recent data demonstrate that the E3-ubiquitin ligase TRAF6 is another important player in this process (Linares et al., 2013). That is, the interaction of TRAF6 with p62 facilitates the lysosomal recruitment of mTORC1 and catalyzes the K63 polyubiquitination of the mTOR subunit of the complex, which is required for its optimal activation by amino acids (Linares et al., 2013). Therefore, the p62/TRAF6 tandem must be considered an important modulator of nutrient sensing through mTORC1. Consistent with this notion, the loss of TRAF6, like that of p62, attenuated proliferation and the transforming properties of cancer cells and led to enhanced autophagy, which could be rescued by the expression of a permanently active RagB mutant, indicating that p62 acts upstream of the Rag proteins

Please cite this article in press as: Linares et al., Amino Acid Activation of mTORC1 by a PB1-Domain-Driven Kinase Complex Cascade, Cell Reports (2015), http://dx.doi.org/10.1016/j.celrep.2015.07.045

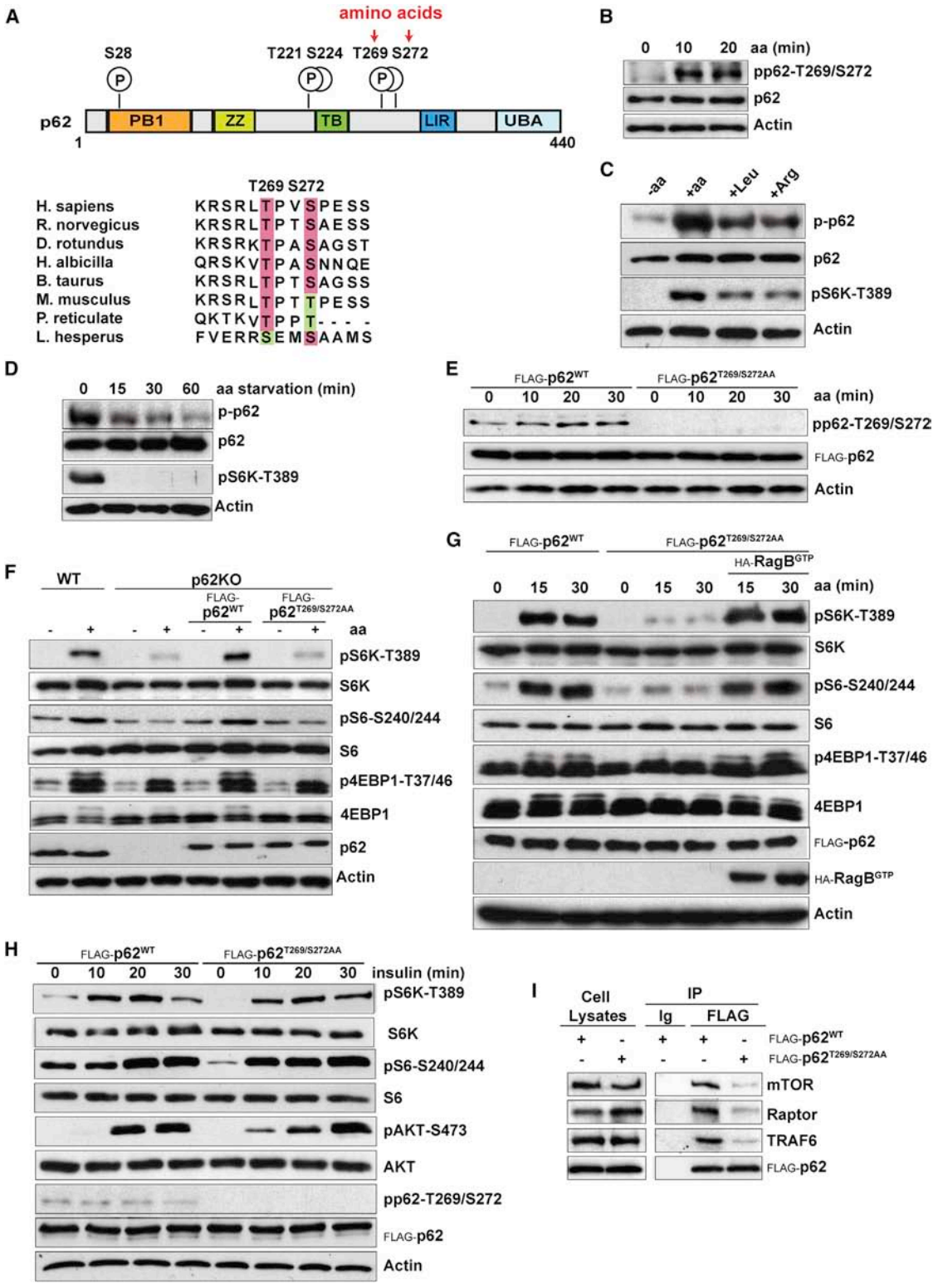

Figure 1. p62 Phosphorylation at T269/S272 Was Required for mTORC1 Activation in Response to Amino Acids

(A) p62 domain organization and phosphorylation sites identified by mass spec. Phosphorylation of T269 and S272 was induced by amino acids (upper panel). Alignment of the amino acid sequence of human p62 (264–276) with orthologs in other species is shown (lower panel).

(B) p62 phosphorylation at T269 and S272 is induced by amino acids. HEK293T cells were starved of amino acids for 50 min and restimulated with amino acids for the indicated durations. Cell lysates were analyzed by immunoblotting.

(legend continued on next page)

(Linares et al., 2013). Thus, p62 acts as a scaffold, bringing components involved in the control of mTORC1 signaling to the correct cellular location (Duran et al., 2011). How mTORC1 is linked to the upstream nutrient-sensing machinery and the potential role of p62 in that process are key unresolved issues.

Here, we demonstrate that p62 phosphorylation at T269/S272 is a critical event in channeling the amino acid response to mTORC1 activation, likely due to its ability to orchestrate the binding of p62 with the different components of the mTORC1-signaling complex. That is, we found that p62 organizes a molecular platform with a kinase cascade that is initiated by MEKK3 and triggers the activation of p38δ, is driven by PB1-domain interactions between p62 and MEKK3, and is located on the lysosomal surface. These kinases, like p62, are selectively required for amino-acid-induced mTORC1 activation whereas dispensable for insulin signaling and are required for effective control of cell growth, autophagy, and transformation. These findings define a critical mechanism to transmit nutrient-sensing signals to the mTORC1 complex, which is mediated by phosphorylation of the scaffold protein p62.

RESULTS

p62 Phosphorylation Is Required for the Activation of mTORC1 by Amino Acids

The mechanisms whereby mTORC1 respond to amino acids are not fully understood. Our previous data demonstrated that p62 is a scaffold in this pathway (Duran et al., 2011; Linares et al., 2013), but the process by which it senses amino acids remains to be elucidated. Recent studies have suggested phosphorylation as a regulatory mechanism for the control of p62 function (Ichimura et al., 2013; Linares et al., 2011; Matsumoto et al., 2011). Therefore, we hypothesized that nutrient-driven p62 phosphorylation might underlie p62-mediated activation of mTORC1 in response to amino acids. To address this possibility, we generated HEK293T cells stably expressing FLAG-tagged p62 or FLAG control. Cells were stimulated with amino acids, after which anti-FLAG immunoprecipitates were subjected to liquid chromatography coupled to mass spectrometry (LC-MS). We found that p62 exhibited low-abundance baseline phosphorylation at residues S28, T221, and S224 that was constitutive and not changed upon amino acid stimulation (Figure 1A, upper panel). In contrast, we found that phosphorylation at residues T269 and S272 was markedly induced by amino acids (Figure 1A, upper panel). These sites, and their surrounding sequences, were highly conserved across species (Figure 1A, lower panel). To establish the relevance of these phosphorylation events in mTORC1 signaling, we used a phosphospecific antibody generated against the human p62 peptide SRLT(P)PVS(P)PES(C), which allowed us to detect phospho-T269/S272. Interestingly, immunoblot analysis revealed the strong phosphorylation of p62 at T269/S272 upon re-addition of all amino acids to cells amino acid starved (Figure 1B). Leucine and arginine, two key amino acids for mTORC1 stimulation, also promoted p62-T269/S272 phosphorylation, which correlated with the magnitude of mTORC1 activation, as measured by phosphorylation of S6K (Figure 1C). Conversely, amino acid starvation resulted in a pronounced inhibition of p62-T269/S272 phosphorylation, concomitant with the decrease of mTORC1 activity (Figure 1D). Mutation of p62-T269/S272 sites to alanine ($p62^{T269/S272AA}$) abolished amino-acid-induced p62 phosphorylation, demonstrating that these are bona fide nutrient-sensitive p62 phosphorylation residues (Figure 1E). To explore whether phosphorylation of p62 has any impact on its ability to regulate mTORC1 activity, we used p62 KO MEFs reconstituted with either $p62^{WT}$ or $p62^{T269/S272AA}$. Consistent with our previously published data, mTORC1 activation in response to amino acids was impaired in p62-deficient cells (Figure 1F) (Duran et al., 2011). Importantly, whereas re-expression of $p62^{WT}$ restored mTORC1 activity in the KO MEFs, that of $p62^{T269/S272AA}$ failed to do so, as demonstrated by phosphorylation of multiple mTORC1 downstream targets including S6K, S6, and 4EBP1 (Figure 1F). Furthermore, overexpression of an active RagB-GTP-bound mutant rescued the mTORC1 inhibition caused by $p62^{T269/S272AA}$ expression (Figure 1G). This is in agreement with p62 acting upstream of the Rag GTPases in the control of mTORC1 signaling in the amino acid pathway and supports the notion that p62 phosphorylation also lies upstream of Rag activation (Duran et al., 2011). In keeping with a specific role for p62 in the amino acid, but not in the insulin pathway, insulin did not promote p62 phosphorylation, which, in turn, was not required for insulin-induced mTORC1 activity (Figure 1H). Notably, p62 phosphorylation was also critical for assembly of the amino-acid-induced p62-mTORC1 complex, as demonstrated by the ability of $p62^{T269/S272AA}$ expression to inhibit the interaction of p62 with the different components of mTORC1,

(C) p62 phosphorylation was determined in response to different amino acids. HEK293T cells were starved of amino acids and restimulated with the indicated amino acids for 30 min.

(D) Amino acid starvation inhibits p62 phosphorylation and mTORC1 activation. HEK293T cells were starved of amino acids for the indicated durations. Total cell lysates were analyzed by immunoblotting.

(E) Mutation of p62-T269/S272 sites to alanine ($p62^{T269/S272AA}$) abolished p62 phosphorylation in response to amino acids. HEK293T cells stably expressing FLAG-$p62^{WT}$ or FLAG-$p62^{T269/S272AA}$ were treated and analyzed as in (B).

(F) The $p62^{T269/S272AA}$ mutant was not able to reconstitute mTOR activation in p62KO MEFs. WT and p62KO MEFs, reconstituted with $p62^{WT}$ or $p62^{T269/S272AA}$, were treated as in (B). Cell lysates were analyzed by western blot.

(G) $RagB^{GTP}$ overexpression rescued the defects in mTOR activation by amino acids in cells stably expressing the $p62^{T269/S272AA}$ mutant. HEK293T cells stably expressing FLAG-$p62^{WT}$, FLAG-$p62^{T269/S272AA}$, or FLAG-$p62^{T269/S272AA}$ and FLAG-$RagB^{GTP}$ were treated as in (B) and immunoblotted for the specified proteins.

(H) p62 phosphorylation was not required for mTOR activation by insulin. HEK293T cells stably expressing FLAG-$p62^{WT}$ or FLAG-$p62^{T269/S272AA}$ were deprived of serum for 24 hr and stimulated with insulin for the indicated durations. Cell lysates were analyzed by western blot.

(I) The $p62^{T269/S272AA}$ mutant eliminated the interaction of p62 with different components of the mTORC1 complex. HEK293T cells stably expressing FLAG-$p62^{WT}$ or FLAG-$p62^{T269/S272AA}$ were treated as in (B). Cell lysates and FLAG-tagged immunoprecipitates were immunoblotted to detect the indicated proteins.

Results are representative of three experiments. See also Figure S1.

Please cite this article in press as: Linares et al., Amino Acid Activation of mTORC1 by a PB1-Domain-Driven Kinase Complex Cascade, Cell Reports (2015), http://dx.doi.org/10.1016/j.celrep.2015.07.045

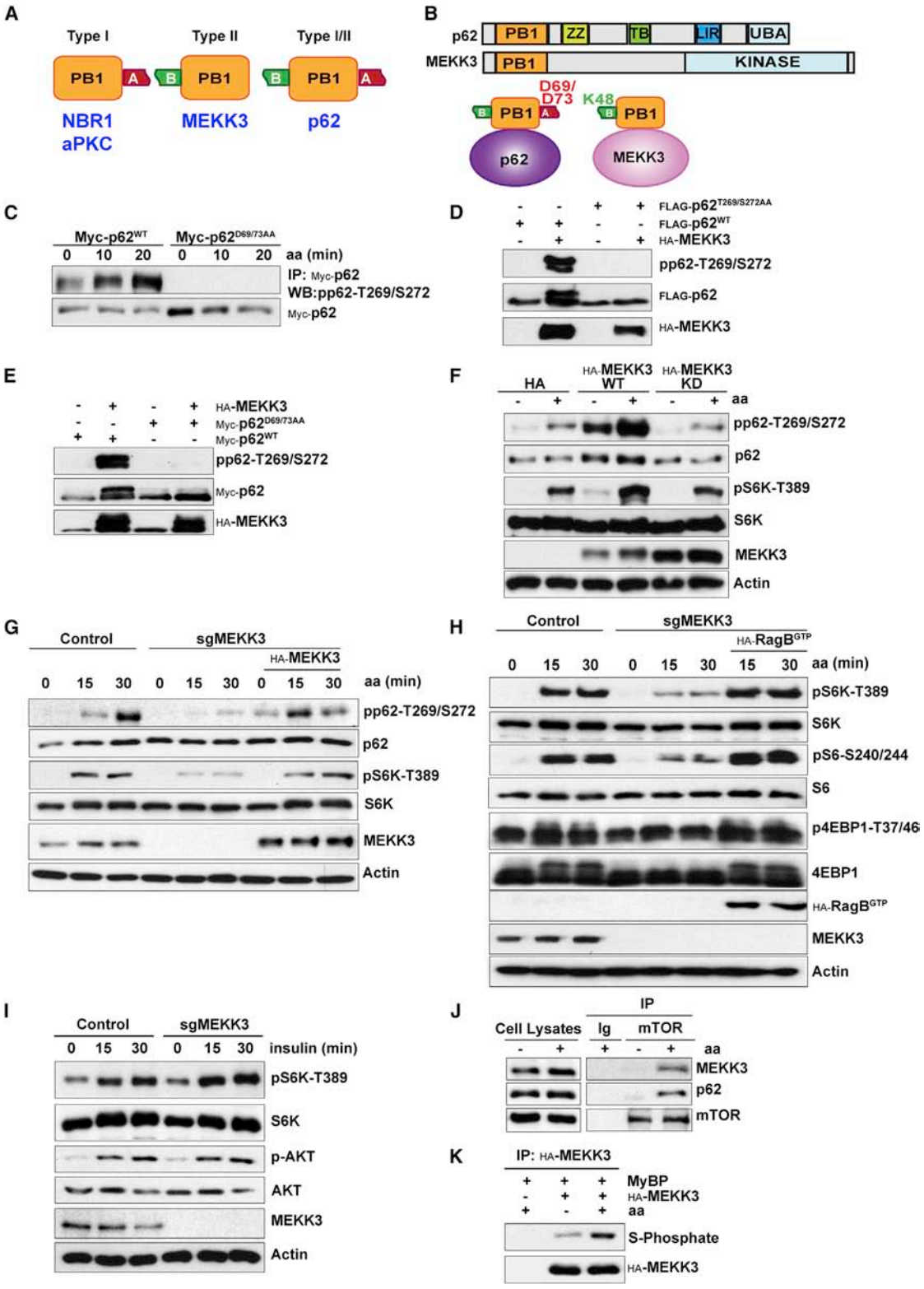

Figure 2. MEKK3 Was a Critical Kinase for p62 Phosphorylation and mTORC1 Activation in Response to Amino Acids

(A) Schematic of the different types of PB1 domains based on the presence of an acid cluster (type I), basic cluster (type II), or both in the same domain (type I/II).

(B) p62 and MEKK3 domain architecture and schematic of the interaction between the acidic cluster of the PB1 domain of p62 and the basic domain of MEKK3.

(legend continued on next page)

including mTOR, raptor, and TRAF6 (Figure 1I). Mutation of p62-T269/S272 sites to aspartic acid did not mimic p62 phosphorylation and did not restore mTORC1 activation or TRAF6 recruitment (Figures S1A and S1B). Together, these findings demonstrate that p62 phosphorylation is a key event in mTORC1 activation, selectively in response to amino acids.

MEKK3 Is a Critical Kinase for Amino-Acid-Induced p62 Phosphorylation

An important question arising from these results is the identity of the amino-acid-activated p62 kinase. In this regard, the structure of p62 includes a PB1 domain, which is a protein-protein interaction module that is present in kinases, such as the atypical PKCs (PKCζ and PKCλ/ι) and MEKK3, as well as in signaling adapters such as Par-6 and NBR1 (Moscat et al., 2006; Sanchez et al., 1998). Protein dimerization occurs by PB1-PB1 interactions through a β-grasp topology in a front-to-back orientation of the two PB1 domains. This involves electrostatic interactions of a cluster of basic residues in one of the PB1 domains that can bind clusters of acidic amino acids in the back of a second PB1 (Figure 2A) (Moscat et al., 2006; Sumimoto et al., 2007). The PB1 domains can be classified into three different types based on the presence of the acid cluster (type I), the basic cluster (type II), or both in the same domain (type I/II; Figure 2A). The PB1 domain of p62 belongs to the type I/II group and, therefore, can accommodate interactions through both faces (Moscat et al., 2006; Sumimoto et al., 2007). In this regard, we previously showed that proteins such as PKCζ, PKCλ/ι, or NBR1, which interact with p62 through its basic cluster, were not required for the activation of mTORC1 (Duran et al., 2011). In contrast, we found that disruption of the acidic cluster of p62, by mutation of D69/D73 to alanine, abolished p62 phosphorylation in response to amino acids (Figures 2B and 2C). This suggests that, if a PB1-domain protein is involved in mTORC1 activation, it must interact with the acidic cluster of p62 using its basic cluster. Interestingly, the PB1-domain-containing kinase, MEKK3, harbors a type II PB1 domain and previous results have shown that the p62 D69A/D73A PB1-domain mutant is unable to interact with MEKK3 (Figure 2B) (Nakamura et al., 2010). Consistent with this, the overexpression of MEKK3 resulted in the phosphorylation of $p62^{WT}$, but not of $p62^{T269/S272AA}$ (Figure 2D). Furthermore, p62 phosphorylation in response to MEKK3 overexpression was eliminated in the p62 PB1-domain mutant (Figure 2E). MEKK3 overexpression, but not that of a kinase-dead mutant, was able to induce the phosphorylation of p62 at T269/S272 (Figure 2F), which correlated with mTORC1 activation (Figure 2F), suggesting that MEKK3 could be a bona fide regulator of p62 phosphorylation and mTORC1 activity. Next, we determined whether MEKK3 is required for mTORC1 activation by using the clustered regularly interspaced short palindromic repeats (CRISPR/Cas9) system to generate MEKK3-deficient HEK293T cells. Notably, the loss of MEKK3 severely reduced p62 phosphorylation and mTORC1 activation in response to amino acids, which were both rescued by the ectopic expression of MEKK3 (Figure 2G). Similar results were obtained with two independent sgMEKK3 clones, as well as by knocking down MEKK3 with a shRNA lentiviral vector in HEK293T, A549, and PC3 cells (Figures S2A–S2D). Of note, the effects of MEKK3 deficiency in mTORC1 activation were rescued by expression of active RagB (Figure 2H). The loss of MEKK3 did not affect insulin-activated mTORC1, consistent with the specificity of p62 in the amino acid pathway (Figure 2I). In keeping with the importance of MEKK3 in this process, we found that, upon cell stimulation by amino acids, endogenous MEKK3 was recruited to an endogenous complex containing p62 and mTOR (Figure 2J). In addition, Figure 2K demonstrates that the kinase activity of MEKK3 was stimulated in amino-acid-treated cells. Collectively, these results demonstrate that p62 is phosphorylated in response to amino acids through a MEKK3-dependent mechanism that is critical for mTORC1 activation and is mediated by the interaction of p62 and MEKK3 through their respective PB1 domains.

MEK3/6 and p38δ Channel MEKK3-Induced Phosphorylation of p62 by Amino Acids

Based on these results, it is possible that p62 could be targeted directly by MEKK3. However, when bacterially expressed

(C) Mutation of p62-D69/73 sites to alanine ($p62^{D69/73AA}$) abolished p62 phosphorylation. HEK293T cells transfected with the indicated plasmids were starved of amino acids for 50 min and restimulated with amino acids for the indicated durations. Myc-tagged immunoprecipitates were analyzed by western blot.
(D) MEKK3 promoted p62 phosphorylation at T269/S272. HEK293T cells were transfected with the indicated plasmids, and cell lysates were analyzed by western blot.
(E) MEKK3-induced p62 phosphorylation required the PB1 domain of p62. HEK293T cells were transfected with the indicated plasmids, and cell lysates were immunoblotted to detect the specified proteins.
(F) Overexpression of MEKK3, but not that of MEKK3 kinase-dead mutant, induced p62 phosphorylation and mTORC1 activation by amino acids. HEK293T cells transfected with the indicated plasmids were deprived of amino acids for 50 min and stimulated with amino acids for 15 min. Cells were analyzed by western blot.
(G) MEKK3 expression rescued p62 phosphorylation and mTOR activation in MEKK3-deficient cells. MEKK3-deficient HEK293T cells generated with the CRISPR/CAS9 system were reconstituted with MEKK3. Cells were deprived of amino acids for 50 min and then stimulated with amino acids for the indicated durations. Cell lysates were immunoblotted for the specified proteins.
(H) $RagB^{GTP}$ overexpression rescued mTOR activation by amino acids in MEKK3-deficient cells. Control and MEKK3-deficient HEK293T cells expressing FLAG-$RagB^{GTP}$ were treated as in (G) and immunoblotted to detect the specified proteins.
(I) MEKK3 was not required for mTOR activation by insulin. Control and MEKK3-deficient HEK293T cells were deprived of serum for 24 hr and stimulated with insulin for the indicated durations. Cell lysates were analyzed by western blot.
(J) MEKK3 is a component of the mTORC1 complex. mTOR immunoprecipitates and cell lysates from HEK293T cells, treated as in (F), were immunoblotted for the indicated proteins.
(K) MEKK3 kinase activity was activated upon amino acid stimulation. HEK293T cells transfected with the indicated plasmids were treated as in (F). HA-tagged immunoprecipitates were used in an in vitro phosphorylation with ATPγS, with myelin basic protein (MyBP) as the substrate, followed by PNBM alkylation and immunoblotting to detect the indicated proteins.
Results are representative of three experiments. See also Figure S2.

Please cite this article in press as: Linares et al., Amino Acid Activation of mTORC1 by a PB1-Domain-Driven Kinase Complex Cascade, Cell Reports (2015), http://dx.doi.org/10.1016/j.celrep.2015.07.045

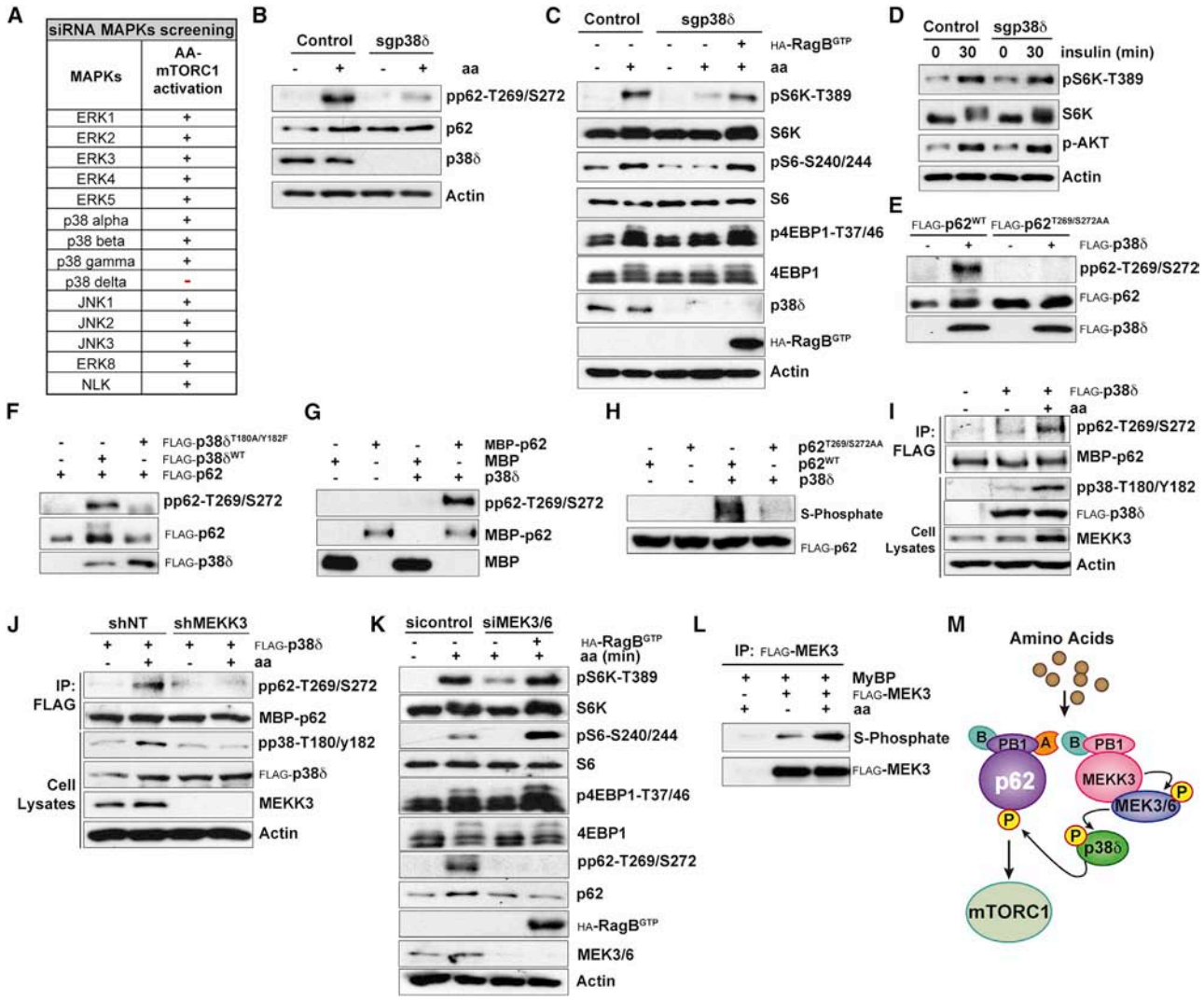

Figure 3. MEKK3/MEK3/6-p38δ Induced p62 Phosphorylation in Response to Amino Acids

(A) p38δ was required for mTORC1 activation in response to amino acids. Results of siRNA screening of MAPKs in mTORC1 activation.

(B) p38δ was required for p62 phosphorylation at T269/S272 in response to amino acids. p38δ-deficient HEK293T cells generated with the CRISPR/CAS9 system. Cells were deprived of amino acids for 50 min and then stimulated with amino acids for 15 min. Cell lysates were immunoblotted for the indicated proteins.

(C) $RagB^{GTP}$ overexpression rescued amino-acid-induced mTOR activation in p38δ-deficient cells. Control and p38δ-deficient HEK293T cells, expressing FLAG-$RagB^{GTP}$, were treated as in (B). Cell lysates were immunoblotted for the indicated proteins.

(D) p38δ was not required for insulin-induced mTORC1 activation. Control and p38δ-deficient HEK293T cells were deprived of serum for 24 hr and then stimulated with insulin for the indicated durations. Cell lysates were immunoblotted to detect the indicated proteins.

(E) p38δ overexpression promotes p62 phosphorylation at T269/S272. HEK293T cells were transfected with the indicated plasmids and immunoblotted for the specified proteins.

(F) p38δ kinase activity was required for p62 phosphorylation. HEK293T cells were transfected with the indicated plasmids and immunoblotted for the specified proteins.

(G) p38δ directly phosphorylated p62 at T269/S272 in vitro. An in vitro phosphorylation assay using recombinant p62 and recombinant p38δ is shown.

(H) T269/S272 sites accounted for p62 phosphorylation by p38δ. FLAG-tagged immunoprecipitates from HEK293T cells were phosphorylated in vitro by recombinant p38δ with ATPγS, followed by PNBM alkylation and immunoblotting for the indicated proteins.

(I) p38δ kinase activity was activated by amino acids. HEK293T cells transfected with the indicated plasmids were treated as in (B). In vitro phosphorylation was carried out with the FLAG-tagged immunoprecipitates and MBP-p62 recombinant protein as a substrate.

(J) MEKK3 was required for p38δ-induced p62 phosphorylation by amino acids. shNT or shMEKK3 HEK293T cells transfected with the indicated plasmids were treated as in (B). In vitro phosphorylation was carried out with the FLAG-tagged immunoprecipitates, and MBP-p62 recombinant protein was used as the substrate.

(K) MEK3/6 was required for p62 phosphorylation and mTORC1 activation in response to amino acids. HEK293T cells transfected with scramble siRNA or MEK3 and MEK6 siRNAs and FLAG-$RagB^{GTP}$ were treated as in (B). Cell lysates were immunoblotted for the indicated proteins.

(legend continued on next page)

recombinant p62 was incubated with active recombinant MEKK3 in an in vitro kinase assay, we found that MEKK3 was not able to directly phosphorylate p62 (Figure S3A). These results strongly suggest the existence of other kinase that acts downstream of MEKK3 to phosphorylate p62 in response to amino acids. Our previously published data showed that CDK1 was able to phosphorylate p62 at residues T269/S272 during mitosis (Linares et al., 2011). However, a selective CDK1 inhibitor did not affect p62 phosphorylation in response to amino acids (Figure S3B). To identify that kinase, because MEKK3 is a MAP3K, we reasoned that a MAP2K/MAPK cascade could act downstream of MEKK3 to phosphorylate p62. To address this possibility, we individually knocked down all the members of the five distinct groups of MAPKs characterized in mammals (Figure 3A). Cells were stimulated with amino acids, as above, and the activation of mTORC1 was determined. Notably, only depletion of p38δ (MAPK13) severely impaired amino-acid-induced activation of mTORC1 (Figures 3A and S3C). Importantly, knockout of p38δ by CRISPR/Cas9 severely abolished p62 phosphorylation and mTORC1 activation in cells stimulated with amino acids, which was rescued by the expression of active RagB (Figures 3B and 3C). Of note, p38δ-deficient cells displayed normal insulin-induced mTORC1 activation (Figure 3D). Similar results were obtained with two other independent CRISPR/Cas9-generated p38δ KO clones (Figure S3D). Furthermore, the pharmacological inhibition of p38δ severely abrogated mTORC1 activation and p62 phosphorylation by amino acids (Figure S3E). Interestingly, we also found that the overexpression of WT, but not of a kinase-inactive p38δ (T180A/Y182F) mutant, was able to induce the phosphorylation of $p62^{WT}$, but not of $p62^{T269/S272AA}$ (Figures 3E and 3F). Taken together, these results demonstrate that p38δ is responsible for p62 phosphorylation and mTORC1 activation by amino acids. To determine whether p62 is actually a direct substrate of p38δ, we incubated bacterially expressed recombinant p62 with active p38δ in an in vitro kinase assay and found that p38δ directly phosphorylated p62 at T269/S272 (Figure 3G). To confirm that these residues account for p62 phosphorylation by p38δ, purified $p62^{WT}$ and $p62^{T269/S272AA}$ were phosphorylated in vitro with ATP-γ-S and recombinant active p38δ. Figure 3H demonstrates that p62 phosphorylation by p38δ was completely abolished in the $p62^{T269/S272AA}$ mutant, as compared to $p62^{WT}$, indicating that p38δ is a bona fide direct p62 T269/S272 kinase that channels MEKK3 signals in amino-acid-activated cells.

If this model is correct, then p38δ should be activated by amino acids in a MEKK3-dependent manner. To determine whether this was the case, HEK293T cells were transfected with FLAG-tagged p38δ, after which cells were treated with amino acids at different times as described above. Transfected p38δ was immunoprecipitated with an anti-FLAG antibody, and its ability to phosphorylate recombinant p62 was determined in an in vitro kinase assay. Interestingly, p38δ from shNT cells that were stimulated with amino acids displayed higher enzymatic activity toward recombinant p62 than p38δ from unstimulated shNT cells (Figure 3I). The finding that amino acid stimulation did not increase the activity of p38δ in shMEKK3 cells (Figure 3J) clearly established that p38δ is a critical downstream target of MEKK3 in the nutrient-sensing cascade that activates mTORC1 through p62 phosphorylation. To identify the kinase that links MEKK3 to p38δ, we tested whether MEK3 and MEK6 might be the MAP2Ks upstream of p38δ. Notably, the simultaneous depletion of MEK3 and MEK6 severely impaired amino-acid-induced mTORC1 activation and p62 phosphorylation, which was rescued by the expression of active RagB (Figure 3K). Furthermore, the kinase activity of MEK3 was stimulated in amino-acid-treated cells (Figure 3L). Collectively, these results demonstrate that MEKK3 is the apical kinase in an amino-acid-sensing cascade that includes MEK3/MEK6 and p38δ and that leads to p62 phosphorylation, which is a critical step for mTORC1 activation in response to amino acids (Figure 3M).

MEKK3 and p38δ Control Lysosomal Translocation of mTOR

To be activated by amino acid stimulation, mTORC1 must undergo translocation from the cytoplasm to the lysosome (Sancak et al., 2008). Given that MEKK3 and p38δ are necessary for amino-acid-induced mTORC1 activity, we next investigated the subcellular localization of MEKK3 and p38δ by confocal immunofluorescence microscopy in both starved and amino-acid-stimulated cells. Double staining of endogenous MEKK3 or p38δ and lysosomal-associated membrane protein 2 (LAMP2) revealed the localization of both kinases at the lysosome, which was independent of nutrient availability (Figures 4A and 4B). The antibodies used in this experiment were validated for immunofluorescence in MEKK3 or p38δ knocked down cells (Figure S4). Cell fractionation confirmed the constitutive localization of MEKK3, p38δ, and p62, along with Lamp2, in the heavy membrane lysosomal fraction (Figure 4C). Of great functional relevance, the knockdown of either MEKK3 or p38δ impaired the colocalization of mTORC1 with LAMP2 in response to amino acids (Figure 4D), demonstrating that p38δ and MEKK3, like p62, are required for mTORC1 translocation to the lysosome.

Role of the MEKK3/p38δ Cascade in the Polyubiquitination of mTOR

TRAF6 is recruited to the p62-mTORC1 complex upon amino acid stimulation, and this promoted the K63 polyubiquitination of mTOR, a key event in amino-acid-dependent activation of mTORC1 (Linares et al., 2013). Our current results link this process to the MEKK3/p38δ cascade, because depletion of either kinase severely impaired the interaction of TRAF6 with p62 (Figures 5A and 5B). This suggests a critical role for the phosphorylation of p62 by the MEKK3/p38δ cascade in the binding of TRAF6 to p62, consistent with the fact that $p62^{T269/S272AA}$ did

(L) MEK3 is activated in response to amino acids. HEK293T cells transfected with the indicated plasmids were treated as in (B). FLAG-tagged MEK3 immunoprecipitates were used in an in vitro phosphorylation, using MyBP as substrate, with ATPγS followed by PNBM alkylation and immunoblotting for the indicated proteins.

(M) Schematic showing that MEK3/6-p38δ channels MEKK3-induced phosphorylation of p62 and mTORC1 activation by amino acids.

Results are representative of three experiments. See also Figure S3.

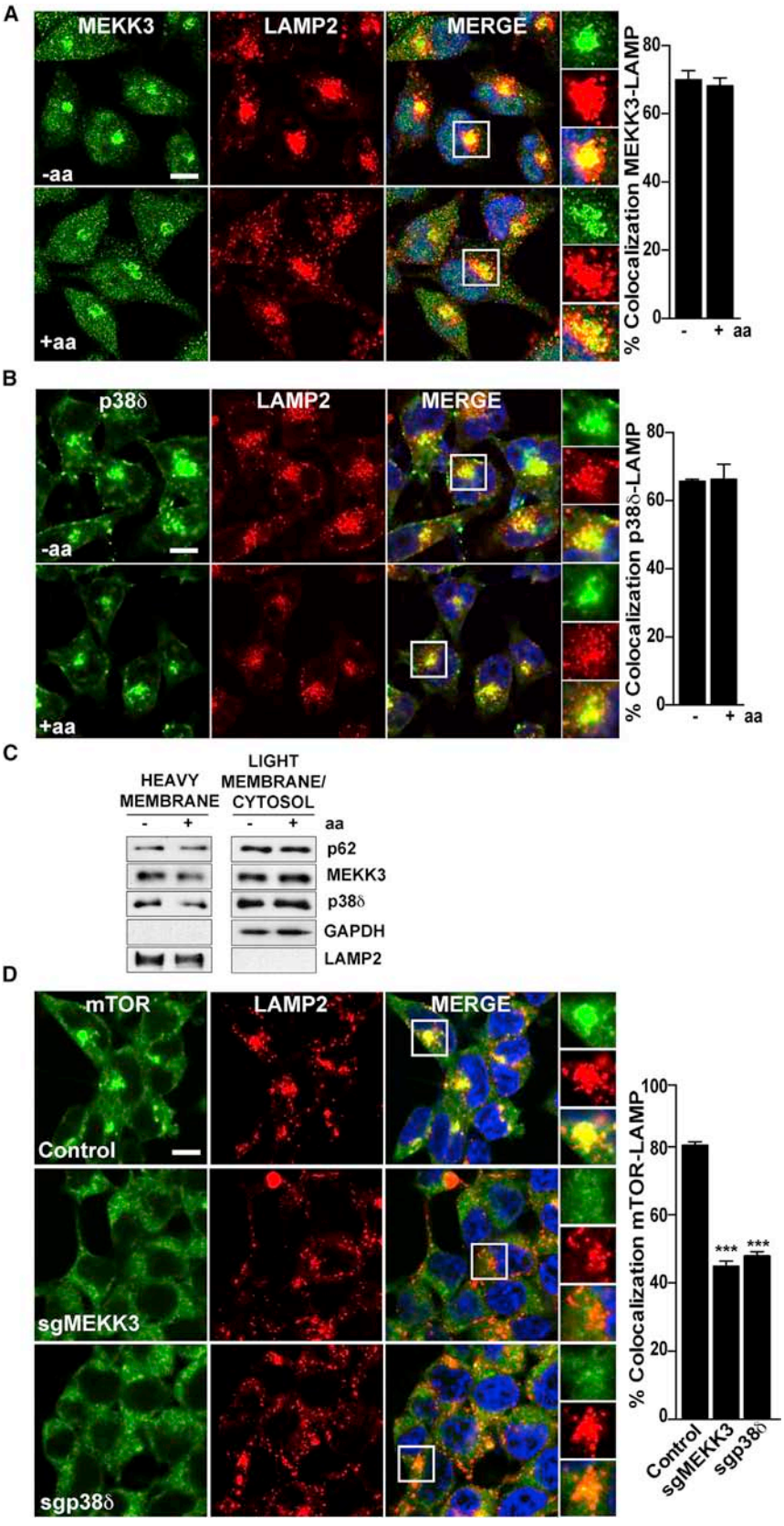

Figure 4. MEKK3/p38δ Cascade Is Required for the Lysosomal Translocation of mTOR

(A and B) MEKK3 and p38δ localize at the lysosome in an amino-acid-independent manner. Images of HeLA cells co-immunostained for MEKK3 and LAMP2 (A) or p38δ and LAMP2 (B) are shown. Cells were starved for 50 min and then stimulated with amino acids for 10 min before processing. In all images, graphs show the areas of staining overlap (merge). The scale bars represent 10 μm. The quantification of colocalization was carried out on at least 15 cells per condition from two independent experiments. Results are shown as means ± SEM.

(C) MEKK3, p38δ, and p62 were present in the lysosomal fraction. HEK293T cells were treated as in (A), and lysates were separated into heavy membrane and light/cytosolic fractions.

(D) MEKK3 and p38δ deficiency prevented amino-acid-induced translocation of mTOR to lysosomes. Images of control, MEKK3-deficient, or p38δ-deficient HEK293T cells treated and analyzed as in (A) that were co-immunostained to detect mTOR and LAMP2 are shown. The scale bars represent 10 μm. Results are shown as means ± SEM. ***$p < 0.001$. Images are representative of two independent experiments. See also Figure S4.

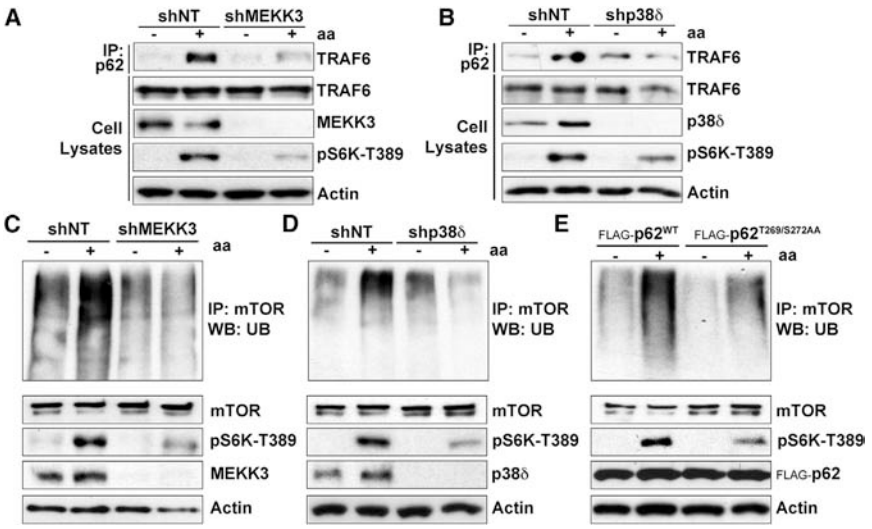

Figure 5. The MEKK3/p38δ Cascade Was Required for TRAF6-Catalyzed K63 Polyubiquitination of mTOR in Response to Amino Acids

(A and B) Knockdown of MEKK3 or p38δ impaired the interaction of TRAF6 with p62 in response to amino acids. shNT, shMEKK3, or shp38δ HEK293T cells were deprived of amino acids for 50 min and then restimulated with amino acids for 30 min. Cell lysates and p62 immunoprecipitates were analyzed by western blot for the indicated proteins.

(C–E) MEKK3, p38δ, and p62 phosphorylation were required for polyubiquitination of mTOR in response to amino acids. shNT, shMEKK3, and shp38δ HEK293T cells or cells stably expressing FLAG-p62^{WT} or FLAG-p62$^{T269/S272AA}$ were treated as in (A). Cell lysates and mTOR immunoprecipitates were immunoblotted for the indicated proteins.

Results are representative of three experiments.

not interact with TRAF6 in amino-acid-stimulated cells (Figure 1I). As predicted by this model, endogenous polyubiquitination of mTOR in response to amino acids was severely inhibited by the deficiency of either MEKK3 or p38δ (Figures 5C and 5D). Furthermore, the endogenous polyubiquitination of mTOR in response to amino acids was inhibited in cells expressing the p62$^{T269/S272AA}$ mutant compared with those expressing p62^{WT} (Figure 5E). Collectively, these data demonstrate that p62 phosphorylation by p38δ is a key event in the recruitment of mTORC1 to the lysosome and in its subsequent activation by TRAF6-mediated polyubiquitination.

The MEKK3/p38δ Cascade Contributes to Cell Proliferation and Autophagy

A well-established function of mTORC1 is to control cell size (Fingar et al., 2002). In keeping with a critical role for MEKK3 and p38δ in the activation of mTORC1, cells deficient in MEKK3, p38δ, or p62 were significantly smaller than WT controls (Figure 6A). On the other hand, it is known that mTORC1 activation promotes cell proliferation and transformation while inhibiting autophagy (Kim et al., 2011; Yu et al., 2010). Consistent with this, the knockdown of MEKK3 or p38δ in PC3 prostate cancer (PCa) cells significantly reduced cell proliferation under normal growing conditions (Figures 6B and 6C), and this effect was rescued by the expression of a constitutively active mutant of RagB (Figures 6D and 6E). Given that nutrient starvation induces autophagy through inhibition of mTORC1 (Kim et al., 2011; Yu et al., 2010), we knocked down MEKK3 or p38δ and determined the effect on autophagy. Interestingly, reduction in the levels of either of these kinases resulted in enhanced LC3 processing, which was even more apparent when cells were incubated with bafilomycin A1, an inhibitor of autophagosomal and lysosomal fusion (Figures 6F–6I). We also analyzed autophagic flux using the reporter GFP-mCherry-LC3 (Kimura et al., 2007), which allows the identification of autolysosomes (mCherry-positive/GFP-negative; red dots) and autophagosomes (mCherry-positive/GFP-positive; yellow dots). Our data showed that the total numbers of autophagosomes and autolysosomes under basal and amino acid starvation conditions were higher in the MEKK3- and p38δ-deficient cells (Figures 6J and 6K). Taken together, these results demonstrate that the MEKK3/p38δ cascade modulates autophagy in response to nutrient starvation, consistent with its role in the regulation of mTORC1 activation.

Relevance of the MEKK3/p38δ/p62/mTOR Axis in Prostate Cancer

To investigate the relevance of the p62/MEKK3/p38δ cascade in the activation of mTOR in PCa, we profited from a recently developed technology for creating 3D prostate organoid cultures (Gao et al., 2014; Karthaus et al., 2014). Murine prostate organoids faithfully recapitulate the in vivo phenotypes of genetic PCa mouse models and can be easily manipulated (Gao et al., 2014; Karthaus et al., 2014). Thus, we isolated prostate epithelial cells from PTEN-deficient mice and subjected them to lentiviral infection to selectively knock down MEKK3, p38δ, or p62 and then cultured them in 3D organoid conditions. Interestingly, we found that the inactivation of MEKK3, p38δ, or p62 decreased the efficiency of organoid formation and size of organoids and reverted the hyperplastic phenotype of the PTEN$^{-/-}$ organoids (Figures 7A and 7B). This strongly suggests an important role for the MEKK3/p38δ cascade in PCa. Notably, the deficiency in p62, MEKK3, or p38δ in these organoids resulted in severe impairment of S6K and 4EBP1 phosphorylation in this model (Figure 7C). Consistent with these observations, immunohistochemical analysis of prostates from PTEN$^{+/-}$ mice showed increased expression of MEKK3, p38δ, and p62, as well as the activation of S6 phosphorylation, which was used as a surrogate marker of mTORC1 activity, in PIN areas of the prostate, as compared to normal glands (Figure 7D). Furthermore, we used double immunofluorescence to analyze the colocalization of p38δ either with p62 or with pS6 in sections of human PCa and normal prostate tissue. Of great interest, we found that p62 and p38δ levels were increased and colocalized with enhanced

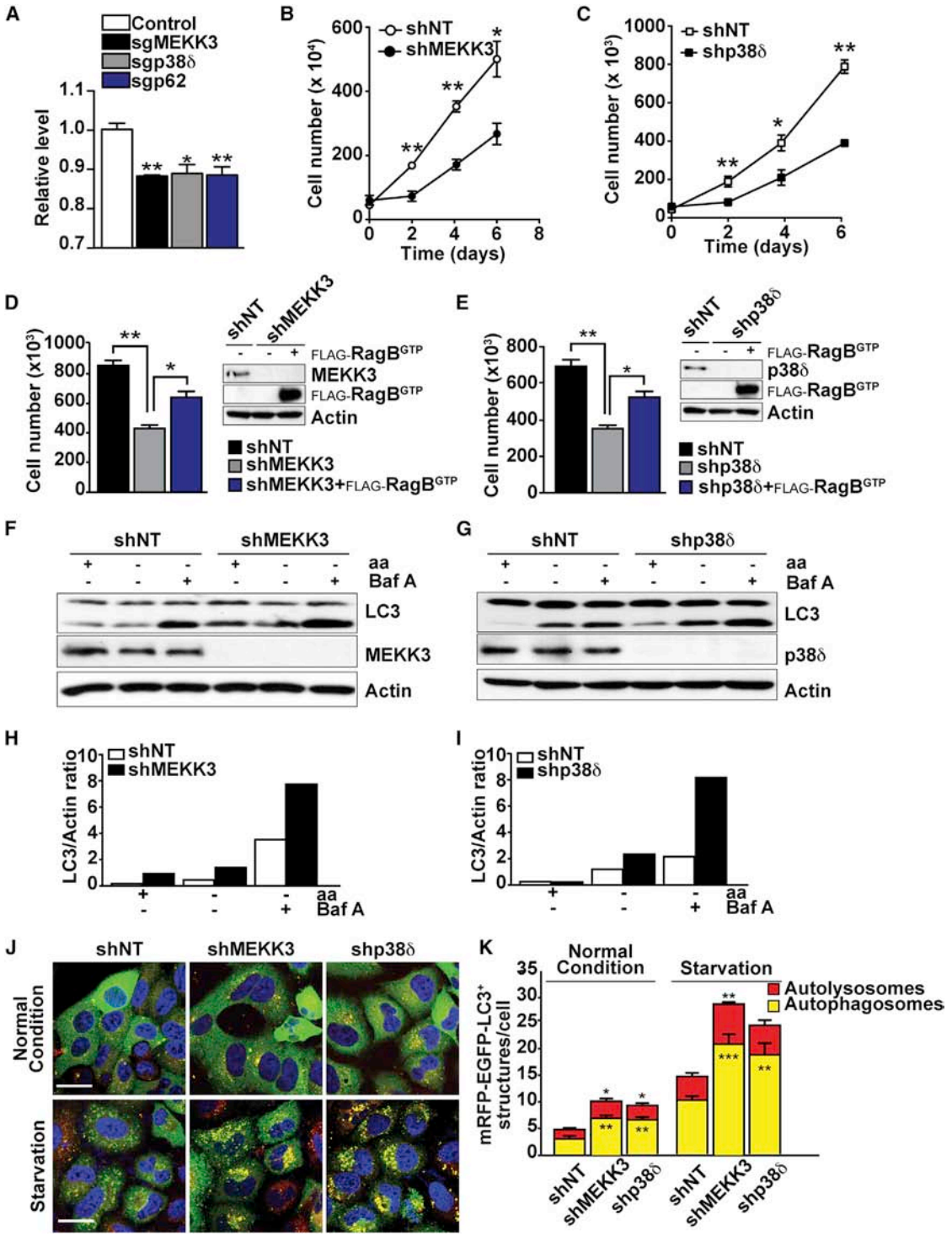

Figure 6. The MEKK3/p38δ Cascade Controlled Cell Proliferation and Autophagy through mTORC1 Activation

(A) MEKK3, p62, or p38δ deficiencies reduced cell size. Results are shown as means ± SEM (n = 3). *p < 0.05; **p < 0.01.

(B and C) Knockdown of MEKK3 or p38δ reduced cell proliferation under normal growing conditions. shNT, shMEKK3, or shp38δ PC3 cells were cultured under normal growing conditions, and cell viability was determined by trypan blue exclusion assay. Results are shown as means ± SEM (n = 3). *p < 0.05; **p < 0.01.

(D and E) RagB^{GTP} overexpression rescued the defects in cell proliferation in MEKK3- or p38δ-knockdown cells. PC3 cells stably expressing FLAG-RagB^{GTP} were infected with shNT, shMEKK3, or shp38δ lentiviral vectors. Cell lysates were analyzed by western blot, and cell viability was determined as in (C). Results are shown as means ± SEM (n = 3). *p < 0.05; **p < 0.01.

(legend continued on next page)

pS6 staining, in tumor tissues as compared to normal controls (Figure 7E). We next analyzed the expression of MEKK3, p38δ, p62, and phospho-S6 in PCa tissue microarrays by immunohistochemistry. Interestingly, our data showed much stronger expression of all these proteins in aggressive tumors with high Gleason score (GS 7–10) than in those with low Gleason score (GS 2–6; Figure 7F). Importantly, MEKK3 and p38δ expression significantly correlated with p62 and phospho-S6 in these human PCa samples (Figure 7G). Taken together, these results established that the PB1-driven MEKK3/p38δ/p62/mTOR pathway is relevant to PCa.

DISCUSSION

The mechanisms whereby cells couple nutrient availability to anabolism and cell growth are being progressively unveiled, and the role of mTORC1 in these processes is well established (Jewell and Guan, 2013; Laplante and Sabatini, 2012; Shimobayashi and Hall, 2014). A major breakthrough in the field was the identification of the lysosome as a critical organelle where mTORC1 is recruited via the Rag proteins and then activated by as-yet-undefined mechanisms. In addition, how mTORC1 senses the availability of nutrients, and specifically of amino acids, is a fundamental problem in the field that needs to be resolved. Here, we show that the signaling adaptor p62, which we previously demonstrated to contribute to mTORC1 activation by amino acids (Duran et al., 2011), is phosphorylated at two specific residues by p38δ through a MEKK3/MEK3/6-driven cascade that enables the recruitment of TRAF6 to the lysosome. This creates a signaling scaffold with the core mTORC1 complex that results in the K63 polyubiquitination of mTOR and its activation in response to amino acids but independent of insulin. Therefore, p62 emerges as a platform that facilitates the recruitment and efficient activation of mTORC1. Interestingly, the specificity of this process is provided by the selective interaction of MEKK3 with p62 through their respective PB1 domains. In this regard, although different MAPKs have previously been implicated in the negative or positive control of mTORC1, primarily in response to stress stimuli (Cully et al., 2010; Li et al., 2003; Wu et al., 2011; Zheng et al., 2011), our data reveal a specific role for p38δ in mTOR activation in the nutrient cascade as part of a PB1-directed complex. Our studies contribute to a better understanding of the activation of mTORC1 by amino acids, but also they provide context for previously reported p62 phosphorylation events. That is, recent data demonstrate that p62 is phosphorylated at S351, which serves to increase its binding affinity for Keap1 and competitively inhibits the Keap1-Nrf2 interaction (Ichimura et al., 2013). This results in the stabilization of Nrf2 and the subsequent expression of genes encoding antioxidant proteins and anti-inflammatory enzymes (Ichimura et al., 2013). Interestingly, at least one of the kinases that can target p62's S351 is mTOR itself. Therefore, it is tempting to speculate that the MEKK3-directed phosphorylation of p62 at T269/S272 serves to activate mTORC1, which then phosphorylates p62's S351 to activate Nrf2 to protect cells from oxidative stress. In cancer, this could be highly relevant because tumor cells need to remove excess ROS while maintaining high levels of proliferation. Therefore, our model predicts that p62 is a crucial regulator of cancer cell proliferation by influencing cell growth through mTORC1 and cell survival through an mTORC1-p62-driven anti-oxidative mechanism.

Interestingly, we have recently reported that MEKK3 is part of another PB1 complex that activates a canonical MEK4/JNK cascade to regulate inflammation in macrophages in response to lipids, another type of nutrients that can trigger an inflammatory response when present in excess (Hernandez et al., 2014). This distinct MEKK3 pathway is orchestrated by the interaction of MEKK3 with NBR1 through their respective PB1 domains (Hernandez et al., 2014). Therefore, two PB1 scaffolds, p62 in mTORC1 and NBR1 in inflammation, use MEKK3 to deliver their respective signals in response to different nutrients. How the interaction of MEKK3 with either p62 or NBR1 orchestrates the p38δ or the JNK pathways, respectively, is not clear and will likely need more-detailed structural studies to be fully understood.

In summary, the work presented here describes a nutrient-sensing pathway that is selectively activated in response to amino acids and is also operative in cancer cells. This kinase cascade is organized by a platform that depends on p62 PB1-domain interactions and is highly upregulated during cancer progression. Different components of the cascade are overexpressed in PCa in a manner that is correlated with tumor stage, which suggests that the cascade is essential for tumor development. Because kinases are eminently druggable targets, our findings have the potential to open new avenues for designing novel treatments for cancer.

EXPERIMENTAL PROCEDURES

Mice

$PTEN^{+/-}$ and $PTEN^{fl/fl}$-PBcre mice were described previously (Fernandez-Marcos et al., 2009). Both mouse strains were generated in a C57BL/6 background. All mice were born and maintained under pathogen-free conditions. Animal handling and experimental procedures conformed to institutional guidelines (Sanford-Burnham Medical Research Institute Institutional Animal Care and Use Committee).

Generation of Knockout Cell Lines

To knock out genes in cell lines, guide RNAs targeting MEKK3, p38δ, and p62 were designed using the CRISPR design tool at http://crispr.mit.edu/ and cloned into a bicistronic expression vector (PX458) containing human-codon-optimized Cas9 fused to EGFP through T2A sequence and the RNA

(F–I) Knockdown of MEKK3 or p38δ promoted autophagy in response to nutrient deprivation. shNT, shMEKK3, or shp38δ PC3 cells were deprived of amino acids and serum for 4 hr in the absence or presence of bafilomycin A1. Cell lysates were immunoblotted for the indicated proteins. Graphs represent LC3-II/actin ratio as measured by densitometry.

(J and K) Knockdown of MEKK3 or p38δ promoted increased autophagic flux. Images of shNT, shMEKK3, or shp38δ cells stably expressing GFP-mCherry-LC3 and treated as in (G) are shown. The scale bars represent 10 μm. Quantification of the number of autophagosomes and autolysosomes per cell is shown. Results are shown as means ± SEM (n = 20). *p < 0.05; **p < 0.01; ***p < 0.001.

Results are representative of three experiments.

Please cite this article in press as: Linares et al., Amino Acid Activation of mTORC1 by a PB1-Domain-Driven Kinase Complex Cascade, Cell Reports (2015), http://dx.doi.org/10.1016/j.celrep.2015.07.045

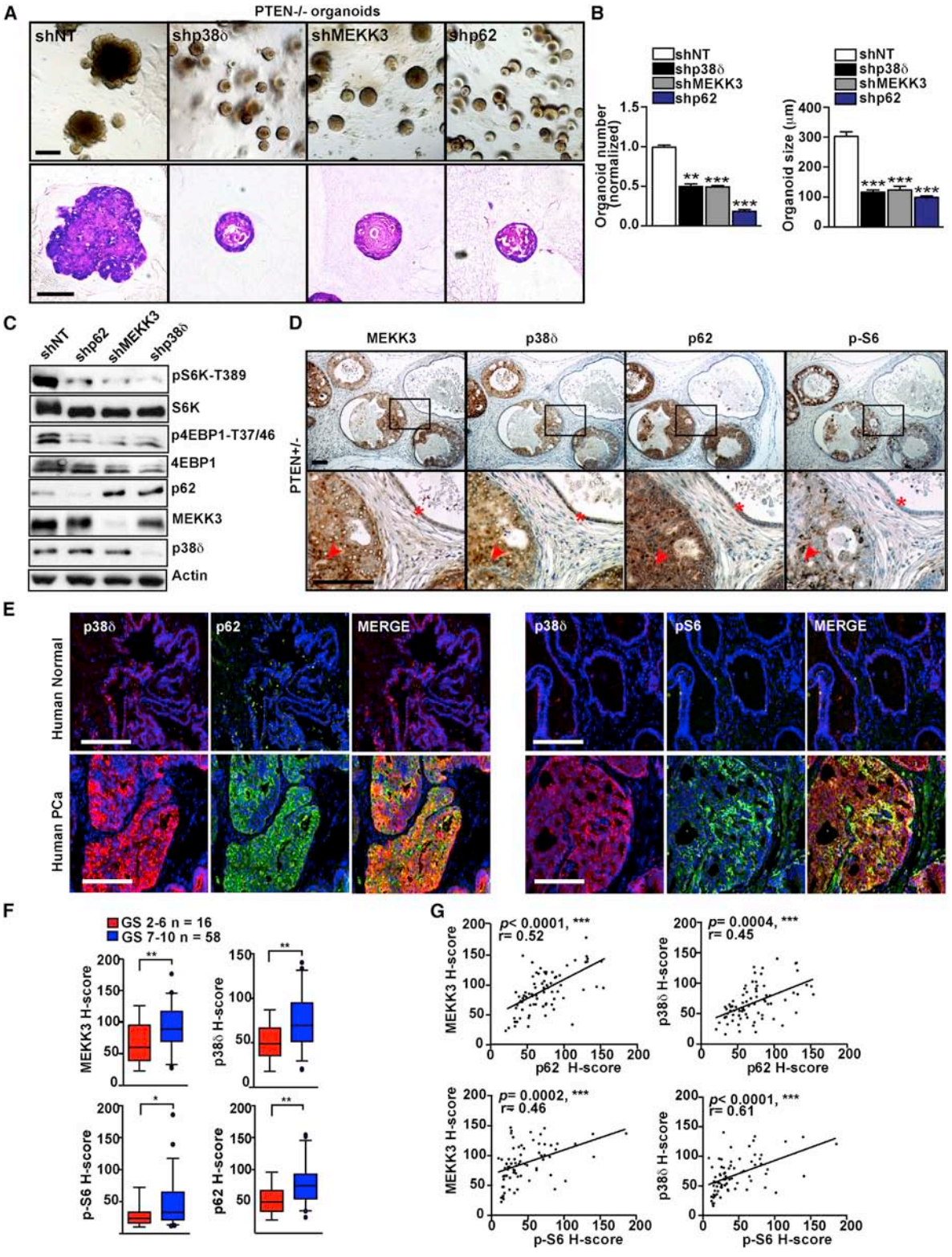

Figure 7. MEKK3/p38δ/p62/mTOR Is Relevant to Prostate Cancer

(A) Knockdown of MEKK3, p38δ, or p62 led to a reduction in the efficiency of organoid formation, size, and hyperplastic phenotype of PTEN-null prostate organoids. Representative images of organoids and H&E staining are shown. Prostate organoids were prepared from PTEN$^{fl/fl}$-PBcre mice and infected with lentiviral vectors for shNT, shp62, shMEKK3, and shp38δ. Organoids were analyzed after 7 days in culture. The scale bars represent 100 μm.

(legend continued on next page)

components (Addgene). Additional detailed procedures are described in the Supplemental Experimental Procedures.

Statistical Analysis

All the statistical tests are justified for every figure. Data are presented as the mean ± SEM. Significant differences between groups were determined using a Student's t test (two-tailed unpaired) when the data met the normal distribution tested by D'Agostino test. If the data did not meet this test, a Mann-Whitney test was used. The significance level for statistical testing was set at $p < 0.05$. All experiments were performed at least two or three times.

SUPPLEMENTAL INFORMATION

Supplemental Information includes Supplemental Experimental Procedures and four figures and can be found with this article online at http://dx.doi.org/10.1016/j.celrep.2015.07.045.

AUTHOR CONTRIBUTIONS

J.F.L. performed most of experiments of this study. A.D. contributed the prostate organoid experiments and IHC staining. M.R.-C. generated CRISPR/CAS9 clones. P.A.-B. contributed to the siRNA screening. A.C. performed the proteomic analysis. M.T.D.-M. and J.M. conceived and supervised the project. M.T.D.-M., J.F.L., and J.M. wrote the manuscript with assistance from all the authors.

ACKNOWLEDGMENTS

NIH grants R01CA132847 (to J.M.), R01CA172025 (to J.M.), R01CA192642 (to M.T.D.-M.), and 5P30CA030199 (to M.T.D.-M. and J.M.) funded this work. Additional support was provided by DoD grants W81XWH-13-1-0353 (to M.T.D-M.) and W81XWH-13-1-0354 (to J.M.). We thank Maryellen Daston for editing this manuscript, Diantha LaVine for the artwork, and Wei Liu and the personnel of the Cell Imaging, Animal Facility, Histology, Functional Genomics, Proteomics, and Viral Vectors Shared Resources at SBMRI for technical assistance.

Received: June 12, 2015
Revised: July 8, 2015
Accepted: July 23, 2015
Published: August 13, 2015

REFERENCES

Bar-Peled, L., Chantranupong, L., Cherniack, A.D., Chen, W.W., Ottina, K.A., Grabiner, B.C., Spear, E.D., Carter, S.L., Meyerson, M., and Sabatini, D.M. (2013). A Tumor suppressor complex with GAP activity for the Rag GTPases that signal amino acid sufficiency to mTORC1. Science *340*, 1100–1106.

Budanov, A.V., and Karin, M. (2008). p53 target genes sestrin1 and sestrin2 connect genotoxic stress and mTOR signaling. Cell *134*, 451–460.

Chantranupong, L., Wolfson, R.L., Orozco, J.M., Saxton, R.A., Scaria, S.M., Bar-Peled, L., Spooner, E., Isasa, M., Gygi, S.P., and Sabatini, D.M. (2014). The Sestrins interact with GATOR2 to negatively regulate the amino-acid-sensing pathway upstream of mTORC1. Cell Rep. *9*, 1–8.

Cully, M., Genevet, A., Warne, P., Treins, C., Liu, T., Bastien, J., Baum, B., Tapon, N., Leevers, S.J., and Downward, J. (2010). A role for p38 stress-activated protein kinase in regulation of cell growth via TORC1. Mol. Cell. Biol. *30*, 481–495.

Durán, R.V., and Hall, M.N. (2012). Regulation of TOR by small GTPases. EMBO Rep. *13*, 121–128.

Duran, A., Linares, J.F., Galvez, A.S., Wikenheiser, K., Flores, J.M., Diaz-Meco, M.T., and Moscat, J. (2008). The signaling adaptor p62 is an important NF-kappaB mediator in tumorigenesis. Cancer Cell *13*, 343–354.

Duran, A., Amanchy, R., Linares, J.F., Joshi, J., Abu-Baker, S., Porollo, A., Hansen, M., Moscat, J., and Diaz-Meco, M.T. (2011). p62 is a key regulator of nutrient sensing in the mTORC1 pathway. Mol. Cell *44*, 134–146.

Efeyan, A., Schweitzer, L.D., Bilate, A.M., Chang, S., Kirak, O., Lamming, D.W., and Sabatini, D.M. (2014). RagA, but not RagB, is essential for embryonic development and adult mice. Dev. Cell *29*, 321–329.

Fernandez-Marcos, P.J., Abu-Baker, S., Joshi, J., Galvez, A., Castilla, E.A., Cañamero, M., Collado, M., Saez, C., Moreno-Bueno, G., Palacios, J., et al. (2009). Simultaneous inactivation of Par-4 and PTEN in vivo leads to synergistic NF-kappaB activation and invasive prostate carcinoma. Proc. Natl. Acad. Sci. USA *106*, 12962–12967.

Fingar, D.C., Salama, S., Tsou, C., Harlow, E., and Blenis, J. (2002). Mammalian cell size is controlled by mTOR and its downstream targets S6K1 and 4EBP1/eIF4E. Genes Dev. *16*, 1472–1487.

Gao, D., Vela, I., Sboner, A., Iaquinta, P.J., Karthaus, W.R., Gopalan, A., Dowling, C., Wanjala, J.N., Undvall, E.A., Arora, V.K., et al. (2014). Organoid cultures derived from patients with advanced prostate cancer. Cell *159*, 176–187.

Groenewoud, M.J., Goorden, S.M., Kassies, J., Pellis-van Berkel, W., Lamb, R.F., Elgersma, Y., and Zwartkruis, F.J. (2013). Mammalian target of rapamycin complex I (mTORC1) activity in ras homologue enriched in brain (Rheb)-deficient mouse embryonic fibroblasts. PLoS ONE *8*, e81649.

Guertin, D.A., and Sabatini, D.M. (2007). Defining the role of mTOR in cancer. Cancer Cell *12*, 9–22.

Hay, N., and Sonenberg, N. (2004). Upstream and downstream of mTOR. Genes Dev. *18*, 1926–1945.

Hernandez, E.D., Lee, S.J., Kim, J.Y., Duran, A., Linares, J.F., Yajima, T., Müller, T.D., Tschöp, M.H., Smith, S.R., Diaz-Meco, M.T., and Moscat, J. (2014). A macrophage NBR1-MEKK3 complex triggers JNK-mediated adipose tissue inflammation in obesity. Cell Metab. *20*, 499–511.

Ichimura, Y., Waguri, S., Sou, Y.S., Kageyama, S., Hasegawa, J., Ishimura, R., Saito, T., Yang, Y., Kouno, T., Fukutomi, T., et al. (2013). Phosphorylation of p62 activates the Keap1-Nrf2 pathway during selective autophagy. Mol. Cell *51*, 618–631.

(B) Quantification of the efficiency of organoid formation and size in the experiment shown in (A). The scale bars represent 100 μm. Results are presented as mean ± SEM. *$p < 0.05$; **$p < 0.01$; ***$p < 0.001$.

(C) Knockdown of MEKK3, p38δ, or p62 in PTEN-null prostate organoids led to decreased mTORC1 activation. Cell lysates from (A) were immunoblotted for the indicated proteins.

(D) Increased expression of MEKK3, p38δ, p62, and S6 phosphorylation in PIN areas (red arrows) of $PTEN^{+/-}$ prostates, compared with normal prostate glands (asterisks). Representative images of MEKK3, p38δ, p62, and phospho-S6 staining of primary PCa samples from $PTEN^{+/-}$ mice are shown. The scale bars represent 25 μm.

(E) Human prostate shows increased expression of p38δ, p62, and S6 phosphorylation in tumor tissue, as compared with normal tissue. Images of human prostate co-immunostained for p38δ and p62 or and p38δ and p-S6 are shown. The scale bars represent 100 μm.

(F) Increased expression of MEKK3, p38δ, p62, and S6 phosphorylation in human prostate tissue microarray (TMA). Box plot graphs show a statistical analysis of MEKK3 ($p = 0.006$), p38δ ($p = 0.004$), p62 ($p = 0.003$), or phospho-S6 ($p = 0.049$) expression in prostate tumors with GS 7–10 compared to prostate tissue with GS 2–6. Results are presented as mean ± SEM. *$p < 0.05$; **$p < 0.01$.

(G) MEKK3 and p38δ expression in human prostate tumors was correlated with p62 and phospho-S6. Correlation plots show the relationship between MEKK3/p62, MEKK3/phosho-S6, p38δ/p62, and p38δ/phospho-S6 (a.u.). The coefficient of correlation (r) and the p value (p) are indicated.

Please cite this article in press as: Linares et al., Amino Acid Activation of mTORC1 by a PB1-Domain-Driven Kinase Complex Cascade, Cell Reports (2015), http://dx.doi.org/10.1016/j.celrep.2015.07.045

Jewell, J.L., and Guan, K.L. (2013). Nutrient signaling to mTOR and cell growth. Trends Biochem. Sci. *38*, 233–242.

Jewell, J.L., Kim, Y.C., Russell, R.C., Yu, F.X., Park, H.W., Plouffe, S.W., Tagliabracci, V.S., and Guan, K.L. (2015). Metabolism. Differential regulation of mTORC1 by leucine and glutamine. Science *347*, 194–198.

Karthaus, W.R., Iaquinta, P.J., Drost, J., Gracanin, A., van Boxtel, R., Wongvipat, J., Dowling, C.M., Gao, D., Begthel, H., Sachs, N., et al. (2014). Identification of multipotent luminal progenitor cells in human prostate organoid cultures. Cell *159*, 163–175.

Kim, J., Kundu, M., Viollet, B., and Guan, K.L. (2011). AMPK and mTOR regulate autophagy through direct phosphorylation of Ulk1. Nat. Cell Biol. *13*, 132–141.

Kimura, S., Noda, T., and Yoshimori, T. (2007). Dissection of the autophagosome maturation process by a novel reporter protein, tandem fluorescent-tagged LC3. Autophagy *3*, 452–460.

Laplante, M., and Sabatini, D.M. (2012). mTOR signaling in growth control and disease. Cell *149*, 274–293.

Li, Y., Inoki, K., Vacratsis, P., and Guan, K.L. (2003). The p38 and MK2 kinase cascade phosphorylates tuberin, the tuberous sclerosis 2 gene product, and enhances its interaction with 14-3-3. J. Biol. Chem. *278*, 13663–13671.

Linares, J.F., Amanchy, R., Greis, K., Diaz-Meco, M.T., and Moscat, J. (2011). Phosphorylation of p62 by cdk1 controls the timely transit of cells through mitosis and tumor cell proliferation. Mol. Cell. Biol. *31*, 105–117.

Linares, J.F., Duran, A., Yajima, T., Pasparakis, M., Moscat, J., and Diaz-Meco, M.T. (2013). K63 polyubiquitination and activation of mTOR by the p62-TRAF6 complex in nutrient-activated cells. Mol. Cell *51*, 283–296.

Matsumoto, G., Wada, K., Okuno, M., Kurosawa, M., and Nukina, N. (2011). Serine 403 phosphorylation of p62/SQSTM1 regulates selective autophagic clearance of ubiquitinated proteins. Mol. Cell *44*, 279–289.

Moscat, J., and Diaz-Meco, M.T. (2009). p62 at the crossroads of autophagy, apoptosis, and cancer. Cell *137*, 1001–1004.

Moscat, J., and Diaz-Meco, M.T. (2011). Feedback on fat: p62-mTORC1-autophagy connections. Cell *147*, 724–727.

Moscat, J., Diaz-Meco, M.T., Albert, A., and Campuzano, S. (2006). Cell signaling and function organized by PB1 domain interactions. Mol. Cell *23*, 631–640.

Nakamura, K., Kimple, A.J., Siderovski, D.P., and Johnson, G.L. (2010). PB1 domain interaction of p62/sequestosome 1 and MEKK3 regulates NF-kappaB activation. J. Biol. Chem. *285*, 2077–2089.

Petit, C.S., Roczniak-Ferguson, A., and Ferguson, S.M. (2013). Recruitment of folliculin to lysosomes supports the amino acid-dependent activation of Rag GTPases. J. Cell Biol. *202*, 1107–1122.

Sabatini, D.M. (2006). mTOR and cancer: insights into a complex relationship. Nat. Rev. Cancer *6*, 729–734.

Sancak, Y., Peterson, T.R., Shaul, Y.D., Lindquist, R.A., Thoreen, C.C., Bar-Peled, L., and Sabatini, D.M. (2008). The Rag GTPases bind raptor and mediate amino acid signaling to mTORC1. Science *320*, 1496–1501.

Sancak, Y., Bar-Peled, L., Zoncu, R., Markhard, A.L., Nada, S., and Sabatini, D.M. (2010). Ragulator-Rag complex targets mTORC1 to the lysosomal surface and is necessary for its activation by amino acids. Cell *141*, 290–303.

Sanchez, P., De Carcer, G., Sandoval, I.V., Moscat, J., and Diaz-Meco, M.T. (1998). Localization of atypical protein kinase C isoforms into lysosome-targeted endosomes through interaction with p62. Mol. Cell. Biol. *18*, 3069–3080.

Shimobayashi, M., and Hall, M.N. (2014). Making new contacts: the mTOR network in metabolism and signalling crosstalk. Nat. Rev. Mol. Cell Biol. *15*, 155–162.

Sumimoto, H., Kamakura, S., and Ito, T. (2007). Structure and function of the PB1 domain, a protein interaction module conserved in animals, fungi, amoebas, and plants. Sci. STKE *2007*, re6.

Thomas, J.D., Zhang, Y.J., Wei, Y.H., Cho, J.H., Morris, L.E., Wang, H.Y., and Zheng, X.F. (2014). Rab1A is an mTORC1 activator and a colorectal oncogene. Cancer Cell *26*, 754–769.

Tsun, Z.Y., Bar-Peled, L., Chantranupong, L., Zoncu, R., Wang, T., Kim, C., Spooner, E., and Sabatini, D.M. (2013). The folliculin tumor suppressor is a GAP for the RagC/D GTPases that signal amino acid levels to mTORC1. Mol. Cell *52*, 495–505.

Valencia, T., Kim, J.Y., Abu-Baker, S., Moscat-Pardos, J., Ahn, C.S., Reina-Campos, M., Duran, A., Castilla, E.A., Metallo, C.M., Diaz-Meco, M.T., and Moscat, J. (2014). Metabolic reprogramming of stromal fibroblasts through p62-mTORC1 signaling promotes inflammation and tumorigenesis. Cancer Cell *26*, 121–135.

Wu, X.N., Wang, X.K., Wu, S.Q., Lu, J., Zheng, M., Wang, Y.H., Zhou, H., Zhang, H., and Han, J. (2011). Phosphorylation of Raptor by p38beta participates in arsenite-induced mammalian target of rapamycin complex 1 (mTORC1) activation. J. Biol. Chem. *286*, 31501–31511.

Yu, L., McPhee, C.K., Zheng, L., Mardones, G.A., Rong, Y., Peng, J., Mi, N., Zhao, Y., Liu, Z., Wan, F., et al. (2010). Termination of autophagy and reformation of lysosomes regulated by mTOR. Nature *465*, 942–946.

Yuan, H.X., Xiong, Y., and Guan, K.L. (2013). Nutrient sensing, metabolism, and cell growth control. Mol. Cell *49*, 379–387.

Zheng, M., Wang, Y.H., Wu, X.N., Wu, S.Q., Lu, B.J., Dong, M.Q., Zhang, H., Sun, P., Lin, S.C., Guan, K.L., and Han, J. (2011). Inactivation of Rheb by PRAK-mediated phosphorylation is essential for energy-depletion-induced suppression of mTORC1. Nat. Cell Biol. *13*, 263–272.

Cell Reports

Supplemental Information

Amino Acid Activation of mTORC1 by a PB1-Domain-Driven Kinase Complex Cascade

Juan F. Linares, Angeles Duran, Miguel Reina-Campos, Pedro Aza-Blanc, Alex Campos, Jorge Moscat, and Maria T. Diaz-Meco

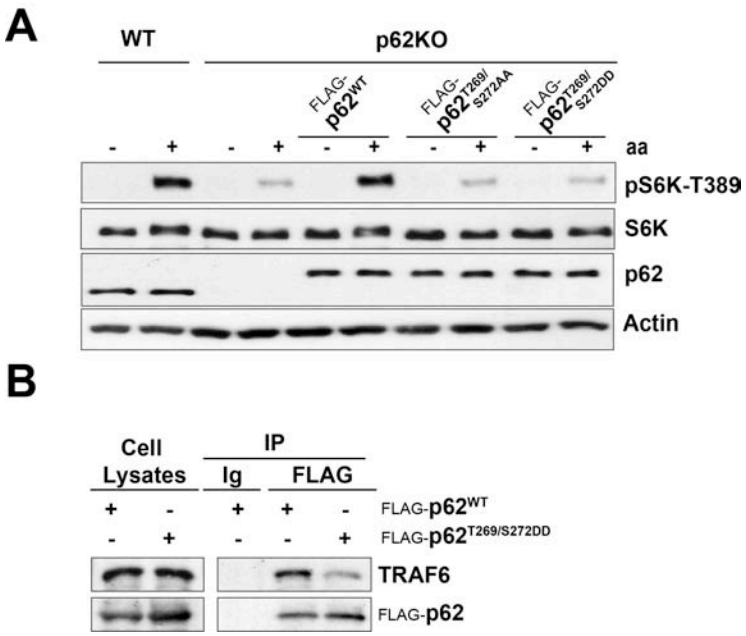

Figure S1. The Mutation of p62 Phosphorylation Sites to Aspartic Acid ,p62$^{T269/S272DD}$, Does Not Mimic p62 Phosphorylation for mTOR Activation and TRAF6 Recruitment in Response to Amino Acids, Related to Figure 1.

(A) The p62$^{T269/S272DD}$ mutant was not able to reconstitute mTOR activation in p62KO MEFs. WT and p62KO MEFs, reconstituted with p62^{WT}, p62$^{T269/S272AA}$, or p62$^{T269/S272DD}$ were starved of amino acids for 50 min and restimulated with amino acids for 20 min. Cell lysates were analyzed by western blot.

(B) The p62$^{T269/S272DD}$ mutant was not able to interact with TRAF6. HEK293T cells, transfected with the indicated plasmid were treated as in (A). Cell lysates and FLAG-tagged immunoprecipitates were immunoblotted to detect the indicated proteins.

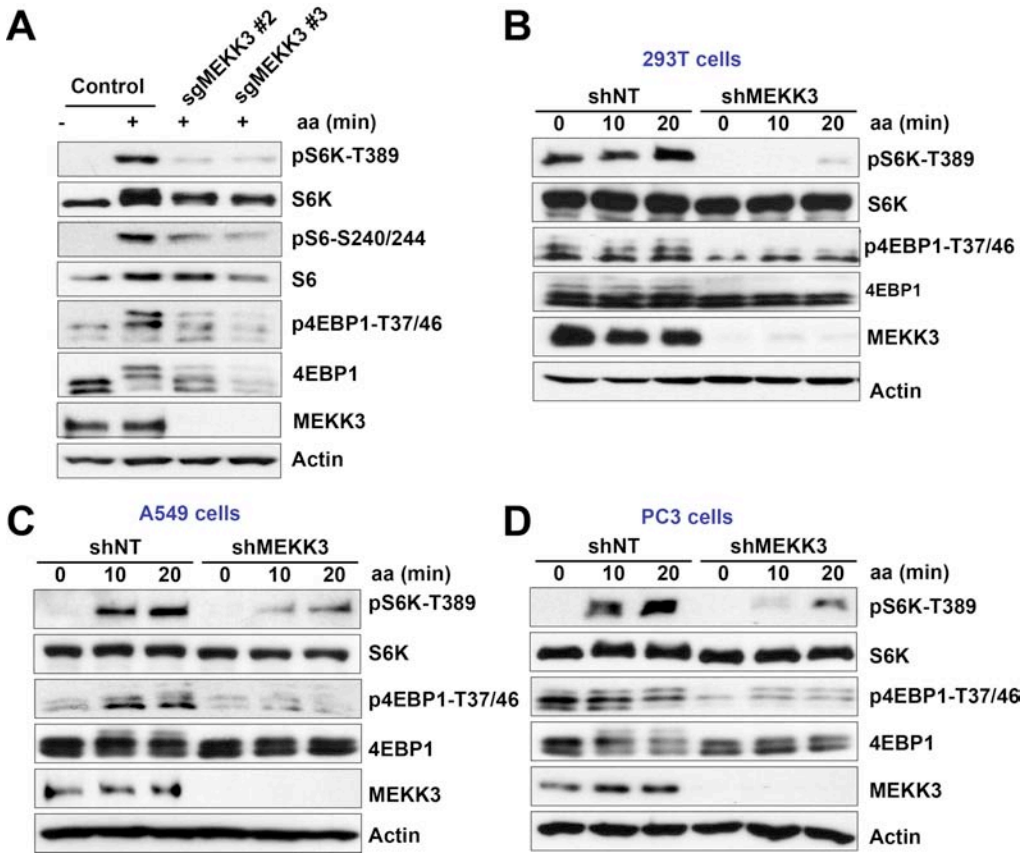

Figure S2. MEKK3 Is Required for mTORC1 Activation in Response to Amino Acids ,Related to Figure 2.

(A) MEKK3 is required for mTOR activation by amino acids. Control or MEKK3-deficient HEK293T cells were deprived of amino acids and serum for 50 min and then stimulated with amino acids for 15 min. Cell lysates were immunoblotted for the specified proteins.

(B) MEKK3 is required for mTOR activation by amino acids. shNT or shMEKK3 HEK293T cells were treated as in (A) and cell lysates were immunoblotted for the specified proteins.

(C-D) MEKK3 is required for mTOR activation by amino acids in different cell lines. shNT or shMEKK3 A549 cells and PC3 cells were treated as in (A), and immunoblotted for the specified proteins.

Results are representative of three experiments.

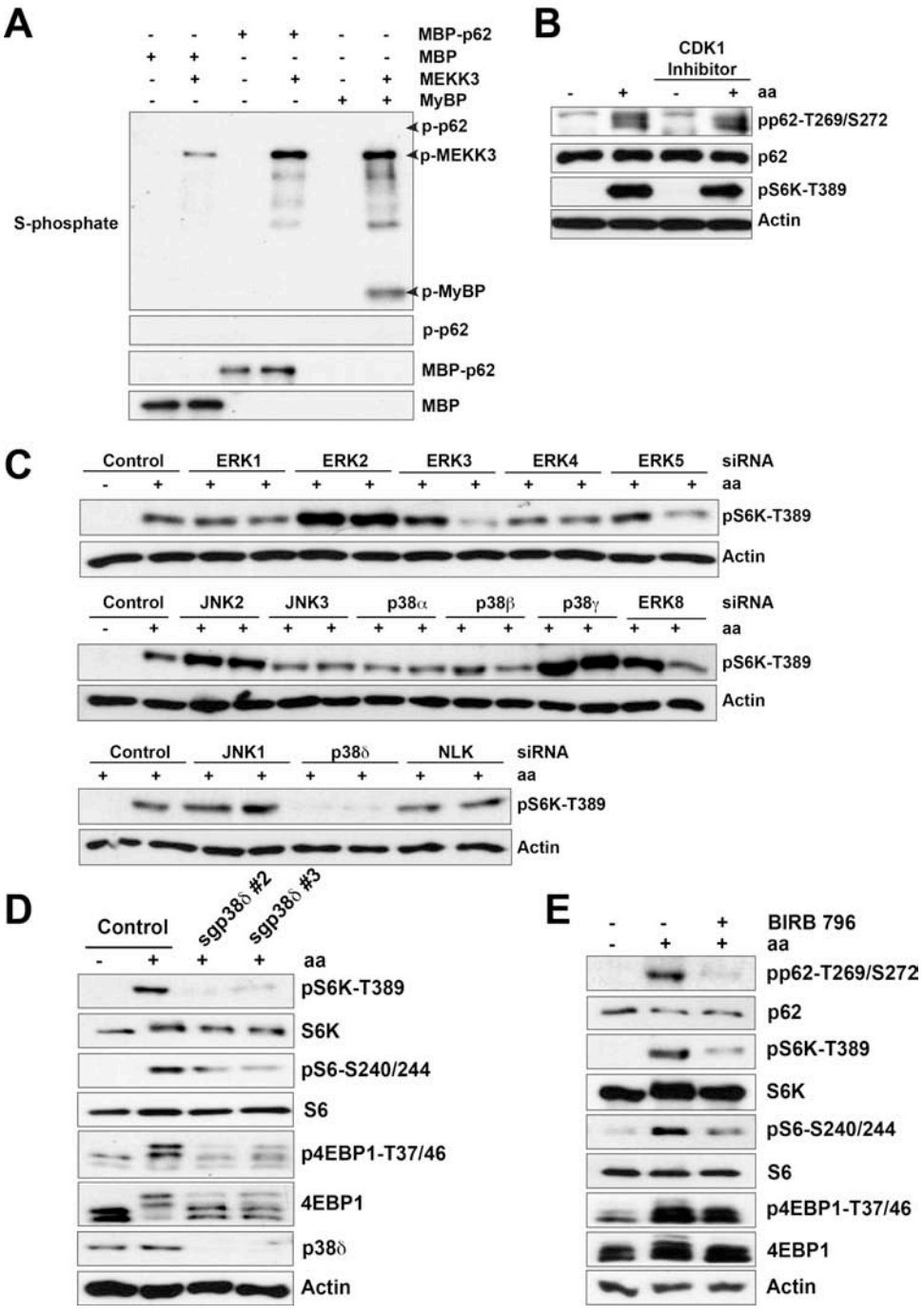
A
MBP-p62
MBP
MEKK3
MyBP
p-p62
p-MEKK3
S-phosphate
p-MyBP
p-p62
MBP-p62
MBP
B
CDK1 Inhibitor
aa
pp62-T269/S272
p62
pS6K-T389
Actin
C
Control
ERK1
ERK2
ERK3
ERK4
ERK5
siRNA
aa
pS6K-T389
Actin
Control
JNK2
JNK3
p38α
p38β
p38γ
ERK8
siRNA
aa
pS6K-T389
Actin
Control
JNK1
p38δ
NLK
siRNA
aa
pS6K-T389
Actin
D
Control
sgp38δ #2
sgp38δ #3
aa
pS6K-T389
S6K
pS6-S240/244
S6
p4EBP1-T37/46
4EBP1
p38δ
Actin
E
BIRB 796
aa
pp62-T269/S272
p62
pS6K-T389
S6K
pS6-S240/244
S6
p4EBP1-T37/46
4EBP1
Actin

Figure S3. p38δ Is Required for mTORC1 Activation and p62 Phosphorylation in Response to Amino Acids, Related to Figure 3.

(A) MEKK3 does not phosphorylate p62 in an in vitro phosphorylation assay with ATPγS.

(B) CDK1 does not phosphorylate p62 in response to amino acids. HEK293T cells, in the presence or absence of purvalanol, were deprived of amino acids for 50 min and then stimulated with amino acids for 20 min. Cell lysates were immunoblotted for the specified proteins.

(C) p38δ is required for mTOR activation by amino acids. HEK293T cells transfected with scramble siRNA or the different MAPK siRNAs were treated as in (B) and cell lysates were then immunoblotted for the specified proteins.

(D) p38δ is required for mTOR activation by amino acids. Control or p38δ-deficient HEK293T cells were treated as in (B) and cell lysates were immunoblotted for the specified proteins.

E) Inhibition of p38 enzymatic activity blocks p62 phosphorylation and mTOR activation by amino acids. HEK293T cells, in the presence or absence of the p38 inhibitor BIRB 796 (10 μM), were treated as in (B). Cell lysates were immunoblotted for the specified proteins

Results are representative of three experiments.

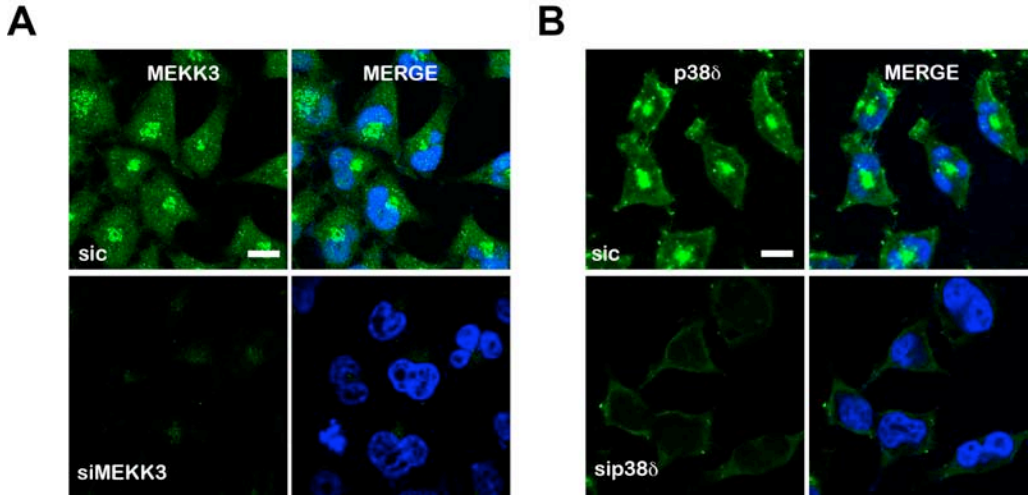

Figure S4. Antibodies Validation for Immunofluorescence, Related to Figure 4.

(A-B) Images of HeLA cells, transfected with scramble siRNA or MEKK3 or p38δ siRNA, coimmunostained for MEKK3 or p38δ and DAPI. Cells were starved for 50 min before processing. Scale bars= 10μm.

Images are representative of two independent experiments.

Supplemental Experimental Procedures

Generation of Knockout Cell Lines

The guide sequences targeting Exon 1 of human MEKK3, p38δ, and p62 are shown below.

MEKK3: 5'- GAACTCAATCATGAACGATC

p38δ: 5'- G TACGTGTCCCCGACGCACGT

p62: 5'-GAAGATCGCCTTGGAGTCCG

The single guide RNAs in the PX458 vector (4μg) were transfected into HEK293T cells using Lipofectamine 2000 according to manufacturer's instructions. 24 hours post transfection, the cells were trypsinized, washed with PBS, and re-suspended in DMEM with 2% FBS and penicillin/streptomycin. GFP-positive cells were single-sorted by FACS (Sanford-Burnham Medical Research Institute FACS core, FACS ARIA) into 96-well plates in DMEM containing 20% FBS and 50μg ml^{-1} penicillin/streptomycin. Single clones were expanded and screened for MEKK3, p38δ, and p62 by protein immunoblotting.

Antibodies and Reagents

Reagents were obtained from the following sources: primary antibodies to HA tag (sc-805), GST tag (sc-138), and Myc tag (sc-40), S6K1 (sc-230), MEKK3 (sc-28769), p38δ (sc-7585), ubiquitin (sc-8017), TRAF6 (sc-7221), and actin (sc-1616); HRP-labeled anti-mouse, anti-mouse IgG1, and anti-goat secondary antibodies were from Santa Cruz Biotechnology. Antibodies to raptor (#2280), phospho-T389 S6K1 (#9205), mTOR (#2983), phospho-T37/46 4EBP1 (#2855), 4EBP1 (#9644), AKT (#9272), phospho-S473 AKT (#4058), LC3 (#4108), phosho-Ser240/244 S6 (#5364), S6 (#2317), and HRP-labeled anti-rabbit secondary antibody were from Cell Signaling Technology. Antibody to

phospho-T269/S272 p62 was from Phospho Solutions. Antibody to LAMP2 (ab25631) was from Abcam, and to human p62 (#610833) from BD biosciences. FLAG antibody (F1804), human recombinant insulin, bafilomycin A1, purvalanol, protein A-sepharose, bovine insulin, RPMI 1640 medium, Y-27632, leucine, and 50x amino acid solution were from Sigma Aldrich. BIRB 796 was from Millipore. DMEM and fetal bovine serum were from Hyclone; FuGENE 6 and Complete Protease Cocktail were from Roche. Alexa 488-, Alexa 555-, and Alexa 568-conjugated secondary antibodies, Lipofectamine 2000, and tyramide signal amplification kits, B27, and Glutamax were from Life Technologies. RPMI 1640 medium modified to be without amino acids was from US Biological; protein G-Sepharose was from Amersham; collagenase type II, DMEM, ADMEM/F12 and TrypLE from GIBCO; EGF 5, R-spondin1, recombinant Noggin from Preprotech; growth factor-reduced Matrigel from Corning; and A83-01 from Tocris.

Isolation and Culture of Prostate Epithelial Cells

Prostate epithelial cells were prepared as previously described (Karthaus et al., 2014) with a few modifications**.** Murine prostates were isolated from 8-week-old $PTEN^{fl/fl}$-PBcre male mice and were placed in 5 mg ml^{-1} collagenase type II in ADMEM/F12 and digested for 1 to 2 h at 37°C. Glandular structures were washed with ADMEM/F12 and centrifuged at 100 G. Subsequently, structures were digested in 5 ml TrypLE with the addition of Y-27632 to 10 µM for 15 min at 37°C. Trypsinized cells were washed and seeded in growth factor-reduced Matrigel. Murine prostate epithelial cells were cultured in ADMEM/F12 supplemented with B27, 10 mM HEPES, Glutamax, and penicillin/streptomycin and containing the following growth factors: EGF 50 ng/ml, R-spondin1-conditioned medium or 500 ng/ml recombinant R-spondin1, 100 ng/ml recombinant Noggin, and the TGF-β/Alk inhibitor A83-01. Murine prostate organoids were passaged either via trituration with a glass Pasteur pipet or trypsinization with

TrypLE for 5 min at 37°C. Lentiviral infections were performed as described previously (Koo et al., 2012) using pLKO.1-puro targeting p62, MEKK3, p38δ, or control scramble. In short, 100,000 single cells were infected with an MOI $1*10^3$. Infection was done during centrifugation for 1 h at 600 G RT. Cells were subsequently placed at 37°C, 5% CO_2 for 3 h to recover. Cells were plated in Matrigel and, 24 h post seeding, 1 µg/ml puromycin was applied for 2 days to ensure only infected cells remained.

Cell Culture

HEK293T, PC3, and A549 cells were from ATCC. p62 KO MEFs were previously described (Duran et al., 2011). Cells were tested for mycoplasma contamination. Cells were cultured in DMEM with 10% FBS. For co-transfection experiments, 0.9 million HEK293T cells were plated in 6 cm culture dishes. 24 hours later, cells were transfected with 500 ng of the expression plasmids. Empty vector was added to transfection mixes to bring the total DNA quantity up to 2 µg. For amino acid starvation, HEK293T cells in 10 cm culture dishes or on coated glass cover slips were rinsed with PBS and incubated in serum and amino acid-free RPMI for 50 minutes. MEFs, PC3, and A549 cells were treated similarly, but starved for 4 hours. Cells were stimulated with a 1X amino acid mixture for different durations, as indicated. After stimulation, the final concentration of amino acids in the media was the same as in RPMI. For insulin stimulation, HEK293T cells were deprived of serum for 24 h and stimulated with 150 nM of insulin. Cells were processed for biochemical or immunofluorescence assays as described below. Cell viability was determined by Trypan Blue exclusion at the indicated times.

Plasmids

pCMV-FLAG-p62, pWZL-Hygro-p62, and pCDNA3-myc-p62 vectors have been described previously (Duran et al., 2011). pCMV-FLAG-p62 T269A/S272A, pCMV-FLAG-p62 T269D/S272D, pWZL-Hygro-p62 T269A/S272A, pCDNA3-myc-p62 D69A/D73A, pCDNA3-FLAG-p38δ T180A/Y182F plasmids were generated by in vitro mutagenesis. The following plasmids were from Addgene: Addgene plasmid 19301, pRK5-HA GST RagBGTP (Sancak et al., 2008); Addgene plasmid 20785, pCDNA3 FLAG-p38δ (Enslen et al., 2000), Addgene plasmid 12186, pCMV5 HA-MEKK3 (Blank et al., 1996); Addgene plasmid 14671, pRc/RSV FLAG MKK3 (Derijard et al., 1995), and Addgene plasmid 22418: mCherry-EGFP-LC3 (Pankiv et al., 2007).

Mammalian Lentiviral shRNAs, siRNAs, and Retroviral Transduction

TRC lentiviral shRNAs targeting human MEKK3 (TRCN0000010692, TRCN0000002305), human p38δ (TRCN0000055428), mouse MEKK3 (TRCN0000025250), mouse p62 (TRCN0000098616) and mouse p38δ (TRCN0000023092) were obtained from Sigma. shRNA-encoding plasmids were co-transfected with psPAX2 (Addgene; plasmid 12260) and pMD2.G (Addgene; plasmid 12259) packaging plasmids into actively growing HEK293T cells by using FuGENE 6 transfection reagent. Virus-containing supernatants were collected 48 hours after transfection, filtered to eliminate cells, and then used to infect target cells in the presence of 8 μg/ml polybrene. Cells were analyzed on the third day after infection. For MAPK siRNA screening, two pools of four siRNAs against each target from two different sources (Dharmacon and Ambion) were used. siRNAs were co-transfected into actively growing cells by using Lipofectamine transfection reagent. Cells were analyzed on the second day after transfection. Retroviruses were produced in Phoenix cells by transient

transfection using Lipofectamine. Culture supernatants were collected 24, 48, and 72 h post-transfection, filtered, and supplemented with 8 μg/ml polybrene. Cells were infected with three rounds of viral supernatants and selected with hygromycin (75 μg/ml).

Cell Lysis, Immunoprecipitation, Fractionation, and Immunoblotting

Cells were rinsed once with ice-cold PBS and lysed in ice-cold lysis buffer (40 mM HEPES [pH 7.4], 120 mM NaCl, 1 mM EDTA, 10 mM pyrophosphate, 10 mM glycerophosphate, and 0.3% CHAPS, and one tablet of EDTA-free protease inhibitors [Roche] per 25 ml). The soluble fractions of cell lysates were isolated by centrifugation at 13,000 rpm for 15 minutes. For immunoprecipitations, primary antibodies were added to the lysates and incubated with rotation overnight at 4°C. 40 μl of a 50% slurry of protein G-sepharose or protein A-sepharose was then added and the incubation was continued for an additional 1 hour. Immunoprecipitates were washed three times with lysis buffer. Fractionation of lysates into heavy membrane and light membrane/cytosolic fractions was performed as described (Menon et al., 2014), In brief, HEK293T cells from two near-confluent 15-cm dishes per treatment were washed with cold PBS, scraped into cold PBS, pelleted by centrifugation at 800 g for 2 min at 4°C, and re-suspended in 300 μl cold hypotonic lysis buffer (10 mM HEPES, pH 7.2, 10 mM KCl, 1.5 mM $MgCl_2$, 20 mM NaF, 100 μM sodium orthovanadate, 250 mM sucrose, with freshly added protease inhibitors). Cells were mechanically lysed by drawing 4 times through a 23G needle and then centrifuged at 500 g for 10 min at 4°C, yielding a post-nuclear supernatant (PNS). The PNS was centrifuged at 20,000 g for 2 hr to separate the soluble supernatant (light membrane/cytosolic fraction) from the insoluble pellet (heavy membrane fraction). The pellet was resuspended in RIPA buffer (40 mM HEPES, pH 7.4, 120 mM NaCl, 1 mM EDTA, 1% Triton X-100, 0.1% SDS, 1% Na deoxycholate, 5% glycerol, 10 mM sodium pyrophosphate, 10 mM glycerol 2-phosphate, 50 mM NaF,

0.5 mM sodium orthovanadate, and 1:100 protease inhibitors). Cell extracts or immunoprecipitated proteins were denatured by the addition of 20 μl of sample buffer and boiling for 5 minutes, resolved by 8%–14% SDS-PAGE, and then transferred to nitrocellulose-ECL membranes (GE Healthcare). The immune complex was detected by chemiluminescence (Thermo Scientific).

In Vitro Kinase-Assay and MS/MS Phosphopeptide Identification

For in vitro phosphorylation assays, 1 μg of recombinant MBP-p62 was incubated at 30 ºC for 60 min in kinase assay buffer containing 25 mM Tris-HCl (pH 7.5), 5 mM $MgCl_2$, 0.5 mM EGTA, 1 mM DTT, and 100 μM ATP in the presence of recombinant MEKK3 or p38δ. For ATP analog-based phosphorylation detection, the protocol described previously (Allen et al., 2007) was followed with minor modifications. Briefly, 100 μM of ATPγS (Biolog) was added to the reaction, after which PNBM (Abcam) and EDTA were added to a final concentration of 2.5 mM and 20 mM, respectively, and incubated for 1 h at room temperature. Immunoblotting detection was performed with anti-thiophosphate ester antibody from Cell Signaling. Protein digestion, TiO2-based phosphopeptide enrichment, electrospray ionization-liquid chromatography tandem mass spectrometry, and MS/MS analysis were performed as described previously (Ma et al., 2013).

Ubiquitin Detection Assay

Detection of endogenous in vivo mTOR ubiquitination was performed as described (Xiong et al., 2009). In brief, HEK293T cells were lysed with cell lysis buffer (2% SDS, 150 mM NaCl, 10 mM Tris-HCl, pH 8.0, with 2mM sodium orthovanadate, 50 mM sodium fluoride, and protease inhibitors). Cell lysates were boiled for 10 min to dissociate protein-protein interactions. The samples were diluted with dilution buffer (10

mM Tris-HCl [pH 8.0], 150 mM NaCl, 2 mM EDTA, 1% Triton). The diluted samples were incubated at 4°C for 60 min with rotation and then centrifuged for 30 min. Cell lysate was incubated with mTOR antibody overnight, after which Protein A beads were added for an additional 1 h. Immunoprecipitates were washed with washing buffer (10 mM Tris-HCl, pH 8.0, 1 M NaCl, 1 mM EDTA, 1% NP-40). Proteins were eluted in SDS-sample buffer, subjected to SDS-PAGE, transferred to nitrocellulose membrane, and immunoblotted with anti-ubiquitin.

Histological Analysis

Prostate organoids and prostates from 10-month-old $PTEN^{+/-}$ male mice were isolated, rinsed in ice-cold PBS, fixed in 10% neutral buffered formalin for 24 h, dehydrated, and embedded in paraffin. Sections (5 μm) were stained with hematoxylin and eosin (H&E). For immunohistochemistry, sections were deparaffinized, rehydrated, and then treated for antigen retrieval. After blocking in avidin/biotin solutions (Vector Laboratories), tissues were incubated with primary antibody overnight at 4 °C, followed by incubation with biotinylated secondary antibody. Endogenous peroxidase was quenched in 3% H_2O_2 in water at room temperature. Antibodies were visualized with avidin/biotin complex (Vectastain Elite; Vector Laboratories) using diaminobenzidine as the chromagen. Human prostate tissue microarray (TMA) slides were obtained from US Biomax. Stained TMA slides were scanned by using the Scanscope XT system (Aperio) and images were captured using the Aperio ImageScope software (v11.1.2.760). For the quantitative analysis, a Histo-score (H score) was calculated based on the staining intensity and percentage of stained cells using the Aperio ScaScope systems.

Immunofluorescence Assays and Colocalization Measurements

HeLa, HEK293T, and A549 cells were plated on fibronectin-coated glass coverslips in 24-well tissue culture plates. 24 hours later, cells were amino acid starved, and then stimulated with amino acids as described above, rinsed with PBS once, fixed with warmed 4% formaldehyde, and permeabilized with 0.1% Triton X-100. Fixed cells on cover slips or sections from human prostate samples, previously deparaffinized, were blocked for one hour in blocking buffer (0.3% BSA in PBS) and then incubated with primary antibody in blocking buffer overnight at 4°C. Samples were then rinsed twice with blocking buffer and incubated with secondary antibodies for one hour at room temperature in the dark, followed by tyramide signal amplification. Slides were mounted on Mowiol and examined with a FluoView 1000 Olympus Laser Point Scanning Confocal Microscope. The colocalization plugin in ImageJ (NIH) was applied to measure co-localization between two channels of confocal z stacks (a constant threshold for all the images within each experiment was applied). A maximum-intensity projection was generated, and the area of co-localizing pixels was quantified using the JACoP plugin in ImageJ, and expressed as the total area of colocalization per cell. Quantification was carried out on at least 15 cells per condition from two independent experiments.

Cell-Size Determinations

For measurement of cell size, triplicates of each sample were analyzed using Countess Automated cell counter (Invitrogen).

Supplemental References

Allen, J.J., Li, M., Brinkworth, C.S., Paulson, J.L., Wang, D., Hubner, A., Chou, W.H., Davis, R.J., Burlingame, A.L., Messing, R.O.*, et al.* (2007). A semisynthetic epitope for kinase substrates. Nat Methods *4*, 511-516.

Blank, J.L., Gerwins, P., Elliott, E.M., Sather, S., and Johnson, G.L. (1996). Molecular cloning of mitogen-activated protein/ERK kinase kinases (MEKK) 2 and 3. Regulation of sequential phosphorylation pathways involving mitogen-activated protein kinase and c-Jun kinase. J Biol Chem *271*, 5361-5368.

Derijard, B., Raingeaud, J., Barrett, T., Wu, I.H., Han, J., Ulevitch, R.J., and Davis, R.J. (1995). Independent human MAP-kinase signal transduction pathways defined by MEK and MKK isoforms. Science *267*, 682-685.

Duran, A., Amanchy, R., Linares, J.F., Joshi, J., Abu-Baker, S., Porollo, A., Hansen, M., Moscat, J., and Diaz-Meco, M.T. (2011). p62 is a key regulator of nutrient sensing in the mTORC1 pathway. Mol Cell *44*, 134-146.

Enslen, H., Brancho, D.M., and Davis, R.J. (2000). Molecular determinants that mediate selective activation of p38 MAP kinase isoforms. EMBO J *19*, 1301-1311.

Karthaus, W.R., Iaquinta, P.J., Drost, J., Gracanin, A., van Boxtel, R., Wongvipat, J., Dowling, C.M., Gao, D., Begthel, H., Sachs, N.*, et al.* (2014). Identification of multipotent luminal progenitor cells in human prostate organoid cultures. Cell *159*, 163-175.

Koo, B.K., Stange, D.E., Sato, T., Karthaus, W., Farin, H.F., Huch, M., van Es, J.H., and Clevers, H. (2012). Controlled gene expression in primary Lgr5 organoid cultures. Nat Methods *9*, 81-83.

Ma, L., Tao, Y., Duran, A., Llado, V., Galvez, A., Barger, J.F., Castilla, E.A., Chen, J., Yajima, T., Porollo, A.*, et al.* (2013). Control of Nutrient Stress-Induced Metabolic Reprogramming by PKCzeta in Tumorigenesis. Cell *152*, 599-611.

Menon, S., Dibble, C.C., Talbott, G., Hoxhaj, G., Valvezan, A.J., Takahashi, H., Cantley, L.C., and Manning, B.D. (2014). Spatial control of the TSC complex integrates insulin and nutrient regulation of mTORC1 at the lysosome. Cell *156*, 771-785.

Pankiv, S., Clausen, T.H., Lamark, T., Brech, A., Bruun, J.A., Outzen, H., Overvatn, A., Bjorkoy, G., and Johansen, T. (2007). p62/SQSTM1 binds directly to Atg8/LC3 to facilitate degradation of ubiquitinated protein aggregates by autophagy. J Biol Chem *282*, 24131-24145.

Sancak, Y., Peterson, T.R., Shaul, Y.D., Lindquist, R.A., Thoreen, C.C., Bar-Peled, L., and Sabatini, D.M. (2008). The Rag GTPases bind raptor and mediate amino acid signaling to mTORC1. Science *320*, 1496-1501.

Xiong, H., Wang, D., Chen, L., Choo, Y.S., Ma, H., Tang, C., Xia, K., Jiang, W., Ronai, Z., Zhuang, X.*, et al.* (2009). Parkin, PINK1, and DJ-1 form a ubiquitin E3 ligase complex promoting unfolded protein degradation. J Clin Invest *119*, 650-660.

Cell Research (2015) 25:537-538.

www.nature.com/cr

RESEARCH HIGHLIGHT

Nutrient stress revamps cancer cell metabolism

Cell Research (2015) **25**:537-538. doi:10.1038/cr.2015.38; published online 31 March 2015

Efforts to identify new therapeutic targets in cancer primarily focused on oncogenes and tumor suppressor genes, and their mechanisms of action. However, there is an emerging alternative strategy that involves identification of target proteins that are not encoded by oncogenes, but are, nonetheless, required to accommodate cancer-specific stresses.

One of the most interesting, and possibly richest, sources for new therapeutic targets is the cellular machinery regulating cancer cell metabolism. Tumor cells normally rely on aerobic glycolysis to maintain cell growth and proliferation, even in the presence of normal concentrations of oxygen [1]. This paradoxical situation makes cancer cells relatively resistant to growth inhibition in conditions of oxygen deprivation, and provides a way to rapidly produce the cellular energy and metabolites required for the high rate of anabolism that drives the dramatically increased proliferation of cancer cells [1]. This is an efficient metabolic mechanism as long as cancer cells have access to a constant supply of glucose. However, cancer cell addiction to a high glucose supply makes them vulnerable and, therefore, susceptible to nutrient stress. Notably, nutrient deprivation has been correlated with poor patient survival [2], suggesting that instead of killing the tumor, the scarcity of nutrients can make the cancer cell stronger. This is likely because the existence of biochemical alterations that allow cancer cells to acquire the plasticity necessary to reprogram their metabolism in response to different nutrient conditions, positioning them better to compete, and thus resulting in a more aggressive tumor. In this regard, the work of Sun and co-workers show that when cancer cells are deprived of glucose or glutamine, the serine biosynthesis pathway (SSP) is activated [3] (Figure 1). These results confirm previous data in colon cancer cells demonstrating that glucose deprivation promotes cell death unless they are deficient in the atypical PKC, PKCζ, and thus they can synthesize serine and glycine from glutamine through a process of "reverse glycolysis" [4]. Interestingly, Sun *et al*. [3] extended these observations and made the important finding that the SSP pathway is activated not only under glucose deprivation condition [4] but also when cells are deprived of glutamine. These observations begged the question, why is the SSP pathway so relevant? The first evidence of the importance of this pathway for tumorigenesis came from the studies of Locasale and co-workers who found that certain cancer cells utilize part of the glycolytic carbon for the serine biosynthetic pathway, which correlated with the amplification of phosphoglycerate dehydrogenase (PHGDH; Figure 1) [5]. Consistent with these data, it was also shown that cell proliferation was severely attenuated by downregulation of PHGDH in cells with an amplified *PHGDH* gene [5]. This suggests that the channeling of glycolytic products to this pathway might have a number of metabolic benefits that cannot be compensated by the import of extracellular serine. Interestingly, Possemato *et al*. [6] also established the 3-phosphoglycerate (3PG) → serine pathway as relevant to cancer, and suggested that the production of α-ketoglutarate from glutamine-derived glutamate during the conversion of phospho-hydroxypyruvate to phospho-serine by PSAT1 was the relevant step for tumorigenesis (Figure 1). More recent data demonstrated that serine-driven one-carbon metabolism, in which oxidation of methylene tetrahydrofolate to 10-formyl-tetrahydrofolate is coupled to reduction of $NADP^+$ to NADPH, is a source of reducing potential with comparable importance to the oxidative pentose phosphate pathway [7]. This pathway also supports another critical component of the cellular redox system, glutathione biosynthesis, as glycine is one of the three amino acids (along with glutamate and cysteine) that compose glutathione. This could explain at least in part why the SSP cascade is so relevant and, according to the recent evidences, so heavily regulated.

In this regard, two very recent studies further support this notion. Gottlieb and co-workers have recently demonstrated that serine is a natural ligand of pyruvate kinase M2 (PKM2), and that serine binding allosterically activates PKM2 enzymatic activity [8]. This has important metabolic implications due to the critical role played by PKM2 in the regulation of the glycolytic flux (Figure 1). Furthermore, Thompson and co-workers presented compelling evidence that PKM2 exerts a regulatory contribution to the serine synthetic pathway [9]. Thus, in the absence of serine, the glycolytic flux to lactate is diminished due to the reduced activity of PKM2, which results in the accumulation of glycolytic intermediates that are diverted to the PHGDH-driven serine biosynthetic pathway [9]. This model implies that cancer cells, by express-

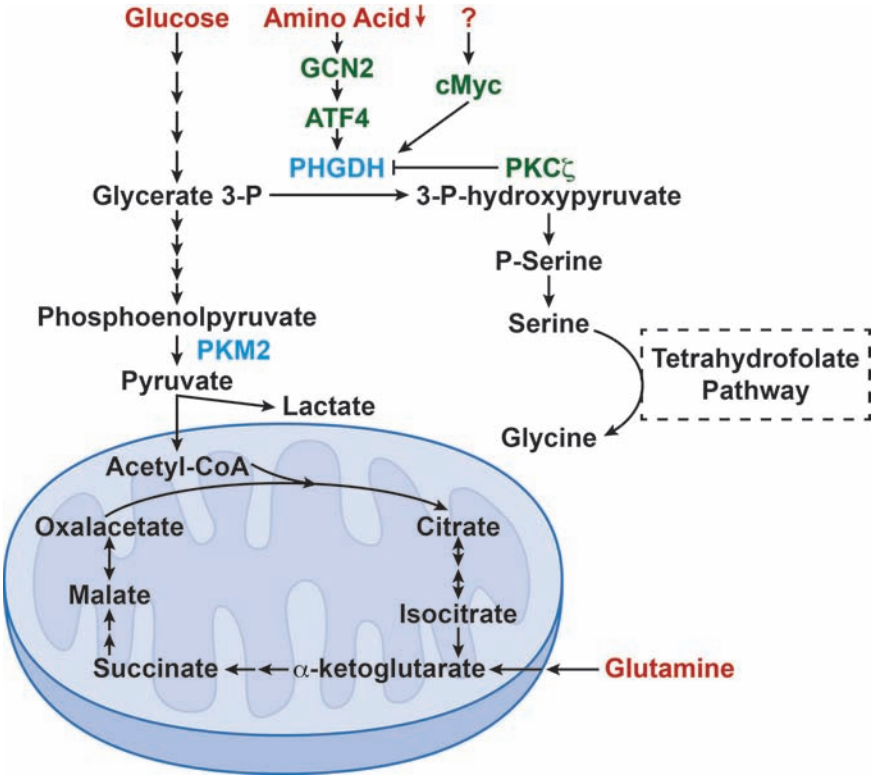

Figure 1 Nutrient sensing and stress in the serine pathway.

ing PKM2, can maintain high levels of anabolism and cell proliferation in the absence of serine in the extracellular milieu. Therefore, the crosstalk between PHGDH and PKM2 appears central to the regulation of cancer metabolism. The results of Sun *et al*. [3] showing that c-Myc stimulated SSP activation by transcriptionally regulating the expression of several SSP enzymes in cancer cells adds another very interesting layer of complexity to the regulation of the pathway. However, much work remains to be done to fully understand this complex regulatory cascades and their relevance in cancer metabolism. For example, it is clear that PHGDH, a critical enzyme in the SSP cascade, is doubly repressed by PKCζ at the transcriptional level and by phosphorylation, which again is consistent with the relevance of this pathway [4]. How this fits with the activation of c-Myc needs to be clarified. In the same vein, the SSP cascade is also controlled by a GCN2 → ATF4 module that acts as a sensor of the extracellular levels of amino acids and that is important for mTORC1 activation [9]. Key questions that remain to be addressed are how nutrient stress regulates c-Myc to impact PHGDH in the context of ATF4 activation and PKCζ activity. Furthermore, recent data from Valencia *et al*. [10] demonstrated that the downregulation of c-Myc in p62/mTORC1-deficient stromal fibroblasts results in impaired SSP that leads to more ROS and inflammation, which creates a more protumorigenic microenvironment in prostate cancer and likely in other tumors. This is important to consider because therapies aimed at blocking c-Myc or mTORC1 at a systemic level will create a more reactive tumor stroma that will likely hamper the therapeutic efficacy of these treatments in the tumor epithelium.

Jorge Moscat[1], Adam Richardson[1], Maria T Diaz-Meco[1]

[1]*Sanford-Burnham Medical Research Institute, La Jolla, CA 92037, USA*
Correspondence: Jorge Moscat
E-mail: jmoscat@sanfordburnham.org

References

1 Vander Heiden MG, Cantley LC, Thompson CB. *Science* 2009; **324**:1029-1033.
2 Le QT, Chen E, Salim A, *et al*. *Clin Cancer Res* 2006; **12**:1507-1514.
3 Sun L, Song L, Wan Q, *et al*. *Cell Res* 2015; **25**:429-444.
4 Ma L, Tao Y, Duran A, *et al*. *Cell* 2013; **152**:599-611.
5 Locasale JW, Grassian AR, Melman T, *et al*. *Nat Genet* 2011; **43**:869-874.
6 Possemato R, Marks KM, Shaul YD, *et al*. *Nature* 2011; **476**:346-350.
7 Fan J, Ye J, Kamphorst JJ, *et al*. *Nature* 2014; **510**:298-302.
8 Chaneton B, Hillmann P, Zheng L, *et al*. *Nature* 2012; **491**:458-462.
9 Ye J, Mancuso A, Tong X, *et al*. *Proc Natl Acad Sci USA* 2012; **109**:6904-6909.
10 Valencia T, Kim JY, Abu-Baker S, *et al*. *Cancer Cell* 2014; **26**:121-135.

Cell

Leading Edge
Minireview

p62 in Cancer: Signaling Adaptor Beyond Autophagy

Jorge Moscat,[1,*] Michael Karin,[2] and Maria T. Diaz-Meco[1]
[1]Cancer Metabolism and Signaling Networks Program, Sanford Burnham Prebys Medical Discovery Institute, 10901 North Torrey Pines Road, La Jolla, CA 92037, USA
[2]Laboratory of Signal Transduction and Gene Regulation Departments of Pharmacology and Pathology, University of California San Diego, 9500 Gilman Drive, La Jolla Ca 92093, USA
*Correspondence: jmoscat@sbpdiscovery.org
http://dx.doi.org/10.1016/j.cell.2016.09.030

Adaptor proteins participate in selective autophagy, which is critical for cellular detoxification and stress relief. However, new evidence supports an autophagy-independent key role of the adaptor p62 (encoded by the gene *Sqstm1)* in signaling functions central to tumor initiation in the epithelium and suppression of tumor progression in the stroma.

Autophagy fulfills two major cellular functions—detoxification through waste removal and conferring resistance to nutrient stress. Autophagy is activated by metabolic emergencies such as nutrient starvation, which results in AMPK activation and mTORC1 inhibition (Galluzzi et al., 2014). The purpose of this "metabolic autophagy" is to provide intracellular energy sources and anabolic building blocks during nutrient shortage, as often happens during cancer progression. In that respect, autophagy might promote tumor growth when cancer cells have limited access to extracellular metabolites and energy sources. This mechanism involves the bulk incorporation of organelles into the autophagosomes without apparent selectivity (Kaur and Debnath, 2015). In contrast, during basal detoxification or waste removal in response to stress, autophagy is thought to require adaptors to target misfolded proteins and dysfunctional organelles to the autophagosomes, while sparing functional cellular constituents (Green and Levine, 2014). This is important because this type of selective autophagy, and its adaptors, maintains cellular wellbeing by preventing ER and oxidative stress. Therefore, selective autophagy, and theoretically its adaptors, function as tumor suppressors by preventing genotoxicity and the accumulation of oncogenic mutations. Consequently, conditions that impair selective autophagy are expected to promote mutagenesis and cancer initiation (Kimmelman, 2011; White, 2012).

Therefore, the signals converging onto the two types of autophagy must be finely balanced to prevent tumor initiation and restrain tumor progression once the cancer cell progenitors have emerged. The incomplete understanding of the intricacies of these pathways is likely the root of the conflicting interpretations of currently available data on the role of autophagy in cancer. Also, the widely accepted conceptual segregation of starvation-induced "bulk" unselective autophagy from nutrient-independent but stress-dependent and adaptor-driven selective autophagy collides with the evidence that the autophagy adaptor p62 is degraded via selective and non-selective autophagy. This, together with the observation that p62 is often upregulated in cancer cells, suggests that a third role of autophagy is to make sure that p62 does not exceed undesired levels. This is important to keep in mind when considering autophagy as a cancer therapeutic target.

Here, we discuss very recent data supporting the notion that p62, in addition to its role in selective autophagy, is a key pro-oncogenic regulator thanks to its function as a signaling hub (Figure 1A). Importantly, high levels of p62 protein in epithelial cells are necessary and sufficient for inducing oncogenic transformation, independent of its autophagy-related functions (Umemura et al., 2016). This model establishes that one of the critical roles of autophagy as a tumor suppressor is to prevent p62-driven tumor initiation and malignant transformation. However, in the non-transformed components of the tumor microenvironment, such as fibroblasts and macrophages, p62 functions as a non-cell-autonomous tumor suppressor that attenuates fibrosis and inflammation (Valencia et al., 2014; Zhong et al., 2016). Therefore, we propose that the homeostatic maintenance of p62 levels in both tumor and stroma by autophagy-dependent or -independent mechanisms will decisively contribute to the final outcome of the tumorigenic process. This has important implications for the design of prospective therapeutic strategies for cancer targeting autophagy or p62-regulated signaling pathways.

p62: An Autophagy Adaptor and Signaling Hub

Although p62 was the first identified autophagy adaptor, four other proteins have similar functions, including NBR1, TAX1BP1, NDP52, and OPTN. p62 was initially found as a signaling regulator residing in the late endosome lysosome (Moscat and Diaz-Meco, 2009). Unlike other autophagy adaptors, with the exception of NBR1, p62 is also a central hub due to its ability to interact with key signaling proteins through well-defined structural elements (Figure 1A)(Moscat and Diaz-Meco, 2009). Thus, p62 can promote the expression of inflammatory genes via NF-κB, which it activates through TRAF6 binding by its TRAF6-binding (TB) domain. p62 also activates the NRF2-dependent anti-oxidant response by sequestering Keap1 through its KIR domain (Figure 1A) (Moscat and Diaz-Meco, 2009). New data also describe that p62 activates mTORC1, which can upregulate c-Myc (Figure 1A) (Duran et al., 2011; Valencia et al., 2014). None of these functions depend on the ubiquitin-associated (UBA) or LC3-interacting region (LIR) domains of p62, which allow it to function as an autophagy adaptor (Figure 1A) (Moscat and

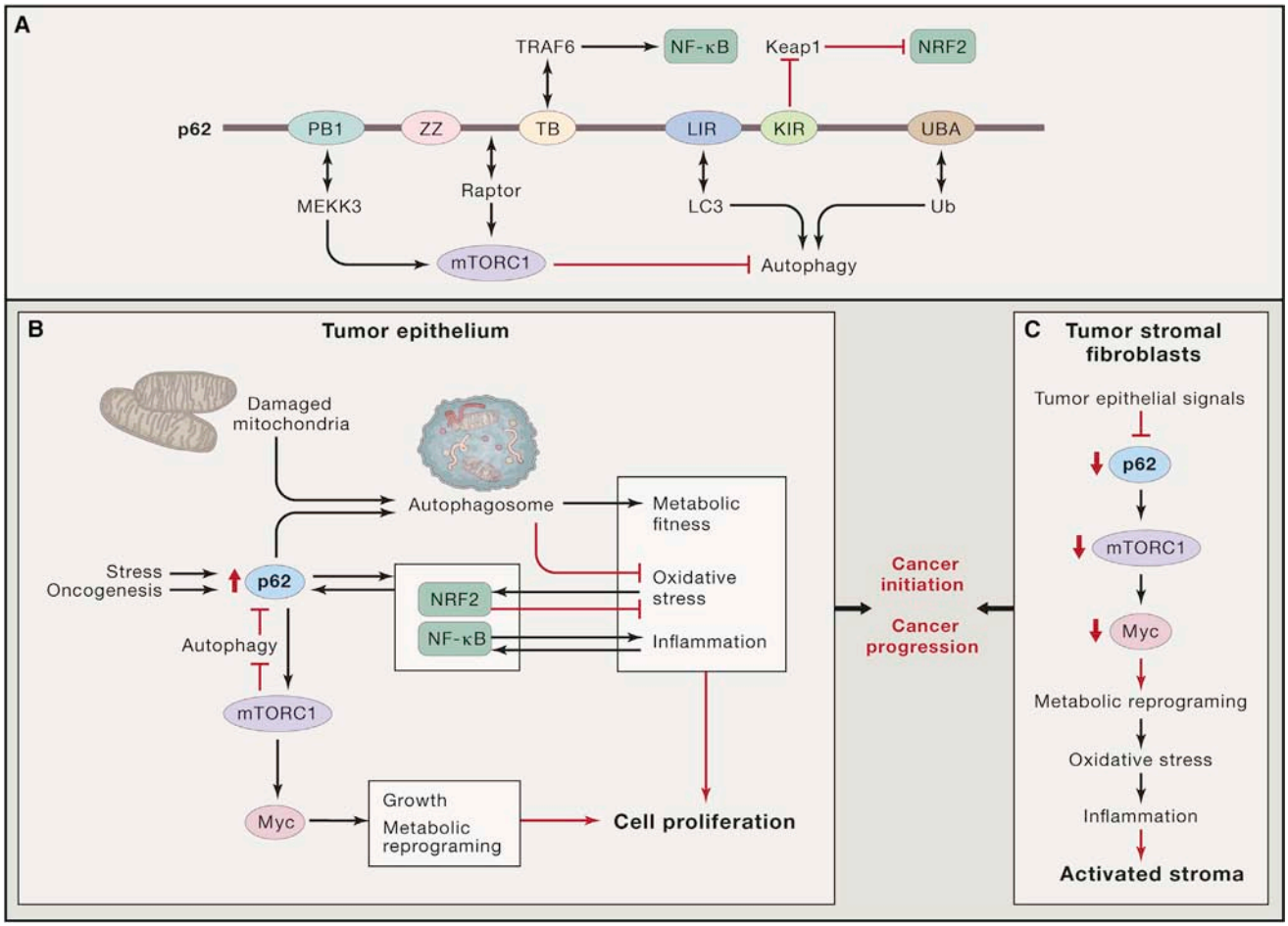

Figure 1. p62 Signaling Functions in the Tumor Epithelium and Stroma

(A) Structural domain organization of p62, binding partners, and signaling functions. p62 has a PB1 domain, a ZZ-type zinc finger domain, a TRAF6-binding (TB) domain, an LC3-interacting region (LIR), a Keap1-interacting region, and a ubiquitin-associated domain (UBA).

(B) Central role of p62 accumulation in the tumor epithelium during cancer initiation through detoxification and mTORC1 activation.

(C) Role of p62 downregulation in the tumor stroma through the inhibition of mTORC1 in metabolic reprogramming and inflammation

Diaz-Meco, 2009). Autophagy, however, plays an important role in the control of p62 levels as it is constantly degraded via non-selective autophagy through its LIR domain that binds to LC3 on autophagosomes' membranes (Moscat and Diaz-Meco, 2009) (Figure 1A). p62 expression is also subjected to positive transcriptional regulation since AP1, NF-κB, and NRF2 can stimulate *Sqstm1* gene transcription (Moscat and Diaz-Meco, 2009) (Figure 1B). Thus, oxidative stress and inflammation induce p62 through NRF2 and NF-κB to promote selective autophagy and cell detoxification. However, just preventing cell death, although it helps tumorigenesis, is not sufficient to initiate cancer since the activation of growth promoting anabolic pathways are required to promote cancer cell growth. In this regard, more recent data demonstrate that p62, due to its location on lysosomes and its ability to bind Raptor and the Rag proteins, regulates mTORC1 activity (Duran et al., 2011). In the presence of growth factors, mTORC1 is activated by the GTPase Rheb (Jewell et al., 2013). Rheb is kept in the inactive GDP form by the tumor suppressive Tsc1/Tsc2 GTPase complex, which is inactivated by PI3K/AKT-mediated phosphorylation triggered by growth factors, and antagonized by the tumor suppressor PTEN (Jewell et al., 2013). Interestingly, p62 deficiency in several cell systems impairs the recruitment of mTORC1 to the lysosomes and its activation in response to amino acids (Duran et al., 2011) and Tsc1 ablation (Umemura et al., 2016).

Of special relevance for the p62-mTORC1 connection, p62 constitutively binds to MEKK3 through their respective PB1 domains (Linares et al., 2015). Upon amino acid stimulation, the p62-MEKK3 complex orchestrates a kinase cascade that includes the activation of MKK3/6 by MEKK3-mediated phosphorylation and the subsequent activation of p38δ (Linares et al., 2015). This results in the direct phosphorylation of p62 at residues T269 and S272 by p38δ, which promotes the recruitment of TRAF6 to the mTORC1 complex resulting in the K63-type polyubiquitination of mTOR, which is important for its efficient activation (Linares et al., 2013) (Figure 1A). Since mTORC1 stimulates several anabolic pathways that promote cell growth and proliferation as well as c-Myc expression, these findings reveal

that p62 not only controls cell survival of normal and cancer cells, but also contributes to cell growth and, when upregulated, to cancer cell proliferation. A link between p62 accumulation and c-Myc expression is observed in prostate cancer stromal fibroblasts (Valencia et al., 2014) and hepatocellular carcinomas (HCC) (Umemura et al., 2016).

p62: Epithelial Cell Stress and Cancer

Accumulation of p62 upon impairment of autophagy may exert deleterious effects in normal epithelial cells. Genetic inactivation of autophagy by ablation of critical autophagy (atg) genes in liver parenchymal cells, including hepatocytes, results in a poorly understood chronic liver damage phenotype that is reversed upon global *Sqstm1* gene ablation (Komatsu et al., 2007). Similarly, genetic inactivation of IKKα in pancreatic epithelial cells (PEC) results in chronic pancreatitis that is alleviated upon selective genetic inactivation of *Sqstm1* in the same cells (Li et al., 2013). Those results are surprising given that p62 accumulation triggers the synthesis of a number of detoxifying enzymes that prevent oxidative stress, likely through the upregulation of NRF2, and one would expect that p62 inactivation under autophagy-deficient conditions should result in more damage. A confounding factor in the study examining autophagy deficiency in the liver is that autophagy is selectively inhibited in the liver parenchyma, whereas p62 is globally ablated in all cells (Komatsu et al., 2007). Therefore, in this case, it is very difficult to know if these effects result from p62 deficiency in the non-parenchyma. This potential shortcoming is rectified in a pancreatitis study in which IKKα and p62 are both knocked out in PEC, the same cell type in which p62 specifically accumulates upon IKKα ablation (Li et al., 2013). In that study, p62 removal does not cause any defects in autophagy, but it does reduce ER stress induced by autophagy inhibition in IKKα-deficient PEC (Li et al., 2013). Although how p62 accumulation in autophagy-deficient epithelia results in increased ER stress is not entirely clear yet, it is likely that unrestrained activation of mTORC1 driven by high p62 levels clogs the ER by excessive protein production, which will be an important contributor to the pancreatitis phenotype. Similar observations are made when p62 is specifically ablated in liver parenchymal cells (Umemura et al., 2016).

Interestingly, chronic p62 accumulation occurs in human pancreatitis (Li et al., 2013) and most liver degenerative diseases in which it is present within cytoplasmic inclusions known as Mallory-Denk Bodies (Umemura et al., 2016). High p62 levels promote the activation of NRF2 (Figure 1B), and increased NRF2 also results in the transcriptional activation of the *Sqstm1* gene, further increasing p62 accumulation through a feed-forward loop that promotes cancer initiation (Umemura et al., 2016). This suggests that although a transient increase in NRF2 levels results in protective anti-oxidant responses (DeNicola et al., 2011), chronic NRF2 activation is a common occurrence in many epithelial cancers, including HCC (Umemura et al., 2016). The pro-carcinogenic p62-NRF2 autoregulatory loop has been recently elucidated by studying several models of HCC induction, either by Tsc1 ablation, which causes chronic mTORC1 activation, or non-alcoholic steatohepatitis (NASH), which is characterized by the accumulation of fat in the liver (like steatosis), along with inflammation and cell damage. Although *Sqstm1* inactivation in liver parenchymal cells abrogates the expression of the NRF2-dependent anti-oxidant response, it also results in the disappearance of hepatocytes that accumulate reactive oxygen species (ROS), which presumably serve as HCC-initiating cells (Umemura et al., 2016). The loss of these cells is most likely due to inactivation of the NRF2-mediated protective response as well as inhibition of mTORC1 activation and c-Myc expression (Umemura et al., 2016). Interestingly, although high-fat diet (HFD)-feeding of wild-type mice, which only develop simple steatosis, does not lead to substantial p62 accumulation, HFD-feeding of MUP-uPA mice, which develop NASH, does result in dramatic p62 accumulation and HCC (Nakagawa et al., 2014; Umemura et al., 2016). Altogether, these studies demonstrate that p62 accumulation in a chronically damaged liver is one of the most important factors, together with compensatory proliferation, that leads to HCC development.

The ultimate proof that p62 is an oncogenic protein is that its overexpression in vivo in the liver was sufficient to induce HCC without carcinogen administration or any other additional stimulus (Umemura et al., 2016). Notably, this correlated with increased mTORC1 and NRF2 activities. This effect of p62 is independent of autophagy because overexpression of a p62 variant lacking the UBA domain, and therefore stripped of its autophagy adaptor function, was also sufficient to drive HCC (Umemura et al., 2016). Therefore, therapies aimed at blocking p62 accumulation, or the activation of its downstream targets, would be a potentially new therapeutic approach for prevention of HCC in high-risk individuals. Targeting p62, or the ability of p62 to activate NRF2 and mTORC1, will have the advantage of not abolishing the basal activity of NRF2 or mTORC1, since both pathways are needed for suppression of liver toxicity and maintenance of hepatic integrity and function (Figure 1B) (Umemura et al., 2014).

p62: In the Tumor Microenvironment

In contrast to cancer cells, in which p62 expression is dramatically elevated, many tumors display reduced levels of p62 in their stroma, especially in cancer-associated fibroblasts (CAF) (Valencia et al., 2014). This observation raises interesting questions regarding the function of p62 in the tumor microenvironment, which also plays a critical role in cancer progression. Investigating p62 function in prostate cancer, we find that p62-deficient stromal fibroblasts exhibit increased production of IL-6, which is critical for TGFβ synthesis that converts CAF into activated myofibroblasts that promote tumor progression (Valencia et al., 2014). Importantly, the downregulation of p62 in CAF is needed for acquiring their tumor-promoting function (Valencia et al., 2014). Decreased mTORC1 activity due to the downregulation of p62 expression results in reduced c-Myc levels that lead to a failure in the synthesis of reduced glutathione due to defective metabolic reprogramming and the concomitant increase in ROS levels under conditions of autophagy competence (Valencia et al., 2014). Interestingly, the increased oxidative stress in these stromal cells translated into higher levels of IL-6 that promoted TGFβ synthesis, being both required for CAF activation in p62-deficient prostate cancer stroma (Valencia et al., 2014) (Figure 1C). An important corollary of these studies is that

blocking p62, or directly inhibiting mTORC1, in the stroma will favor tumor progression, which suggests that anti-cancer treatments aimed at reducing the pro-tumorigenic mTORC1 signaling in tumor cells will be counteracted by the undesired effects of mTORC1 inactivation in the stroma. This renders therapies that target mTORC1 in cancer inefficient or even counter-effective. Future studies in other cancer model systems, together with the analysis of more extensive patient's samples will establish the generality of these observations.

The ability of p62 to act as a tumor suppressor in constituents of the tumor microenvironment might also apply to tumor-associated macrophages (TAM), which serve as an important source of tumor-promoting inflammatory signals (Grivennikov et al., 2010; Ruffell and Coussens, 2015). In this regard, selective autophagy dependent on p62 has been reported to be important for clearance of mitochondria that have been damaged due to exposure of macrophages to different stimuli capable of activating the NLRP3 inflammasome (Zhong et al., 2016). Such stimuli induce mitochondrial damage and the release of direct NLRP3-inflammasome activators such as mtDNA and ROS (Zhou et al., 2011). Damaged mitochondria undergo mitophagic clearance through p62 resulting in termination of inflammasome activation and reduced production of the tumor-promoting cytokines IL-1β and IL-18 (Zhong et al., 2016). Many stimuli that lead to NLRP3 inflammasome activation, such as silica microcrystals and asbestos fibers, are carcinogens even though they do not induce any oncogenic mutations. Altogether, these results can explain why genetic inactivation of p62 at an organismal level is associated with increased tumor progression (Valencia et al., 2014), whereas the selective inactivation of p62 in cancer epithelial cells restrains cancer initiation (Umemura et al., 2016).

Conclusions and Outstanding Questions

Although we now know a lot more about p62 and its role in cancer, many issues still need to be investigated. For example, why is p62 degraded during nutrient stress-induced autophagy if this process does not need adaptors? But, even if it does, how can p62 distinguish between different cargos during "bulk" versus "selective autophagy"? And during selective autophagy, how is specificity of cargo recognition achieved? It is unlikely that just the PB1 and the UBA domains will be sufficient for cargo selection by p62. How about the other UBA-containing adaptors? Are they specific for different cargos or do they recognize the same cargos, but the specificity is cell type dependent? Do other adaptors have autophagy-independent signaling capabilities like in the case of p62? Our recent data demonstrating that NBR1 is a new scaffold for JNK activation in response to hyper-nutrition in macrophages suggest that this is the case (Hernandez et al., 2014). However, more data are required to address all these fundamental questions whose resolution will help us understand the function of these proteins in physiologically relevant models including cancer and devise new therapeutics by targeting p62-regulated functions.

ACKNOWLEDGMENTS

Our research is funded by NIH grants R01DK108743 (J.M.), R01CA172025 (J.M.), R01CA163798 (M.K.), R01CA118165 (M.K.), P01DK098108 (M.K.), R01CA192642 (M.T.D.-M.), and 5P30CA030199 (M.T.D-M. and J.M) and by DoD grants W81XWH-13-1-0354 (J.M.) and W81XWH-13-1-0353 (M.T.D-.M.) M.K. holds the Ben and Wanda Hildyard Chair for Mitochondrial and Metabolic Diseases. We thank Diantha LaVine for the artwork.

REFERENCES

DeNicola, G.M., Karreth, F.A., Humpton, T.J., Gopinathan, A., Wei, C., Frese, K., Mangal, D., Yu, K.H., Yeo, C.J., Calhoun, E.S., et al. (2011). Nature *475*, 106–109.

Duran, A., Amanchy, R., Linares, J.F., Joshi, J., Abu-Baker, S., Porollo, A., Hansen, M., Moscat, J., and Diaz-Meco, M.T. (2011). Mol. Cell *44*, 134–146.

Galluzzi, L., Pietrocola, F., Levine, B., and Kroemer, G. (2014). Cell *159*, 1263–1276.

Green, D.R., and Levine, B. (2014). Cell *157*, 65–75.

Grivennikov, S.I., Greten, F.R., and Karin, M. (2010). Cell *140*, 883–899.

Hernandez, E.D., Lee, S.J., Kim, J.Y., Duran, A., Linares, J.F., Yajima, T., Muller, T.D., Tschop, M.H., Smith, S.R., Diaz-Meco, M.T., et al. (2014). Cell Metab. *20*, 499–511.

Jewell, J.L., Russell, R.C., and Guan, K.L. (2013). Nat. Rev. Mol. Cell Biol. *14*, 133–139.

Kaur, J., and Debnath, J. (2015). Nat. Rev. Mol. Cell Biol. *16*, 461–472.

Kimmelman, A.C. (2011). Genes Dev. *25*, 1999–2010.

Komatsu, M., Waguri, S., Koike, M., Sou, Y.S., Ueno, T., Hara, T., Mizushima, N., Iwata, J., Ezaki, J., Murata, S., et al. (2007). Cell *131*, 1149–1163.

Li, N., Wu, X., Holzer, R.G., Lee, J.H., Todoric, J., Park, E.J., Ogata, H., Gukovskaya, A.S., Gukovsky, I., Pizzo, D.P., et al. (2013). J. Clin. Invest. *123*, 2231–2243.

Linares, J.F., Duran, A., Yajima, T., Pasparakis, M., Moscat, J., and Diaz-Meco, M.T. (2013). Mol. Cell *51*, 283–296.

Linares, J.F., Duran, A., Reina-Campos, M., Aza-Blanc, P., Campos, A., Moscat, J., and Diaz-Meco, M.T. (2015). Cell Rep. *12*, 1339–1352.

Moscat, J., and Diaz-Meco, M.T. (2009). Cell *137*, 1001–1004.

Nakagawa, H., Umemura, A., Taniguchi, K., Font-Burgada, J., Dhar, D., Ogata, H., Zhong, Z., Valasek, M.A., Seki, E., Hidalgo, J., et al. (2014). Cancer Cell *26*, 331–343.

Ruffell, B., and Coussens, L.M. (2015). Cancer Cell *27*, 462–472.

Umemura, A., Park, E.J., Taniguchi, K., Lee, J.H., Shalapour, S., Valasek, M.A., Aghajan, M., Nakagawa, H., Seki, E., Hall, M.N., and Karin, M. (2014). Cell Metab. *20*, 133–144.

Umemura, A., He, F., Taniguchi, K., Nakagawa, H., Yamachika, S., Font-Burgada, J., Zhong, Z., Subramaniam, S., Raghunandan, S., Duran, A., et al. (2016). Cancer Cell *29*, 935–948.

Valencia, T., Kim, J.Y., Abu-Baker, S., Moscat-Pardos, J., Ahn, C.S., Reina-Campos, M., Duran, A., Castilla, E.A., Metallo, C.M., Diaz-Meco, M.T., and Moscat, J. (2014). Cancer Cell *26*, 121–135.

White, E. (2012). Nat. Rev. Cancer *12*, 401–410.

Zhong, Z., Umemura, A., Sanchez-Lopez, E., Liang, S., Shalapour, S., Wong, J., He, F., Boassa, D., Perkins, G., Ali, S.R., et al. (2016). Cell *164*, 896–910.

Zhou, R., Yazdi, A.S., Menu, P., and Tschopp, J. (2011). Nature *469*, 221–225.